University of Canterbury

Effects of electrostatically charging pesticide sprays and quantitative methods for measuring spray efficacy

A thesis submitted to the University of Canterbury in partial fulfilment of the requirements for the Masters of Engineering (Mechanical Engineering)

Luke Longworth
6-30-2020

1 ABSTRACT

Traditional pesticide spraying procedures are often wasteful, with large proportions of the spray missing the target plants and drifting to unwanted locations. Electrostatically charging the spray can enhance the process, reducing loss and improving coverage on hidden surfaces. This thesis describes an investigation into the various parameters that can increase the effectiveness of an electrostatic nozzle, and how these and geometric parameters can increase the efficacy of spray. Additionally, an investigation into the use of capacitive wetness sensors to test spray efficacy was performed.

Increasing liquid flow rate through the nozzle was a major contributor to increasing nozzle charge-to-mass ratio, with increasing electrode voltage playing a more minor, but still noticeable role. The sensor specifications of the PHYTOS 31 capacitive wetness sensors were measured and recorded, and two calibration functions that convert sensor output to areal coverage were produced; one for large droplets (>1 mm) and the other for fine sprays (<1 mm). These sensors were also compared to water sensitive papers and found to be a suitable substitute for spray coverage measurements, though it should be noted that whilst papers measure the integral of coverage over time, the capacitive sensors measure instantaneous coverage. Finally, it was found that the wrap-around effect of electrostatic sprays is most effective on surfaces facing 0° – 60° away from the spray axis, and on surfaces 8° below the spray axis. Additionally, canopy penetration was improved by charging the spray, though this effect does not persist at the back of the canopy. Canopy penetration is found to improve as voltage increases, though there is a peak voltage of around 3.5 kV beyond which there is no clear evidence of further improvement.

TABLE OF CONTENTS

2 INTRODUCTION

2.1 SPRAYING IN AGRICULTURE

The spraying of pesticides is an essential part of most growing operations around the world. In 2001 the world reached an average global cost of $25 billion (USD) associated with 2.25 billion kg of active ingredient sprayed (Law E. S., 2001). Between 2010 and 2014 the mean annual pesticide use was 2.784 kg/ha, or 645 mg/kg of crop (Zhang, 2018). Pesticide use alleviates a number of concerns, including reducing the proportion of plants that die due to infection, or due to insects or other animals eating them, as well as by reducing the competition in the soil due to weed growth (Nazarko, et al., 2002). An exception to this ubiquity is in the market for organic farming, in which customers are willing to spend more money to receive produce grown with little to no pesticide. Whilst this is a viable option for that market, the increased cost of sale and lower productivity per unit land due to crop loss due to pests indicates that organic farming is not economically viable for the majority of food production.

There are several difficulties encountered in a spraying operation, most of which can be condensed to one issue: Spray frequently lands in the wrong place. In traditional spraying procedures, as much as 60 – 70% of spray will entirely miss the target plant (Law E. S., 2001), with this pesticide spray being deposited onto the soil or being caught in wind. Furthermore, of the 30 – 40% of spray that lands on the surface of the plant, the spatial distribution is skewed to the top surfaces of leaves (Longworth, Hendrickson, Steel, Cannon, & Gleadow, 2018), and often to the outer layers of leafy canopies (Ferguson, et al., 2016). Thus, there have long been pressures from multiple sources to improve the processes of pesticide spraying due in part to economic reasons, in part from legislature, in part from social health concerns (Kishi, et al., 1995), and in part from environmental concerns (Law E. S., 2001) (Malborough District Council, 2015) (World Health Organisation, 2018).

Viticulture is a large New Zealand industry for which spraying is eminently necessary. Grapes are subject to infection from mildews (downy and powdery) and botrytis, aggressive fungi which grow from spores carried in the air (MacGregor, 2016). To protect the plant from infection the entirety of the plant surface must be covered (Syngenta, 2019). This presents issues, as not only are the grape bunches of complex shape (as opposed to apples or oranges, for example) with complex surface areas and some individual fruits shielding others from spray, but the fruits are often protected by a leafy canopy. Due to the necessity of total coverage, most spraying operations spray until there is visible run-off from the plant due to the expense of conducting thorough tests to verify good coverage (The Australian Wine Research Institute, 2010). This usually provides adequate coverage, but it vastly exacerbates the wastefulness and damaging aspects of spraying.

This excess of spray is one of the key issues causing a number of problems for agriculturalists in New Zealand, including viticulturists. The World Health Organisation has identified the necessity for pesticide use in ensuring bountiful harvests to support growing populations, but also warns against overuse due to health concerns in people with primary or secondary contact with the chemicals (World Health Organisation, 2018). The Marlborough District Council in New Zealand has developed a stricter focus on spray drift as a result of growing industry in the area and as such there are increased restrictions on use of agrichemicals on local farmers (Malborough District Council, 2015). Whilst pesticides are apparently necessary, we should use and waste less where possible.

Electrostatic spraying is one method that has been proposed to reduce the negative impacts of pesticide spraying.

2.2 ELECTROSTATIC SPRAYING AT PRESENT

Electrostatic spraying was not a viable option for most industries until the 1990s, and many industries (including viticulture) still do not see it in widespread use. It consists of imparting a charge to the spray before it reaches the target plant, thus inducing an opposite surface charge in the grounded target plant, which in turn attracts the spray (Law E. S., 2001). This attraction serves two main purposes: firstly, the space-charge field of the spray cloud is drawn to the plant, which aids the travel of the spray from the nozzle to the plant; and secondly, when the spray is close enough to the plant (usually cited as within millimetres due to the inverse relationship between separation distance and attraction force, as well as the total charge being limited by conductivity of the plant and the Rayleigh limit, outlined below) (Law E. S., 2001), the electrostatic attraction forces can overcome the inertia, drag and gravitational pull of the droplets, and alter the flight path such that the droplets will land on the target plant.

The former of these two effects is useful for preventing spray drift, with the bulk attraction to the plants adjusting the flight path of droplets that may otherwise miss the plant. This effect ceases to affect the spray when wind forces are present, but other techniques such as air-assisted sprays may be employed to help minimise losses (Zhao, Castle, & Adamiak, 2008) (Law E. S., 2001) (Wei, et al., 2017). The latter effect helps to provide even coverage of the plant surface, as well as providing a mechanism for spray to adhere to hard-to-reach, or "shadowed" surfaces. This tendency for electrically charged spray to reach the back or undersides of surfaces is often referred to as the wrap-around effect (Law E. S., 2001) (Longworth, Hendrickson, Steel, Cannon, & Gleadow, 2018).

There are multiple ways to charge an aqueous spray, with three of the more common options being via corona discharge, contact, and induction charging (Hislop, 1988). Contact charging nozzles provide very low charge-to-mass ratios, and so these are not commonly used (Law E. S., 2001). Corona discharge nozzles work by spraying the liquid flow through a mesh of corona wires (such as those in a printer) at a high electric potential. The fluid around the wires is then ionised, transferring charge without a spark. This method is more effective, but it also produces ozone and nitrous oxide (Peyrous & Lapeyre, 1982) which are noxious gases. Thus, induction charging is the preferred option for agricultural sprays. The electrode is placed at the tip of the nozzle with a high electric potential applied to it and the water tank is grounded. The electrode causes the body of water to gain a total charge, which is concentrated at the tip of the emergent water column due to its high curvature. The charged tips then break off from the main flow, isolating them from ground. This produces a charged spray (Bailey, 1988). Figure 1 shows a representative illustration of induction charging.

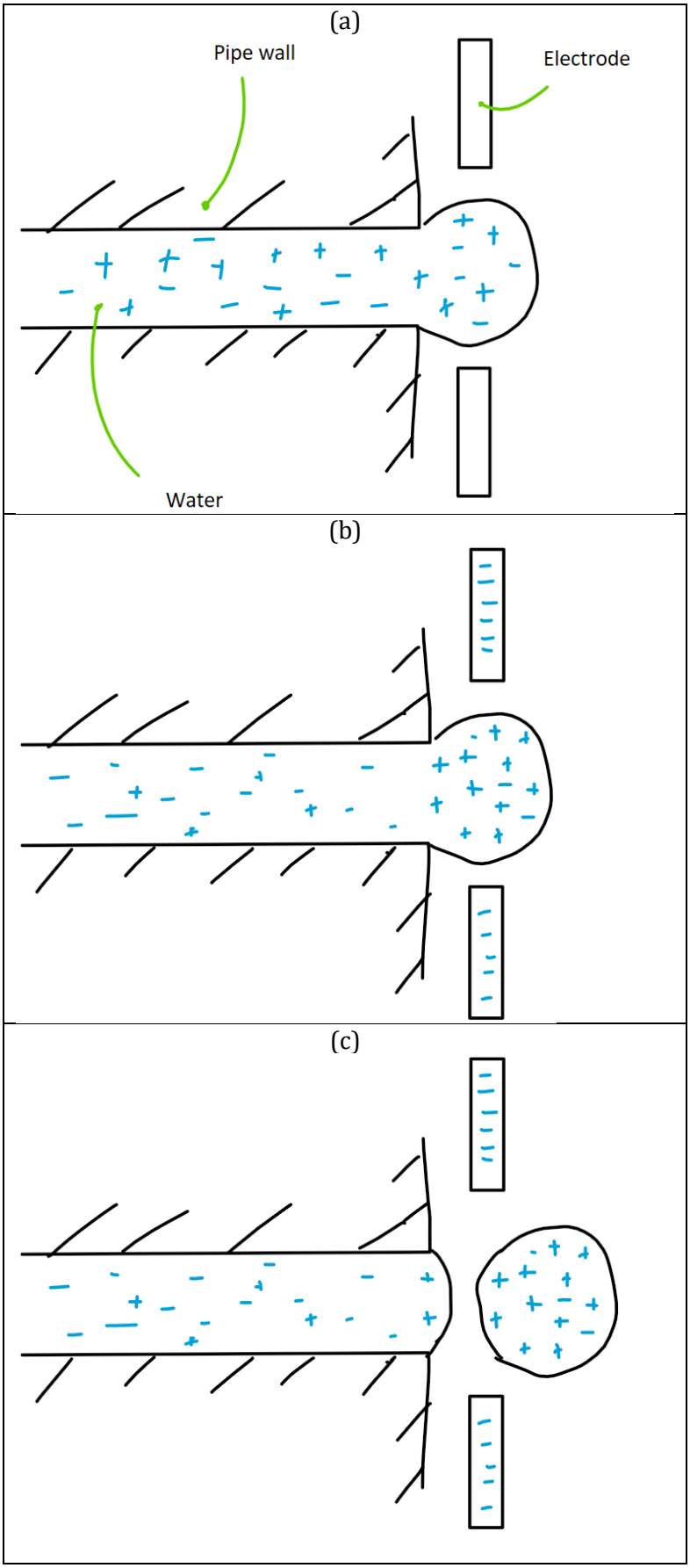

Figure 1: Induction charging process - (a) shows water flowing out of a pipe with an uncharged electrode, (b) shows water flowing with a charged electrode (charge concentrating at the tip of the water column), (c) shows the charged tip of the water column breaking off and producing a charged droplet

One issue that was discovered in early induction charging nozzles is that the charged spray often deviated from its course to instead wrap around onto the highly charged electrode. The way this problem was initially solved, and which solution is used in most systems today, is by using a high-velocity air sheet that emits from the nozzle around the water column. This has the added advantage of drawing out and breaking up the water column, meaning that the water supply does not need to be pressurised to spray. The air pushes any spray deviating towards the electrode far away from the nozzle at a higher velocity than can be overcome by the electrostatic forces. This air-assisted spraying system is also helpful in propelling droplets from the nozzle to the target plant, allowing for spraying from a greater distance and with higher external wind velocities.

One useful metric for predicting nozzle effectiveness is the *charge-to-mass ratio*. The electric force on the droplets is proportional to the charge on the droplet, and thus the acceleration of the droplets is proportional to the charge-to-mass ratio. Optimising the charge to mass ratio is thus an important part of designing an electrostatic spraying nozzle (Gomez & Tang, 1998). The charge-to-mass ratio experiences a limiting maximum in the form of the Rayleigh limit (equation 1) the point at which the electrostatic repulsion forces exceed the surface tension and cause the droplet to become unstable. Existing nozzles tend to produce sprays with droplets that reach only 10% of the Rayleigh limit (Post & Roten, 2018) on average, suggesting that the charge-to-mass ratio may see increases in future. ε_o is the permittivity of free space (8.85e-12 $C^2N^{-1}m^{-2}$), σ is the surface tension (Nm^{-1}), ρ is the density of the liquid (kgm^{-3}), and d is the droplet diameter (m).

$$\frac{q_{max}}{m} = \frac{\sqrt{2} \times 2\pi\sqrt{\varepsilon_o \sigma}\, d^{\frac{3}{2}}}{\rho \frac{\pi}{6} d^3} = \frac{\sqrt{2} \times 12\sqrt{\varepsilon_o \sigma}}{\rho\, d^{\frac{3}{2}}} \quad 1$$

Electrostatic spray charging also affects the droplet-size distribution of the spray. Conventional nozzles usually see average droplet sizes on the order of hundreds of microns (Dorr, et al., 2013) (Asano, 1999) whilst electrostatic nozzles produce droplets that are significantly smaller, often 30 – 80 microns (Law E. S., 2001) (Electrostatic Spraying Systems, 2011) due to larger droplets approaching their individual Rayleigh limit, experiencing Coulomb fission and splitting into smaller droplets (Gomez & Tang, 1998). This relaxing effect is exacerbated for higher charge-to-mass ratios, as smaller droplets have a higher surface area to volume ratio. This simultaneously helps and hinders the spraying process, as smaller droplets tend to provide a more uniform spread of droplets over the target plant (Balsari, Grella, Marucco, Matta, & Miranda-Fuentes, 2019), but they are also more prone to drift in the wind (Zhao, Castle, & Adamiak, 2008).

All sprays will feature a distribution of different drop sizes, so a mean value is often used to describe them. When referring to average droplet size, this investigation will generally mean the Sauter Mean Diameter (SMD), as this is related to the fraction of the Rayleigh limit that the spray reaches (Post & Roten, 2018). It is defined as the diameter of the droplet whose volume to surface area ratio is the mean of the entire spray, and in practice is generally found to be a linear multiple of the volume median diameter (the diameter producing the median volume). It is defined as follows:

$$SMD = \frac{\sum_{i=1}^{n} d_i^3}{\sum_{i=1}^{n} d_i^2} \quad 2$$

2.3 Equipment used in Spray Studies

One difficulty encountered by those choosing to study agricultural sprays is the resistance of sprays to quantitative measurement. The volume of liquid that is just leaving the nozzle can be measured with relative ease; a commonly used unit to describe the effectiveness of a spray is the litres of active ingredient required per hectare. However, a measurement of exactly where the

spray lands and how it gets to that location is much more difficult. Several methods are commonly employed today to quantify the distribution patterns of sprays. One employs the use of a fluorescent dye mixed in with the spray liquid, which can then be visually inspected by eye, with a UV-sensitive camera, or (most commonly) with a fluorometer, or can be washed off and isolated, producing a total volume deposited (Inculet, Castle, Menzies, & Frank, 1981) (Law, Marchant, & Bailey, 1985). Another method avoids any direct measurements, instead opting to compare the quality of the harvest for two sections of crop that were treated differently, or by noting pest population differences between the two. (Kabashima, Giles, & Parrella, 1995). One common method is the water sensitive paper, a small paper treated with a yellow, waxy coat that reacts with water to turn blue (or another colour change). These can be placed in strategic locations within an orchard, vineyard or similar farm to give insight into where the spray is going and spray density at different locations (Ferguson, et al., 2016). Similar methods involve oil-sensitive papers or coloured dyes sprayed onto white cards.

All these methods are effective to varying degrees, but also require a significant amount of work hours to collect and process the samples. The water sensitive papers have a variety of software options that can scan and automatically produce a percentage coverage from a phone camera, but these may not be reliable in all cases (especially with small droplet sizes) and still require people to collect and scan each paper manually. An ideal spray sensor would be able to report information in real time with a strong indication of spray distribution patterns.

One sensor that achieves this is the PHYTOS 31 leaf wetness sensor (Meter Group, Pullman, WA, USA). This sensor is sensitive to changes in dielectric constant near the surface of the sensor due to interdigitated wires covered in a thin, hydrophobic surface. These are referred to as capacitive wetness sensors and have the advantage of being able to output a voltage signal reflecting the state of the sensor in real time. However, their use in research is limited, with the sensors' main uses currently being to determine whether the crop is dry enough to begin a spraying operation and as part of weather stations that help to predict diseases such as fungal infections. Just like other intrusive sampling devices, measurements using these sensors will rely on collection efficiency (which depends heavily on spray conditions), and droplet spreading.

Meter Group have previously performed calibration tests on their PHYTOS sensors, producing graphs such as the one seen in Figure 2, but these calibration functions are difficult to compare to other spray sensing methods such as water sensitive papers, as well as not generalising to other situations such as alternative chemical compositions of spray (due to variations in dielectric constants and surface contact angle of droplets).

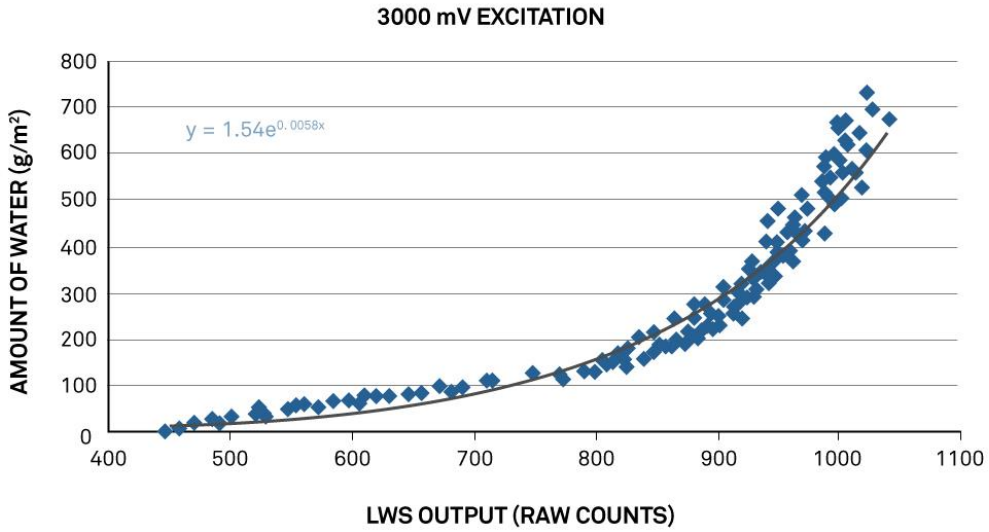

Figure 2: PHYTOS 31 Leaf wetness sensor calibration performed by Meter Group (retrieved from https://www.metergroup.com/environment/articles/predicting-amount-water-surface-lws-leaf-wetness-sensor/ on 15/06/2020)

Capacitive wetness sensors have been used for estimating spray coverage, detecting rain, and detecting moisture content in stored crops. Clark (Clark, 2018) used a Decagon capacitive leaf wetness sensor (LWS) as an alert for rainfall. In this case, the sensor was used as a binary on/off and was not calibrated to area or mass. The Decagon LWS is structurally identical to the LWS marketed by Meter as the PHYTOS 31 (used in this study) and by Campbell Scientific. Camuffo et al. (Camuffo, della Valle, & Becherini, 2018) used LWS to measure humidity and condensation in buildings, but did not seek liquid water coverage measurements. Kawahara et al. (Kawahara, Lee, & Tentzeris, 2012) constructed a novel LWS using inkjet printing with silver nanoparticle ink to produce their sensors, and Hernero et al. (Hornero, Gaitan-Pitre, Serrano-Finetti, Casas, & Pallas-Areny, 2017) developed a sensor very similar to the PHYTOS 31 and compared the two, finding that the different sensors differed particularly in terms of drying time. Ehlert et al. (Ehlert, Himmelmann, Beinhorn, & Kollar, 2019) performed a 3 year outdoor test on six different commercially available capacitive or resistive sensors, finding the Decagon model to be the most stable, though they did comment that it (and two other sensors) reported moisture in some periods where it was not visible on a timelapse camera in the area.

Acharya et al. (Acharya, Stebler, & Zou, 2017) used LWS underneath the leaf litter on a forest floor to measure moisture levels, and when calibrating the sensor output to gravimetrically measured percent water content they found a quadratic function to be suitable. Meter Group produced a calibration between sensor output and mass per unit area and fitted an exponential function to it. Wang et al. (Wang, Yu, Ou, Gong, & Jia, 2019) calibrated the PHYTOS sensors and found a linear relationship between mass and sensor output, with non-ionic solutions (pure water and non-ionic herbicides) having the same slope and ionic solutions having a different slope. Foque et al. (Foque, Dekeyser, Langenakens, & Nuyttens, 2018) calibrated a Delta OHM HD3901 sensor, which is similar to the PHYTOS 31. Single droplets were detectable down to a threshold of 2 L/ha. They also performed spray tests on these sensors, using water sensitive papers to measure areal coverage and comparing this to sensor output. In these tests, they found a linear correlation between sensor output and spray areal application rate, with signal depending on droplet size (attributed to contact angle and coalescence). Similarly, Hernero et al. attributed a spike and

decay time-pattern in sensor signal to coalescence of droplets on the surface, reducing coverage slightly after the droplets were deposited.

Taking a different approach, Wen et al. (Wen, Zhang, & Chen, 2019) developed a spray coverage sensing system that is not capacitive, but uses a fluorescent dye in the spray, deposited onto kraft paper strips which are later analysed in a spectrometer. This circumvented some of the handling issues of water sensitive papers and has low ongoing costs.

No publication to date has reported a calibration of a capacitive LWS that compares sensor output to areal coverage over the full range from dry to fully covered. This study aims to fill this gap by producing a calibration of the PHYTOS 31 sensors that covers a wider range of sensor output values and to describe them in the context of percent sensor output. It also compares differences in sensor behaviour for large droplets and fine sprays. Finally, the areal coverage of the sensor is measured directly rather than inferred from nearby water sensitive papers, finding that droplet deposition on the two different surfaces are not identical.

2.4 Research opportunities

Several studies have been conducted that confirm the efficacy of electrostatic spraying, in terms of total coverage, plant survival rate and pesticide use per hectare (Inculet, Castle, Menzies, & Frank, 1981) (Law & Lane, 1981) (Law, Marchant, & Bailey, 1985). Both the top and bottom surfaces of leaves find improved coverage, though the bottom surface sees this to a greater degree. This effect, known as the wrap-around effect, has long been known as an effective way to cover back surfaces (Law S. E., 1983).

However, existing knowledge tends to lack specificity. This investigation seeks to understand further the changes that could be made to electrostatic spraying technology to maximise these already-understood benefits. One considered change is altering the operation of the nozzle by changing the volumetric flow rate and electrode voltage. Another is to adjust the positioning and orientation of the nozzle with respect to the plant.

The PHYTOS 31 sensors discussed above are used frequently throughout this investigation, both as a primary method of recording changes in spray deposition and as a subject of study in their own right. Calibration functions exist to compare a raw sensor output (either as a bitstream of raw counts, or as a measured capacitance output) to mass deposition, but a non-dimensionalised calibration from sensor voltage output to areal coverage that spans the entire sensor range has not been produced. Additionally, neither an investigation into the effect of droplet size on sensor signal nor a comparison with water sensitive papers in identical situations have been performed. This investigation described in this thesis sought to produce these calibration functions and apply them to different scenarios, as well as to provide the comparison to water sensitive papers by analysing the output of the two sensing methods on both whole-sensor and individual droplet scales.

This report is divided into three main sections:

1. Firstly, an investigation into the nozzle used, characterising its inputs and outputs, and then measuring important variables such as charge-to-mass ratio and droplet size distributions. This enables any efficacy studies performed with this nozzle to be contextualised, drawing links between changes in spray deposition to the theory of induction charging.
2. Secondly, the PHYTOS 31 leaf wetness sensors are studied. Their electrical properties are investigated, datalogging equipment is produced, and a series of calibration functions are

evaluated. Following this, they are compared to the water sensitive papers in multiple ways.

3. Finally, the nozzle and sensors, having been characterised, are used to study and measure different spray scenarios in the laboratory and the field so as to produce new insight into the mechanisms and advantages of electrostatic spraying.

3 NOZZLE CHARACTERISATION

3.1 SUMMARY OF RELEVANT LITERATURE

- Patel (Patel, Sharma, Nayak, & Ghanshyam, 2015) used COMSOL modelling to predict that increased charge-to-mass ratio increases spray cloud uniformity and deposition, but increases radial drift
- Zhao (Zhao, Castle, & Adamiak, 2008) also showed this relationship between deposition rates and radial drift.
- Balsari (Balsari, Grella, Marucco, Matta, & Miranda-Fuentes, 2019) showed that cannon- and hand-type nozzles both have strong negative correlations between droplet size and driftability, and showed that increasing air speeds (and decreasing liquid flow rates) increases driftability
- Gomez (Gomez & Tang, 1998) investigated the relationship between individual droplet size and charge-to-mass ratio near the Rayleigh limit, and described the fission undergone by droplets with high charge
- Patel (Patel, et al., 2015) designed an air-assisted electrostatic nozzle similar to that used in this experiment and discussed the advantages and disadvantages of the nozzle. They tested the nozzle and produced depositions two- to three-fold as high as a non-electrostatic spraying nozzle
- Jahannama (Jahannama, Watkins, & Yule, 1999) measured droplet size and charge-to-mass ratio, and found that the droplet size distribution for charged and uncharged sprays varied much more for sprays with a horizontal nozzle than with a vertical nozzle.

This chapter describes new measurements of the air and water flow rates, charging efficiency, and droplet size distribution of a modified ESS BP1 sprayer.

3.2 NOZZLE AND MODIFICATIONS

The nozzle used in the majority of the tests was a modified BP1 backpack sprayer manufactured by Electrostatic Spraying Systems (Electrostatic Spraying Systems, 2011) (an unmodified BP1 sprayer can be seen in Figure 3, and scans produced by the MARS scanner (a spectrographic CT scanner) at the University of Canterbury can be seen in Figure 4 and Figure 5). This nozzle is marketed as a backpack sprayer that is useful for small home orchards and gardens and comes with a built-in electrode and high voltage circuit. However, the nature of a handheld sprayer is that variance due to user error is high, and so the nozzle was modified. The primary change in equipment was to remove the handhold and associated trigger and charging mechanism. The backpack that contains the liquid used for spraying and the nozzle were thus separated into two discrete components. An intermediary component was constructed to manage the inputs to the nozzle.

Figure 3: An unmodifed BP1 sprayer. Retrieved from https://asrhealthcare.com/product/ess-bp1-backpack-sprayer-and-spraywand-only-compressor-needed/ on 15/06/2020

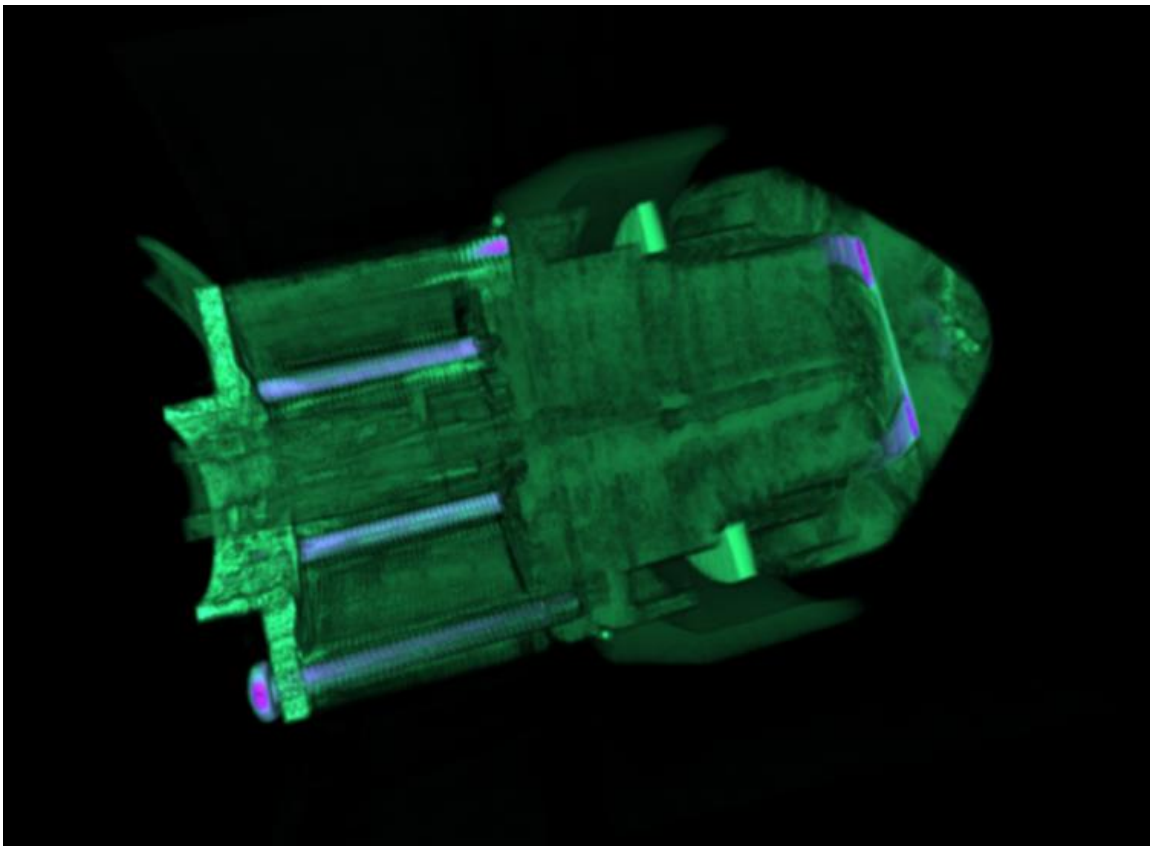

Figure 4: Cross section of the BP1 nozzle head. Blue sections are metallic; Green are plastic.

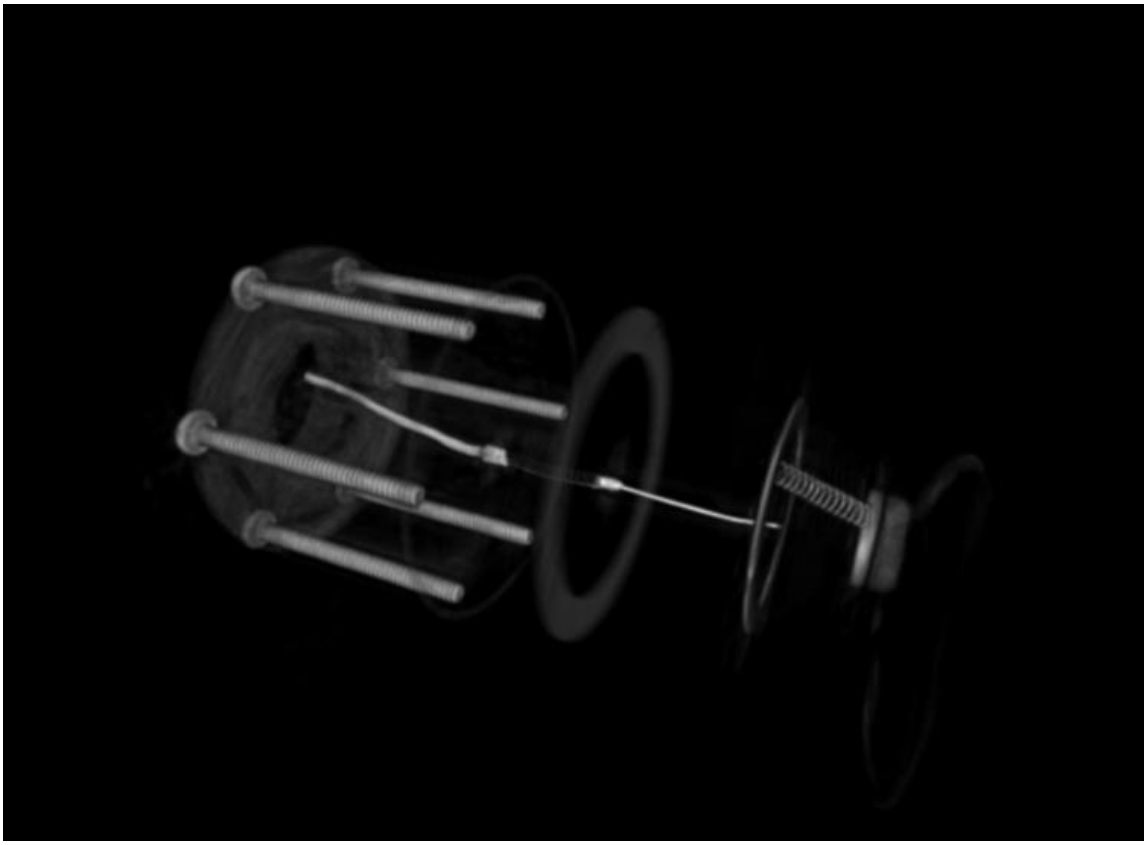

Figure 5: MARS scan of the BP1 nozzle head showing the electrical pathway (wire to metallic washer to spring to electrode)

This intermediary component will hereinafter be referred to as the control box, and was initially constructed by Hugh Hendrickson (with input from others including the author) as part of an engineering honours project. It consists of a steel box containing two solenoid valves and a control circuit driven by an Arduino Uno. Each solenoid valve exists between the nozzle and supply of water or pressurised air respectively, with the Arduino activating op-amps to allow or disallow power to each valve. Thus, the nozzle can be simply programmed to spray for a known amount of time from a location separated from the test. Alternatively, spray patterns can be programmed, with several early tests featuring a set of 2-second pulses to see how spray coverage changes over time. The Arduino also managed the DC-DC step-up voltage convertor (FS60P-12) that provides a configurable high voltage to the nozzle electrode up to approximately 8kV, two features the original lacked. The output from this convertor was connected to the nozzle via crocodile clips, which allowed for easy activation and deactivation of the electrostatic charging mechanism. The interior of the control box can be seen in Figure 7.

Figure 6 shows a symbolic layout for the components of the spraying system.

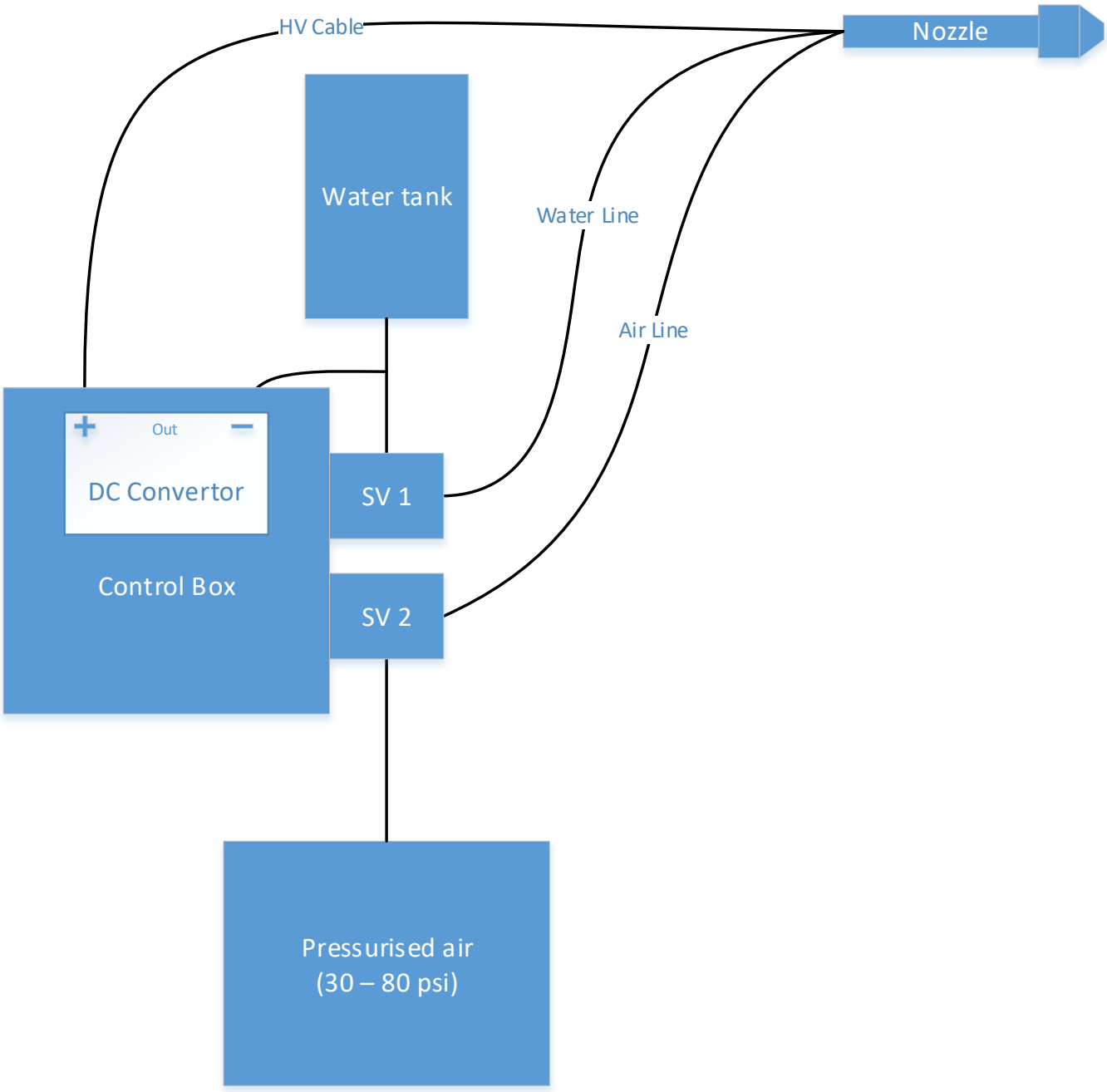

Figure 6: Symbolic schematic for electrostatic nozzle equipment

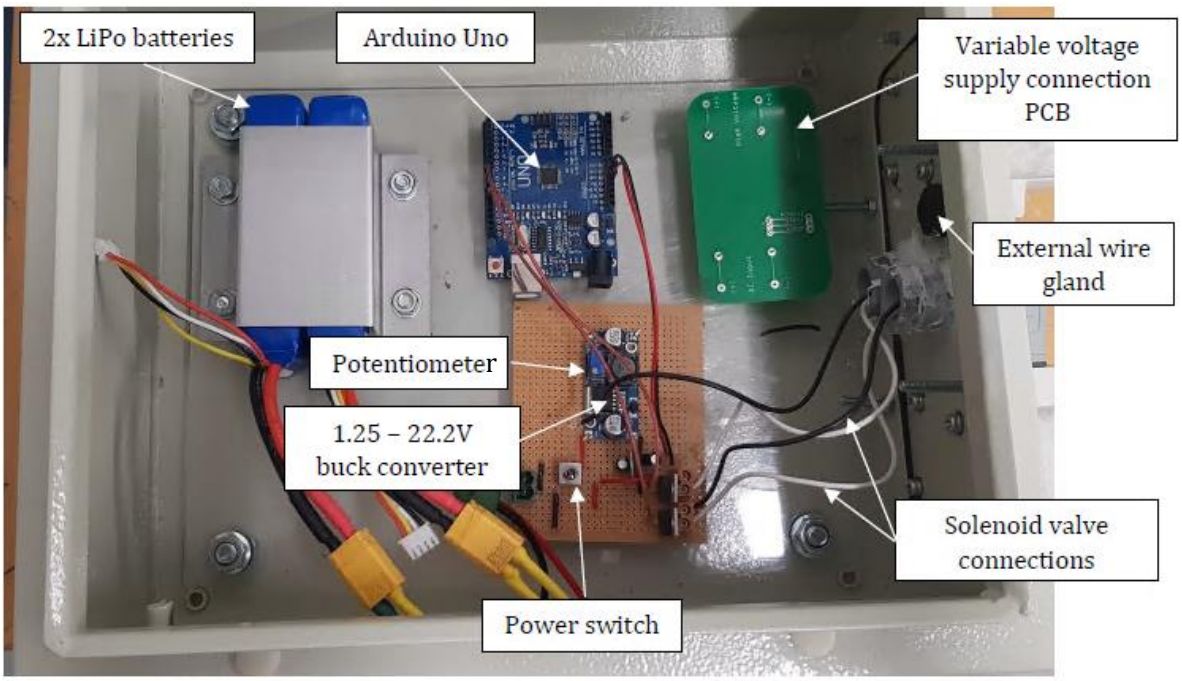

Figure 7: Interior of nozzle control box

This system features two primary inputs that are controllable by the user: Air pressure, and voltage input to the step-up convertor. These two factors influence both the amount of liquid leaving the nozzle in a given space of time and the amount of charge on the droplets leaving the nozzle. For a complete understanding of the phenomena at play, the interplay of these input variables on the output variables must be understood first. Thus, investigations were carried out with the goal of converting air pressure and input voltage into more useful metrics.

3.3 CHARACTERISING INPUT (LIQUID, AIR, VOLTAGE)

The first input-output pair to be investigated was the effect of the DC-DC step-up convertor. This was simple, only requiring a pair of voltmeters. For a series of input voltages, the output voltage was measured using a high-voltage voltmeter that operates up to 10kV. Figure 8 shows the comparison between the two.

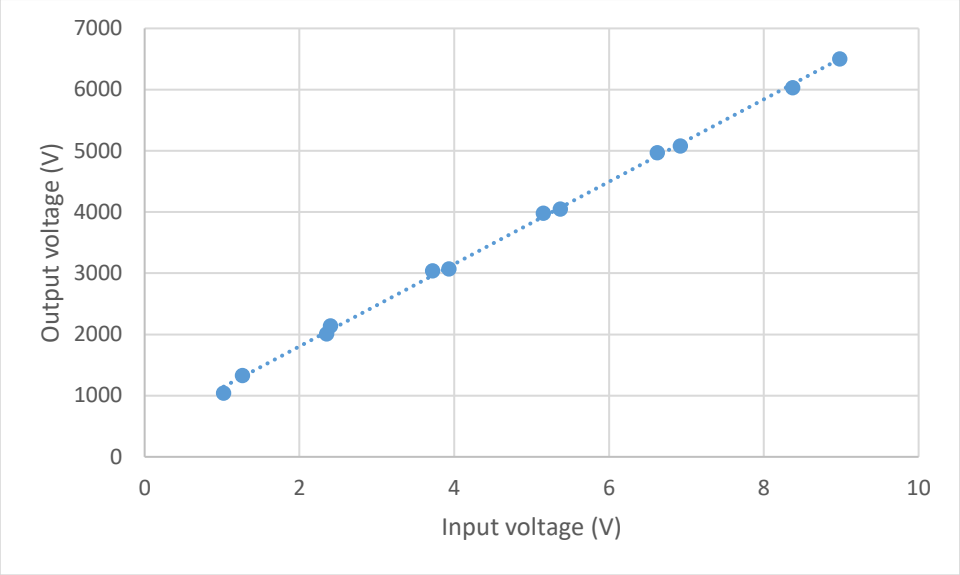

Figure 8: Calibration function from DC-DC step-up convertor input voltage to output voltage

The calibration function for the convertor is clearly linear, with regression producing the below equation (3) with an R^2 of 0.999. V_{in} and V_{out} are input and output respectively, both in V.

$$V_{out} = 673V_{in} + 459 \quad (3)$$

This calibration suggests an output range of 1kV to 6.5kV, but in practice this was limited to outputs of 1kV to about 4kV, because voltages at or above this upper threshold tended to produce electrical breakdown, observed as audible crackling when attached to the nozzle, and would trigger the alarm response of the convertor, shutting off the control circuit. The nozzle is originally rated for 1kV, so it seems reasonable that there is some unknown discharge path inside the nozzle for higher voltages.

The second input-output pair to be considered was the effect of air pressure on the flow rate. Both the liquid flow rate compared to pressure and the air flow rate compared to pressure were measured. These two metrics are not independent, as the liquid is not pressurised and relies on the air flow to draw it out of the tank.

The liquid flow rate was measured first. This test was performed by angling the nozzle into a large measuring cylinder for several minutes. The exit from the cylinder was covered, apart from a few square millimetres to allow pressure equalisation, such that the vast majority of the liquid stayed inside whilst some air was able to escape. At higher air pressures, there may be more loss, but this is accounted for with error bars. The time and final volume of liquid were recorded so that an average liquid flow rate could be accounted for. The results can be seen in Figure 9.

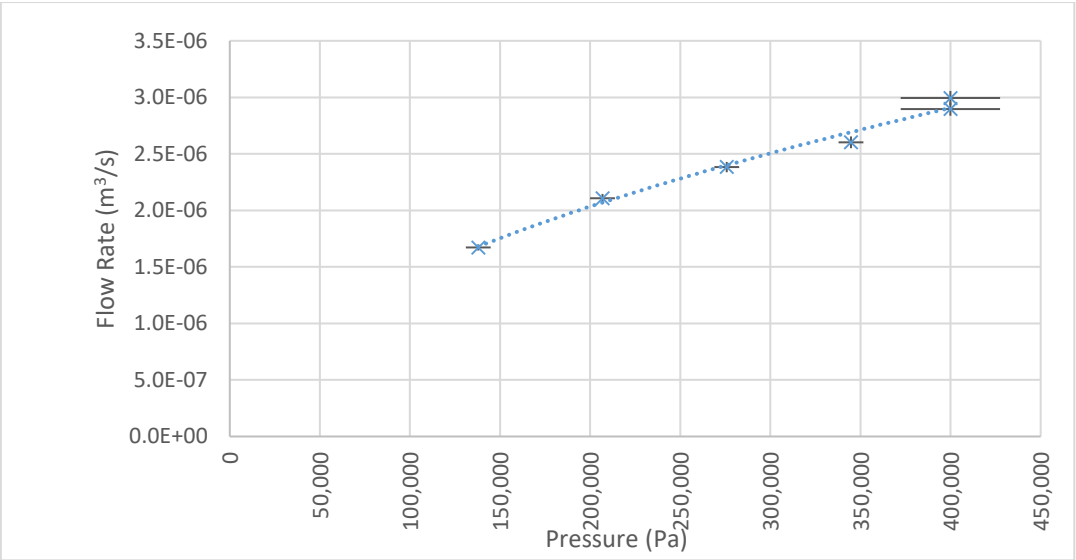

Figure 9: Average liquid flow rate from the nozzle compared to pressure of air supply

A power regression was used to generate the equation *4* with an R^2 of 0.990. Q is volumetric liquid flow rate (m^3s^{-1}), and P is pressure (Pa).

$$Q = (3.78 \times 10^{-9})P^{0.515} \quad 4$$

Bernoulli's equation predicts a square root relationship between the pressure of the liquid and the velocity of the liquid, so an equivalent equation was found by taking the square root of the pressure terms and performing linear regression. This function had an R^2 of 0.986.

$$Q = \left(4.72\sqrt{P} - 0.79\right) \times 10^{-9} \quad 5$$

The difference between these two functions reaches a maximum of approximately 8e-08 Pa. This difference amounts to 5% or less of the typical measured value, and therefore they were considered equivalent and were used interchangeably.

A similar test was performed to test the air flow rate through the nozzle, but this time the water input was left disconnected, and the nozzle was directed through a flowmeter (TSI model 4040) to measure the flow rate directly. Error bars are given as ±10 kPa in pressure based on the previous liquid flow rate measurements and a generous ±5 LPM in flow rate (converted to m^3s^{-1}), even though data was recorded to 1 decimal place.

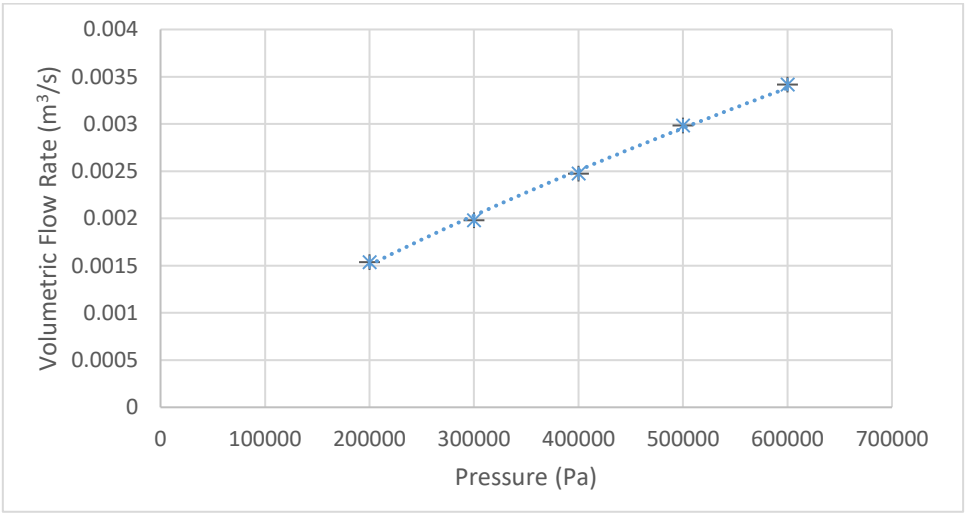

Figure 10: Average air volume flow rate compared to pressure of air supply

The air flow rate is not well described by a square root relationship. A power regression was used to generate the following equation 6.

$$Q = (2.0 \times 10^{-7})P^{0.74} \quad 6$$

The air flow rate and liquid flow rate experience a different relationship with the air supply pressure. This suggests that liquid mass fraction in the spray plume may also change with pressure. The proportion of the spray that is liquid by mass is shown in Figure 11. It shows that as air pressure increases, a smaller proportion of the flow is liquid. Error bars are calculated as the quadrature sum of air and liquid flow rate errors.

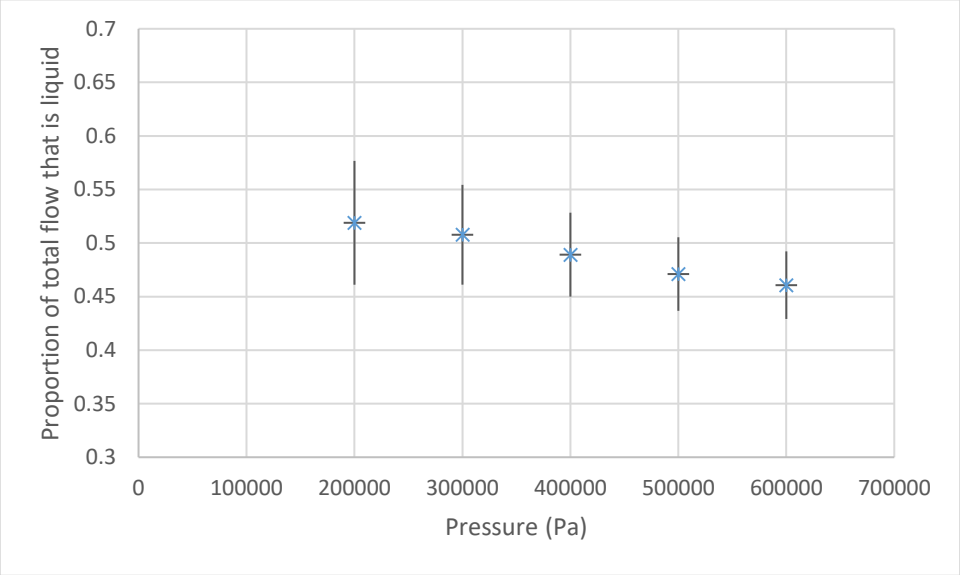

Figure 11: Mass fraction of total nozzle output that is liquid compared to pressure of air supply

3.4 CHARACTERISING OUTPUT (CURRENT, DROPLET SIZE)

With the two primary equations (3 and 4) describing the relevant input variables (electrode voltage and liquid flow rate), investigations into the output variables of the nozzle are possible. Two main tests were performed as part of these investigations. The first of these sought to understand the relationship between the controllable input variables and the amount of charge in the flow. This investigation used the same nozzle and Christchurch city water supply, so the only variables allowed to change are the input variables described above; liquid flow rate and electrode voltage. The goal of electrostatically enhanced spraying is ultimately to maximise the forces that attract spray droplets to plants, which is often characterised by the charge-to-mass ratio of the spray, but this investigation also considered other metrics: spray current, nozzle power output, and the charging effectiveness (also Sauter Mean Diameter and size distribution, but this is discussed later in the section). These are described below (where q refers to charge, Q refers to flow rate, and V refers to electrode voltage):

$$Current = I = \frac{dq}{dt} \quad 7$$

$$Charge\ to\ mass\ ratio = CTM = \frac{I}{Q} \quad 8$$

$$Power\ output = P = IV \quad 9$$

$$Charging\ effectiveness = CE = \frac{I}{QV} \quad 10$$

Current refers directly to the amount of charge leaving the nozzle over a given period and can be measured by an ammeter connected to a conducting vessel which collects the spray. The charge-to-mass ratio gives an indication of the strength of attractive forces compared to inertial forces. The power output indicates the energy consumption of the nozzle and can give an estimate of the energy imparted to the spray. The charging effectiveness indicates the amount of added attractive force given for each extra unit of voltage added to the electrode.

Each of these metrics are based on the current. To measure the current, an aluminium barbecue tray was wrapped in two layers of stainless steel wire with an average hole diameter of 0.5mm. This was isolated from ground on a plastic tray, and then was connected to the ground pin of a wall socket via a microammeter. This setup can be seen in Figure 12. When the nozzle was sprayed into this tray, a theoretical 100% of the spray would impact some surface of this tray before escaping, discharge to the metal surface, and then run to ground through the ammeter. The nozzle was sprayed into the tray for a variety of different air pressures and input voltages in order to investigate the effect of these two input variables on the current output of the nozzle. Figure 13 shows the results of this experiment, with liquid flow rate and electrode voltage as input variables.

Figure 12: Setup for spray current measurements

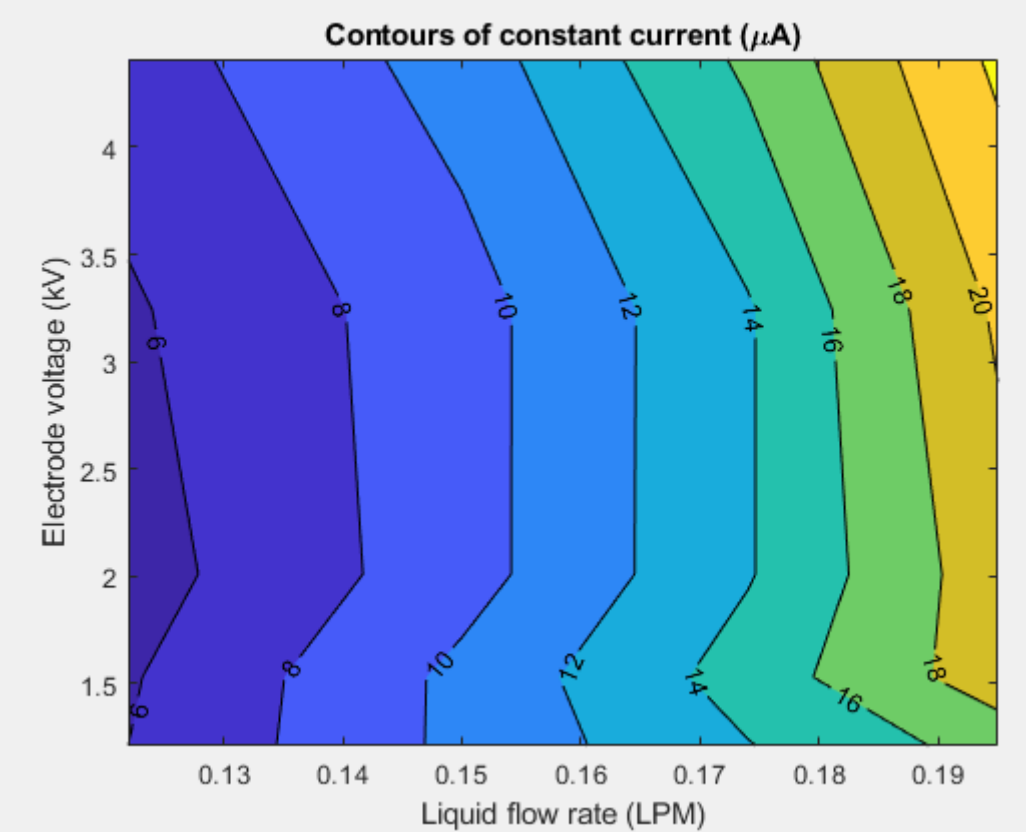

Figure 13: Current output of nozzle over a variety of liquid volume flow rates and electrode voltages

It is clear that the flow rate has a much more significant impact on the current than the electrode voltage, though there is a distinct increase occurring between 3.24 and 4.41 kV. This is expected, as the induction charging mechanism is based on the release of droplets from the main water column, so higher flow rates should be expected to produce higher currents. Additionally, the increased electric field strength due to the higher electrode voltage should increase the amount of charge added per drop, so the higher voltages should be expected to produce higher currents. It is not clear why there is a valley around the 2 kV mark.

This current data was converted to charge-to-mass ratio by dividing each current value by the flow rate at which it was measured. This has the advantage of removing the time dimension (an increase in liquid flow rate is – not surprisingly – found to increase the "charge flow rate") in an effort to see any differences in charge per droplet with flow rate (as opposed to charge per unit time). Figure 14 shows the resulting surface.

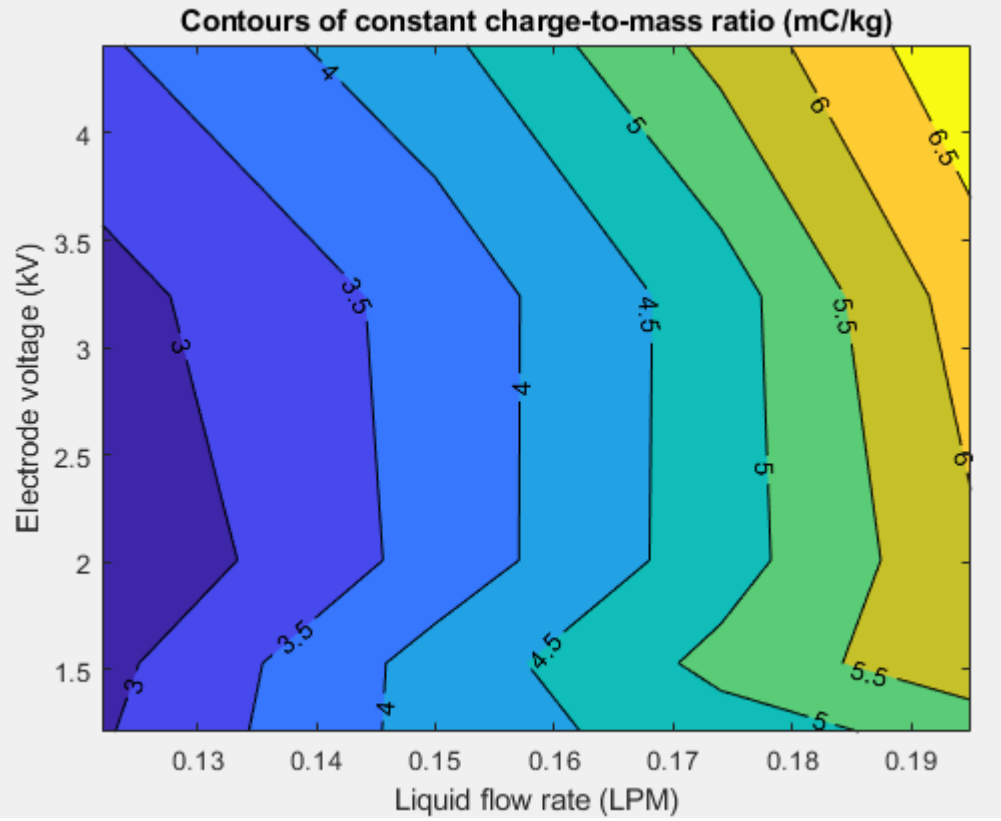

Figure 14: Charge-to-mass ratio of spray over a variety of volume flow rates and electrode voltages

Interestingly, the flow rate still seems to have a much more significant impact than the electrode voltage over the ranges considered, with the form of the surface remaining much the same.

The charge-to-mass ratio is arguably the most important metric to consider, as it represents the balance between inertial components (mass), that act to prevent the droplet flight path from changing, with the forcing components (electrostatic attraction), that act to change the flight path. A higher charge-to-mass ratio indicates that, on average, drops are more likely to reach the target surface due to electrostatic forces. This figure suggests that the best way to maximise this variable is to increase the liquid flow rate. This corresponds to higher liquid velocity, which may mean that more impulse is required to change the droplet trajectory, though many sprays are performed at such a distance that droplet velocity is much lower by the time the stream reaches the plant. This distance between the nozzle and the plant thus becomes an important metric of consideration.

This relationship between liquid flow rate and charge-to-mass ratio may impact droplets differently based on their individual size. If the flow rate is increased, then velocity necessarily increases too. Larger droplets will maintain this velocity for longer and will experience greater weight and drag forces than smaller droplets. Whilst the charge-to-mass ratio would be on average higher, these effects may counteract the improvements. Smaller droplets may then be preferred in instances where bulk drift can be minimised by techniques such as air-assistance.

There are two more metrics of interest. Firstly, total power passing through the nozzle, generated by multiplying the current by the electrode voltage. Secondly, the charge-to-mass ratio of spray per unit voltage on the nozzle. This latter metric has been dubbed “charging effectiveness” to indicate that it measures the amount of charge imparted to the spray for each unit voltage on the electrode. These can be seen in Figure 15.

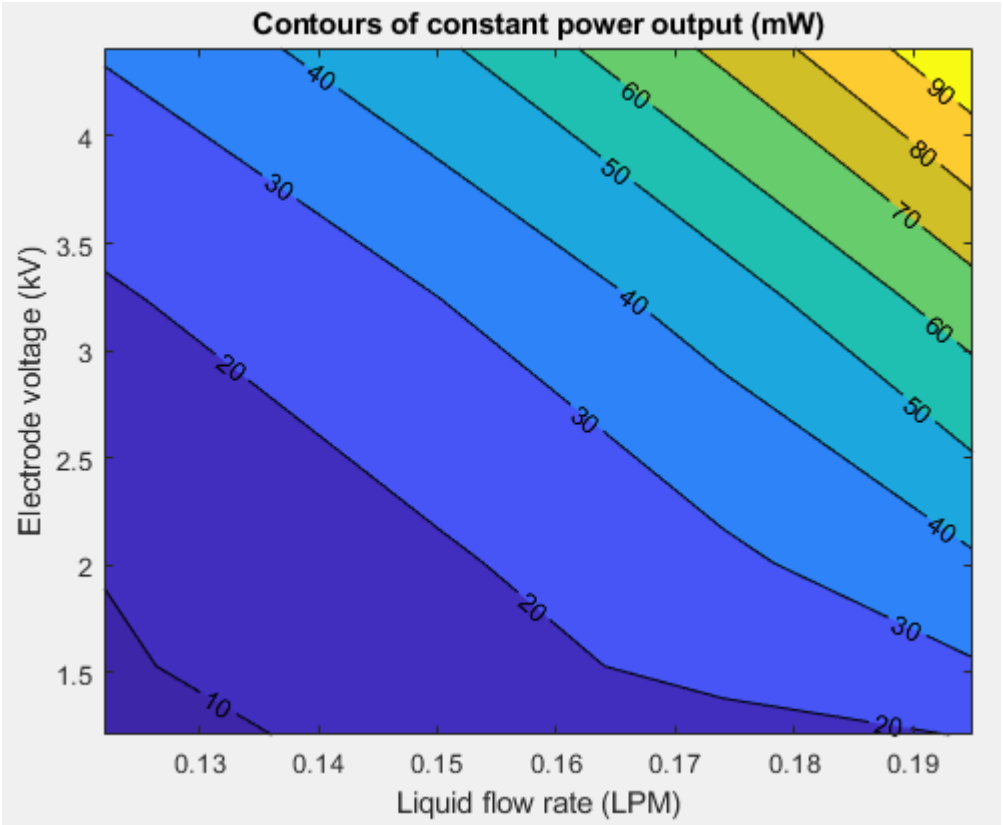

(a)

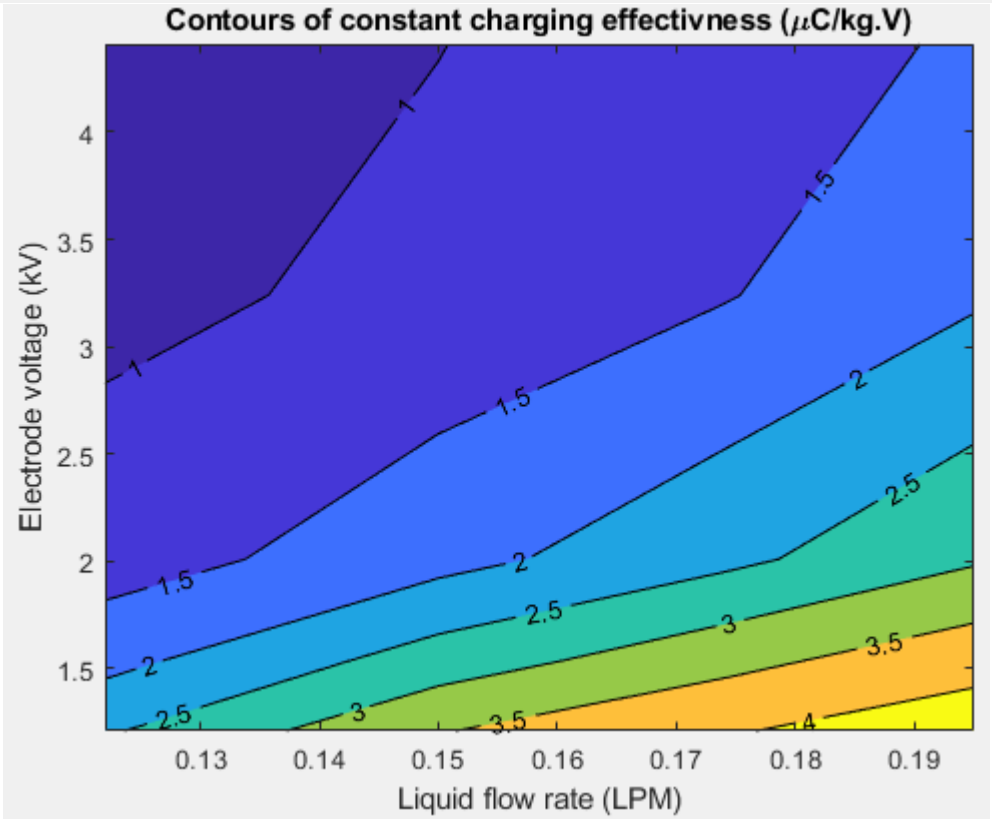

(b)

Figure 15: (a) Power output and (b) charging effectiveness of nozzle for a variety of volumetric flow rates and electrode voltages.

Given a fixed flow rate, the power output and charging effectiveness follow inverse curves – with power output increasing with voltage and charging effectiveness decreasing with voltage. As the flow rate increases, these patterns stay the same, but the increase or decrease is more drastic.

Additionally, the whole curve raises. The power output result is expected, as current depends largely on the flow rate, so increases in either flow rate or voltage should produce a higher value. The charging effectiveness, however, suggests that voltage increases produce diminishing returns, with each successive kilovolt added to the nozzle only contributing small amounts to the increased charge on the droplets. This is discussed in more detail later in this section.

Various regression models were investigated to produce a reasonable calibration to estimate charge to mass ratio. Specifically, those considered were linear, quadratic, and power. The forms of these equations can be seen in equations 11, 12 and 13.

$$CTM = aV + bQ + c \tag{11}$$

$$CTM = aVQ + bV^2 + cQ^2 + dV + eQ + f \tag{12}$$

$$CTM = cV^a Q^b \tag{13}$$

Linear regression in multiple dimensions was used to evaluate suitable coefficient values in each case, utilising the data analysis add-on for Microsoft Excel. In the case of equation 11, no data processing took place before regression for a function of two variables was performed. In the cases of equations 12 and 13, logarithms were used to transform the equation into the following linear form:

$$\log(CTM) = \log(c) + a\log(V) + b\log(Q) \tag{14}$$

In the middle case, regression was performed as if the charge-to-mass ratio was a function of 5 independent variables; VQ, V^2, Q^2, V and Q.

The final equations and associated R^2 can be seen in Table 1.

Table 1: Possible equations to describe droplet charging as a function of control variables and their associated R^2 values. CTM is the charge to mass ratio (Ckg^{-1}), V is voltage (V), Q is volumetric liquid flow rate (m^3s^{-1})

Type	Function	R^2	
Linear	$CTM = 2.49 \times 10^{-7}V + 2310Q - 0.00242$	0.8800	15
Quadratic	$CTM = 0.381VQ + 1.41 \times 10^{-10}V^2 - 3.6 \times 10^{8}Q^2 - 1.6 \times 10^{-6}V + 3365Q - 0.00159$	0.9238	16
Power	$CTM = 284300V^{0.110}Q^{1.47}$	0.9060	17

Though the quadratic approximation has the highest R^2 value, it is more complex than either of the other equations. The power fit has a similar R^2, so this complexity seems excessive. The power fit was thus selected as the preferred option.

This offers some insight into the relationship between the input variables and the charge to mass ratio, notably that both are related non-linearly. Flow rate has increasing returns, so any feasible increase to flow rate should make appreciable differences. Conversely, electrode voltage has diminishing returns, such that an initial change from zero produces drastic changes in output, but following this initial rise there is very little output change from even large input changes. This is expected, as increasing voltage is associated with increased polarisation within the liquid. The repulsion of like charges will resist further polarisation, hence diminishing returns. Figure 16 shows just the level curves of the function, first with curves at fixed flow rate values, then with curves at fixed voltage values. These show visually that within reasonable ranges of voltage and flow rate, the voltage contributes very little to the charge-to-mass ratio in this nozzle.

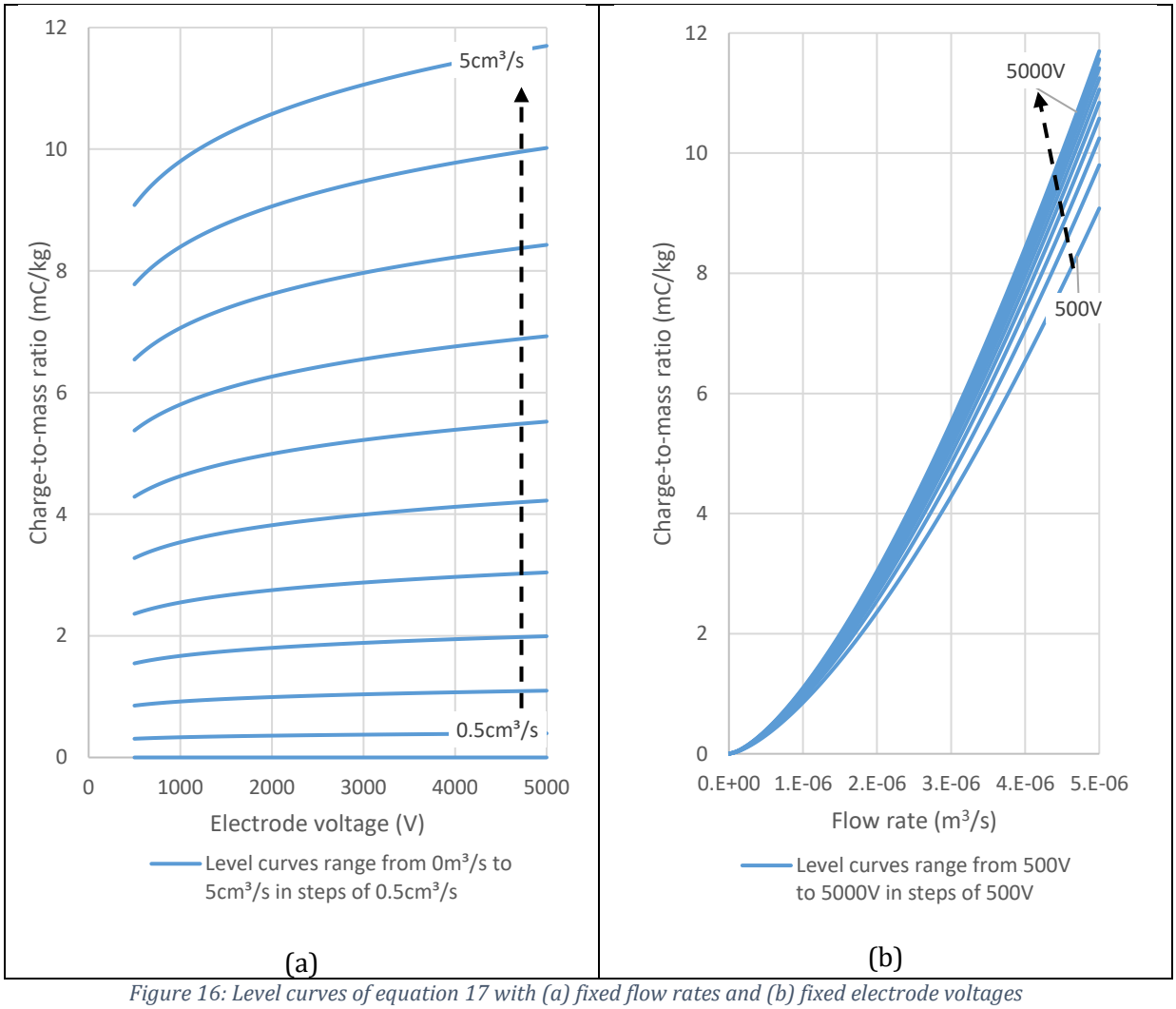

Figure 16: Level curves of equation 17 with (a) fixed flow rates and (b) fixed electrode voltages

The charge-to-mass ratio should be dependent on the average droplet size (or vice versa). To investigate the relationship between current from the nozzle and the droplet size, the nozzle was taken to the Centre for Spray Technology Application Research and Training (C-START) at the University of Queensland in Gatton, QLD, Australia. This aspect of testing was undertaken by project sponsor Dr Scott Post, with the data passed on for use in this thesis. The following is an excerpt from his write-up, followed by a photograph of the test set-up (Figure 17):

"The instrument used was an Artium (Sunnyvale, CA, USA) TK1 Phase-Doppler Interferometry (PDI) probe, with a static range of 4.3 – 640.5µm. PDI user settings are photo-multiplier tube (PMT) gain of 600V, analogue threshold of 100mV, and peak DC offset of 600mV. Fixed settings are 532 nm, focal length of 100 mm, beam diameter of 0.08 mm, and collection angle of 40°. The working fluid was tap water. The PMT voltage gain was selected to provide high validation rates. All data points had data validation rates of 93%-99.7%, and the relatively high gain also helps to detect the very small drops present (drops were detected all the way down to the device minimum, with maximum drop size typically 100 µm)."

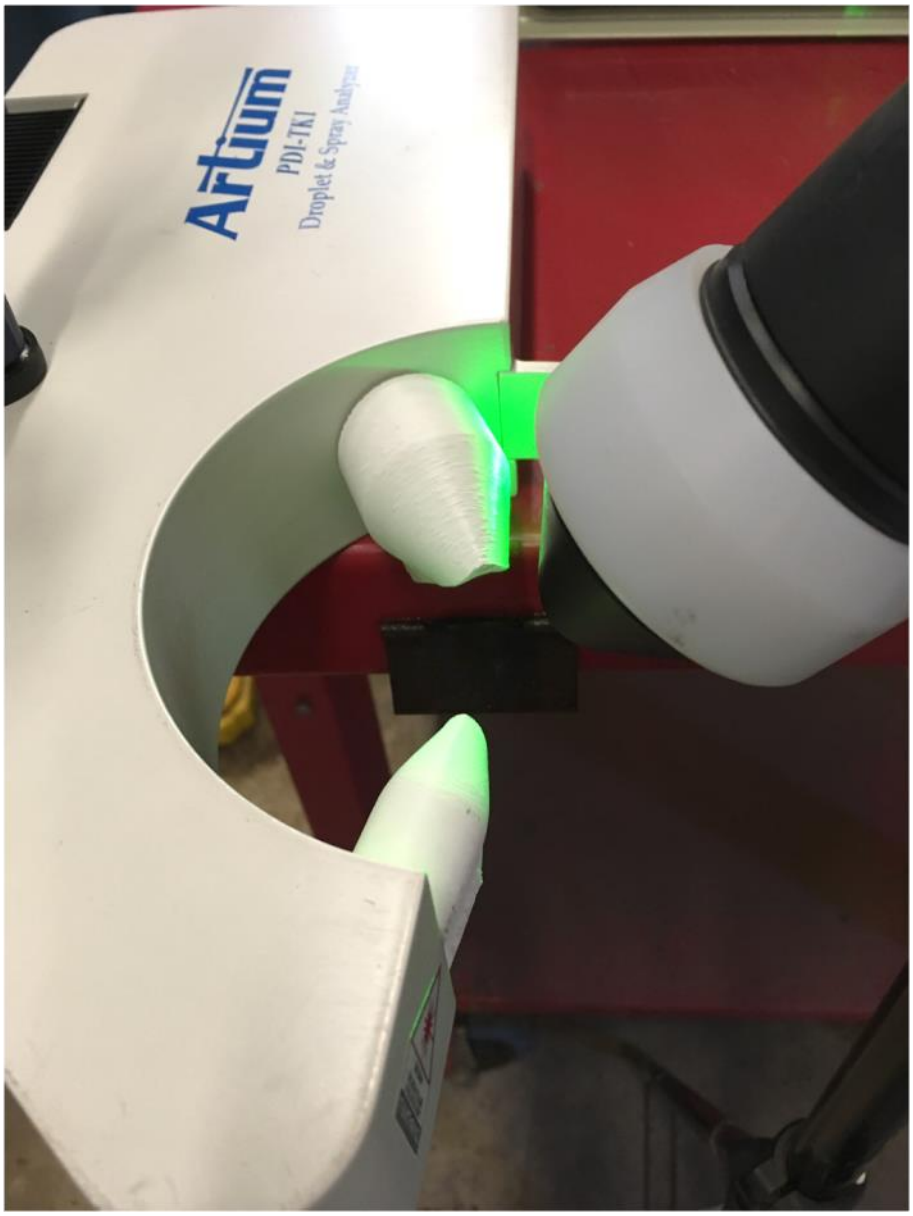

Figure 17: Arrangement of nozzle and PDI used for measuring droplet size

The input voltage and air pressure values were chosen to match the initial current tests. Because the testing was done at different times and different locations, there may be some variation in spray quality. The results can be seen in Table 2, with each unique voltage/flow rate pairing the charge to mass ratio (left, grey, $mCkg^{-1}$) with the Sauter Mean Diameter (right, white, μm). The charge to mass ratios have an uncertainty of 0.14 to 0.22 based on cumulation of error at each step of calculation. The error in SMD was not recorded in the data made available for this investigation.

Table 2: Charge to mass ratios (left, grey, mC/kg) and Sauter Mean Diameters (right, white, microns) for different combinations of liquid flow rate and electrode voltage.

	0.122Lmin^{-1}		0.150Lmin^{-1}		0.174Lmin^{-1}		0.196Lmin^{-1}	
1.21kV	2.95	61.9	4.19	48.7	4.79	45.9	5.16	39.7
1.53kV	2.86	56.7	4.19	47.7	5.13	43.1	5.87	38.9
2.01kV	2.60	53.0	3.68	42.9	4.90	39.6	6.25	36.9
3.24kV	2.82	53.9	3.68	38.9	4.80	35.6	6.70	25.1
4.41kV	3.44	45.7	4.36	37.6	5.66	29.8	6.89	24.6

There is a clear tendency for the SMD to decrease both with increased flow rate and increased electrode voltage. Applying a power regression to the data produces the following function (in SI units) with $R^2 = 0.900$ (SMD is Sauter Mean Diameter (m), V is voltage (V), Q is volumetric liquid flow rate (m^3s^{-1}):

$$SMD = \frac{6.8 \times 10^{-10}}{V^{0.2}Q} \qquad 18$$

As with the charge-to-mass ratio, the flow rate through the nozzle has a much more significant effect on the diameter for the tested values of voltage and flow rate, though the effects of each is more muted in the case of SMD, as well as inverted relationship. If the two are plotted against one another, Figure 18 is produced, with a linear trendline superimposed.

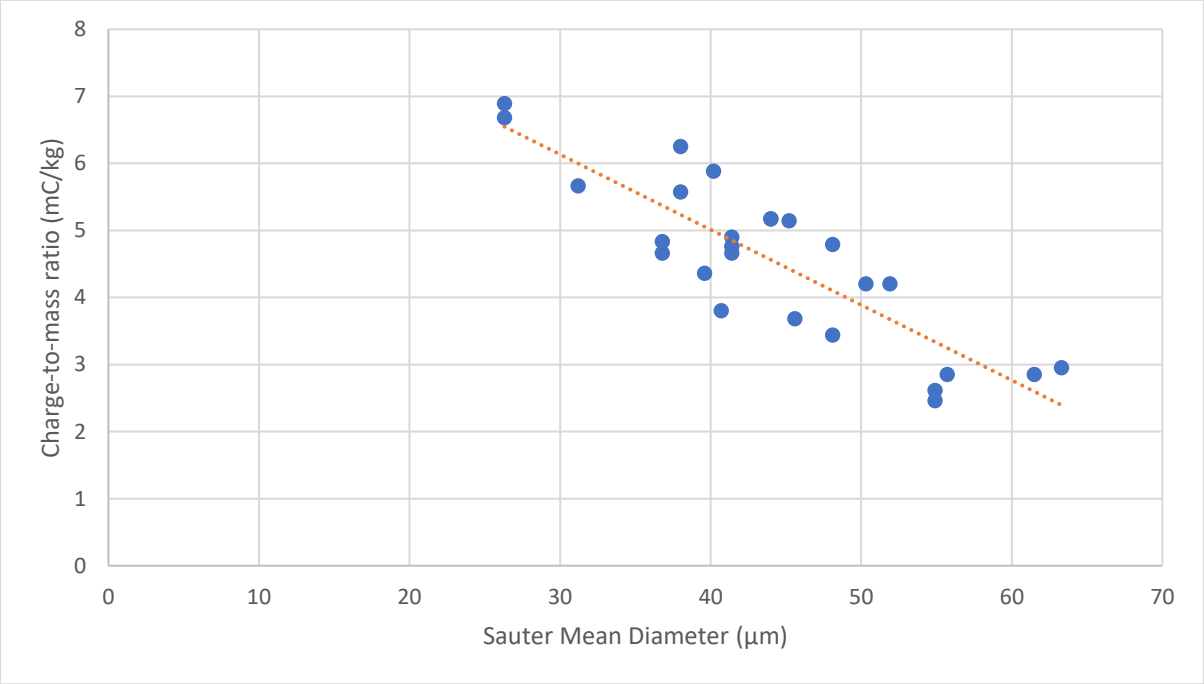

Figure 18: Scatterplot of Sauter Mean Diameter (SMD) and charge-to-mass ratio of spray with associated linear line of best fit

The line of best fit shown in Figure 18 was generated using linear regression in Excel and has an R^2 value of 0.7433. The units of charge-to-mass ratio and SMD are mC/kg and µm respectively.

$$CTM = 9.5 - 0.112(SMD) \qquad 19$$

(Gomez & Tang, 1998) suggests that there are three main modes for droplet size distribution with variation of charge-to-mass ratio; one for small droplets (<50 microns), one for medium droplets (50 – 150 microns), and one for large droplets (>150 microns). The former follows a relationship in which the charge to mass ratio is proportional to D^{-1}, the middle follows a $D^{-1.5}$ relationship, and the latter drops off rapidly. Figure 19 shows the scatterplot on log-log axes with lines of gradient -1 and -1.5.

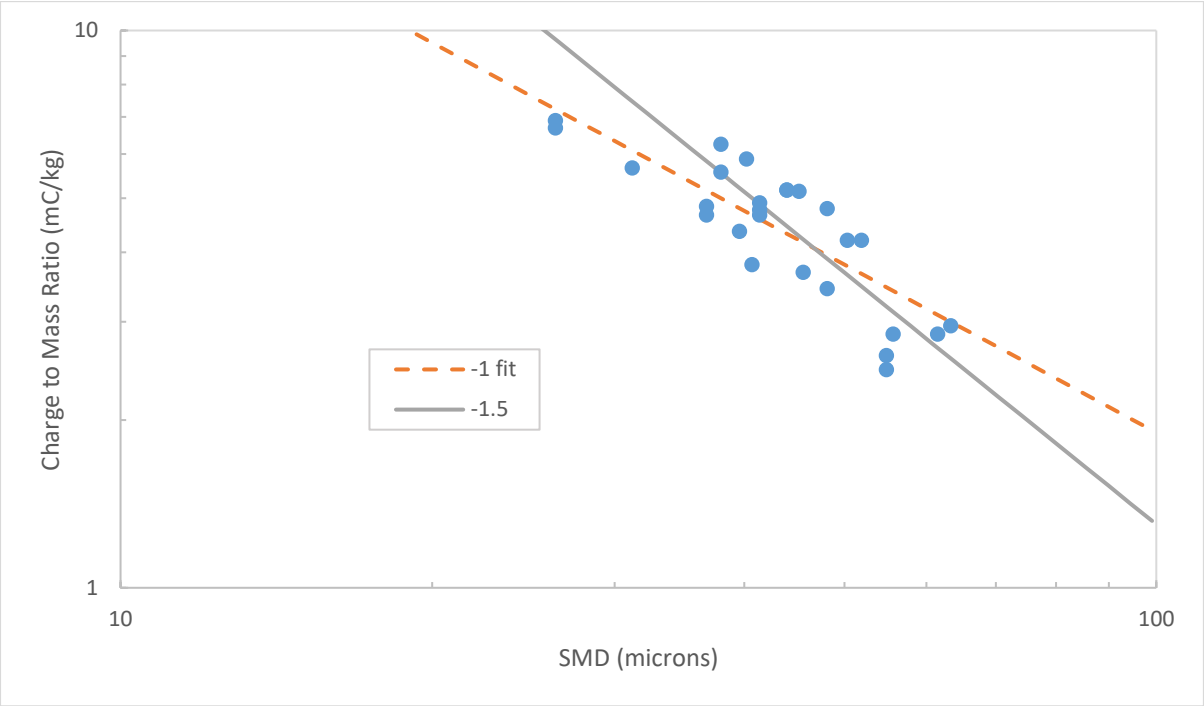

Figure 19: Log-log plot of Sauter Mean Diameter (SMD) and charge-to-mass ratio of spray with overlaid lines of gradient -1 and -1.5

This may follow the expected pattern of droplets smaller than 50 microns following a gradient of -1, with droplets larger than 50 microns following the -1.5 line. However, this is unclear due to the large spread of the data. A power regression for the charge-to-mass ratio as a function of the droplet diameter gives the following equation (20) with $R^2 = 0.699$:

$$CTM = (8 \times 10^{-8}) * SMD^{-1.08} \qquad 20$$

This supports the expected pattern further, as the majority of the sprays are below 50 microns in SMD and the power is close to -1. The R^2 value indicates a correlation but is not large enough to state with certainty that this is the best model.

This suggests that sprays seeking high charge to mass ratios will encounter more spray drift issues due to lower average droplet sizes. The tendency of a spray with a high charge-to-mass ratio to be attracted to, wrap around, and stick to a target plant will be counteracted by the tendency of a spray with a low average diameter to be caught on gusts of wind and be blown off track. Spray systems that utilise high charging mechanisms may wish to prioritise aspects of nozzle design that allow the nozzle to get very close to the target plant, or to increase the power of the air-assistance to keep the droplets in the desired location.

Note that these conclusions are stemming from bulk data (i.e. an average droplet size) and so there may be differences in behaviour for sprays with different droplet size distributions.

4 WETNESS SENSOR CHARACTERISATION

4.1 SUMMARY OF RELEVANT LITERATURE

- Foque (Foque, Dekeyser, Langenakens, & Nuyttens, 2018) tested a leaf wetness sensor similar in design to the PHYTOS sensors, finding a good correlation between spray coverage and sensor output signal (V). However, spray coverage was measured with water sensitive papers rather than directly on the sensor itself.
- Shujie (Shujie, et al., 2016) measured the contact angle of droplets on a variety of leaves, though they measured maximum possible contact angle rather than a variety of contact angles compared to droplet volume. Contact angles varied from 40° to 140° for different plants
- Ebert (Ebert, Taylor, Downer, & Hall, 1999) investigated the relationship between droplet size and efficacy of spray, finding that smaller, more even deposits are not always more efficacious than deposits of larger droplets.
- Kesterson (Kesterson, Luck, & Sama, 2015) and Salyani (Salyani & Serdynski, 1990) developed wetness sensors that utilise changes in resistance across sensor surface. Both produced results in which increased water deposition led to increased sensor signal, but the latter encountered problems with oxidation and the former could not separate the droplet size effects from the application rate effects. Salyani et al also found that solutions with higher concentration of ions produced lower signals.
- Lyashchenko (Lyashchenko, Loginova, Lileev, Ivanova, & Efimenko, 2009)and Mohsen-Nia (Mohsen-Nia & Amiri, 2013) found that water with lower concentrations of contaminants (the former using salt solutions, the latter using alcohol solutions) has a higher dielectric constant

This chapter details the specifications, advantages and limitations of the PHYTOS 31 capacitive leaf wetness sensors. The sensors are calibrated such that raw output can be used to infer areal coverage, and then the sensors are compared to the existing industry standard for spray coverage measurement: water sensitive papers.

4.2 PHYTOS 31 LEAF WETNESS SENSORS

PHYTOS 31 capacitive leaf wetness sensors produced by Meter Group (Pullman, WA, USA) (seen in Figure 20) were a central part of this investigation. Existing spray coverage sensing methods such as water sensitive papers and fluorescent dyes are capable of producing data that reflects the specific proportion of area covered (*areal coverage*) but require significant post-processing to generate this data. The PHYTOS sensors are primarily used at present to determine whether a section of crops is wet or dry, with the associated data logger being pre-programmed to produce a binary output of dry or wet based on thresholds. There is no demonstration of the accuracy of these sensors to date, nor a comparison to water sensitive papers.

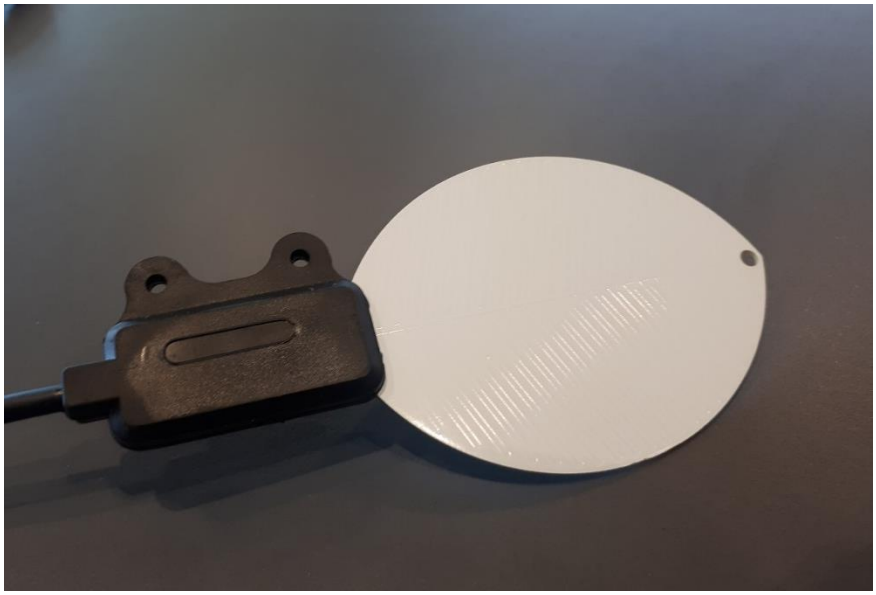

Figure 20: PHYTOS 31 leaf wetness sensor

This investigation hypothesised that these sensors could be used to produce more detailed data than a dry/wet binary threshold. Several tests were carried out to find general properties of the sensors, as well as to produce a calibration curve that could be used to give areal coverage of the sensor and quantify uncertainty. These sensors were then used in the other tests described later in this thesis.

4.3 DATA LOGGING METHODOLOGY

The manufacturers of the PHYTOS sensor recommend their ZL6 data logger to accompany these sensors, but this was not considered a necessary expense. Instead, two data logging circuits were created: Firstly, a National Instruments ADC and LabView data acquisition script, and secondly, an Arduino Nano-based data logger.

The LabView circuitry made use of a USB-6009 I/O device to power and receive data from the sensors. An excitation voltage of 5V and a ground line was connected to each of the four PHYTOS 31 sensors from the I/O device, and then the output signals from the sensors were wired into the ADC input ports of the I/O device. A pre-existing data acquisition LabView script was used to provide the excitation voltage and record the data measurements after they were converted from a bitstream to voltage. This data logger was excellent for lab use, as the data was saved directly to the computer, and the real-time sensor output was displayed on screen. This allowed for easy troubleshooting and reliable data. However, it was limited to lab use only, as transporting this equipment to a vineyard would be time consuming and difficult, and providing stable power to all the components without access to electrical mains would be difficult. Additionally, it would be difficult to ensure that equipment did not overheat or get damaged by the spray. Thus, the second data logger was created.

The Arduino data logger is formed from the following components:

- Arduino Nano
    - This provides the logic to operate the circuit as well as providing power to other components
- SD Card Port

        - This is an off the shelf component that provides an interface between the Nano and an SD card.
- DC to DC Step-Up Transformer
    - This was powered by a pair of AA batteries. The power output was a USB-B, so a USB-B to mini-USB cable was used to connect this to the Nano.

This datalogger solves the portability problem but is more difficult to troubleshoot as there is no visual signal when the circuit malfunctions like the LabView circuit.

Initially the Arduino Nano itself was used to perform analogue to digital conversion (ADC) but, because 10 bits of resolution was deemed unsuitably low, an ADS1115 16-bit signed integer ADC unit was retrofitted to the board in between the sensor output and the Nano.

These two data logging circuits (LabView and Arduino) were used interchangeably depending on where the tests were taking place. It was assumed that these circuits produced equivalent results (verified to be true within an error of 5% - usually less and strictly less than the imposed error bounds - for a fixed areal coverage in section 4.5.2).

4.4 SENSOR FEATURES AND SPECIFICATIONS

4.4.1 Testing the minimum and maximum sensor outputs over time

The capabilities and limitations of the PHYTOS 31 sensors were tested in several ways. The first involved submerging each of them in a bucket of water for five minutes, removing them one by one and drying with a towel, leaving them to dry for five minutes, and then repeating. This provided information about rise time, settling time, sensor-to-sensor interaction, and sensor output range. Each sensor was labelled as sensor A through to D, and this labelling was used in all subsequent tests. The results can be seen in Figure 21 and Figure 22, a collection of graphics that show the bitstream recorded by the Arduino over time. The first shows all four sensors together over the full range, whilst the second shows each sensor individually and cuts out the rise and fall sections.

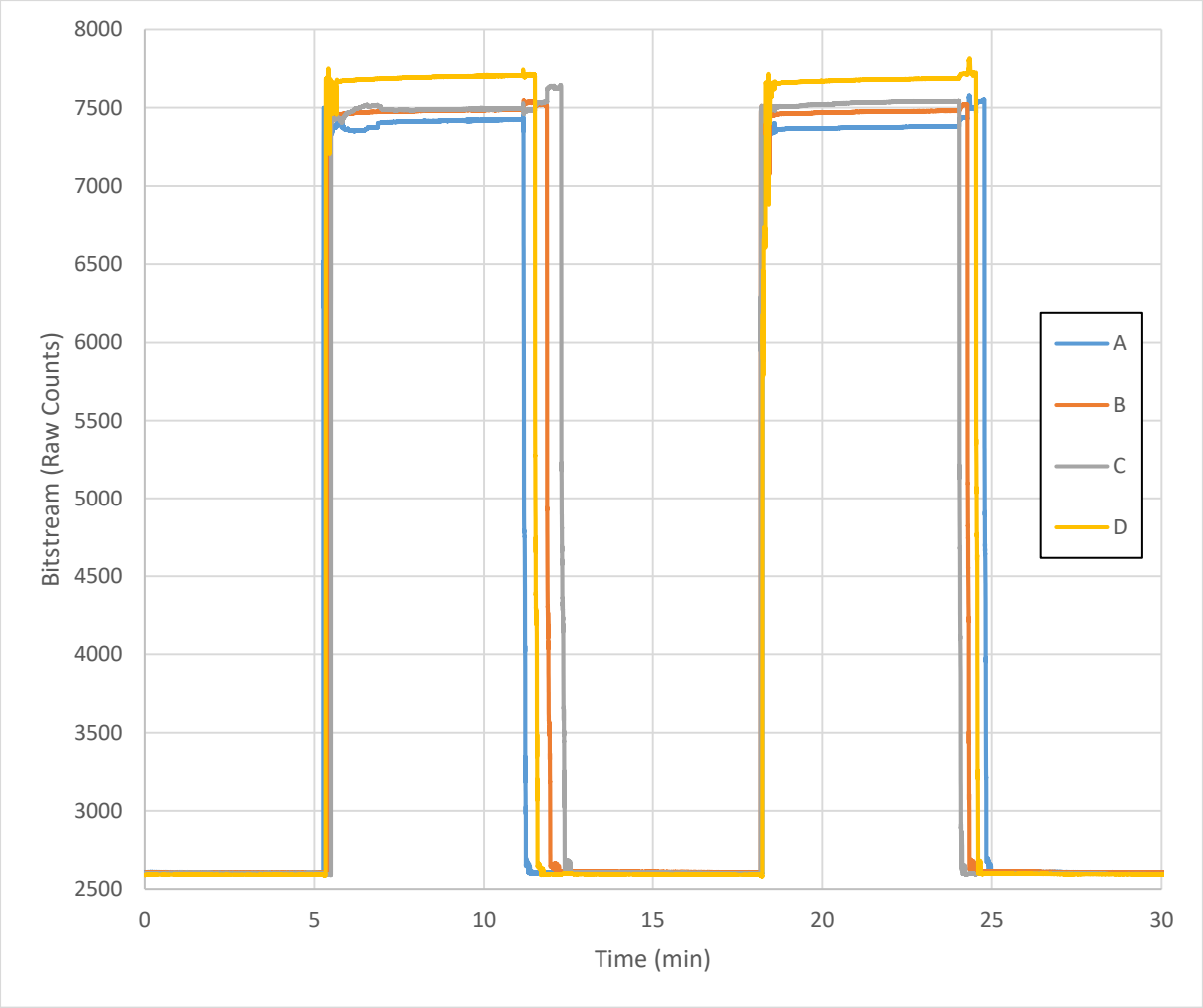

Figure 21: Sensor output over time for successive submerge-dry cycles

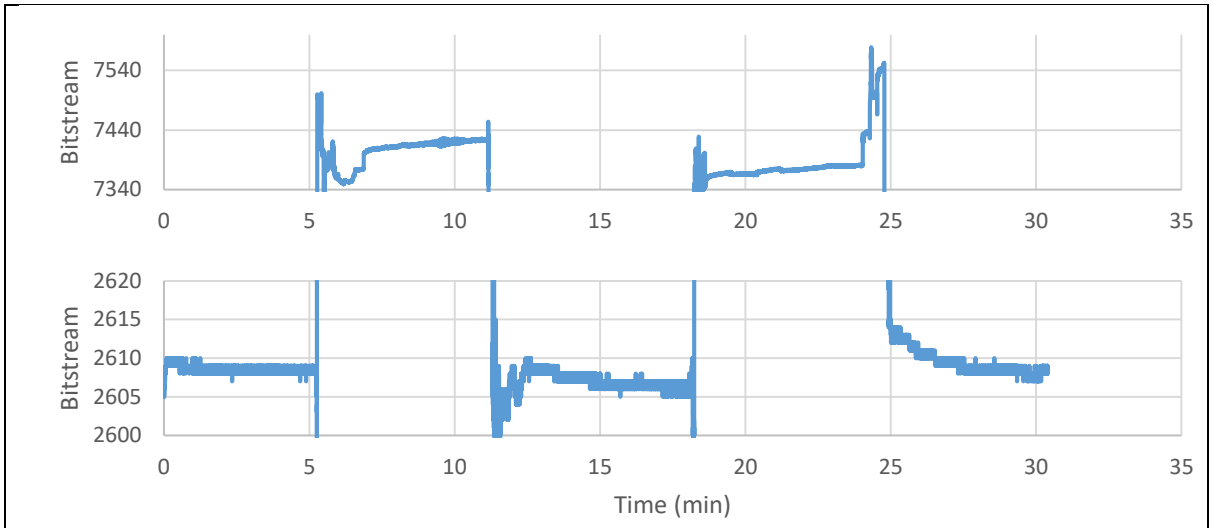
Bitstream
7540
7440
7340
0
5
10
15
20
25
30
35
Bitstream
2620
2615
2610
2605
2600
Time (min)

(a)

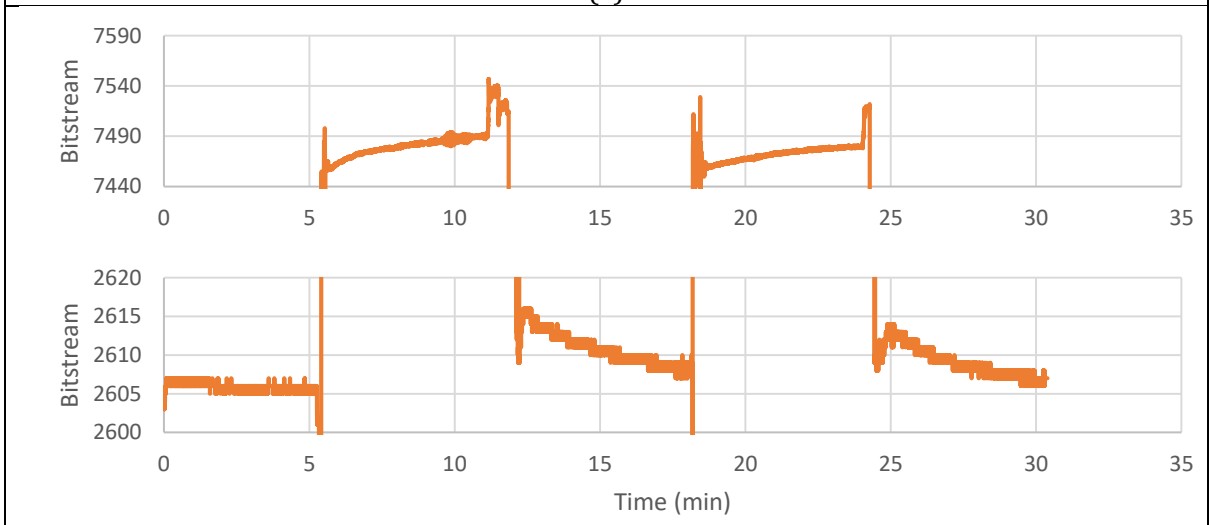
Bitstream
7590
7540
7490
7440
0
5
10
15
20
25
30
35
Bitstream
2620
2615
2610
2605
2600
Time (min)

(b)

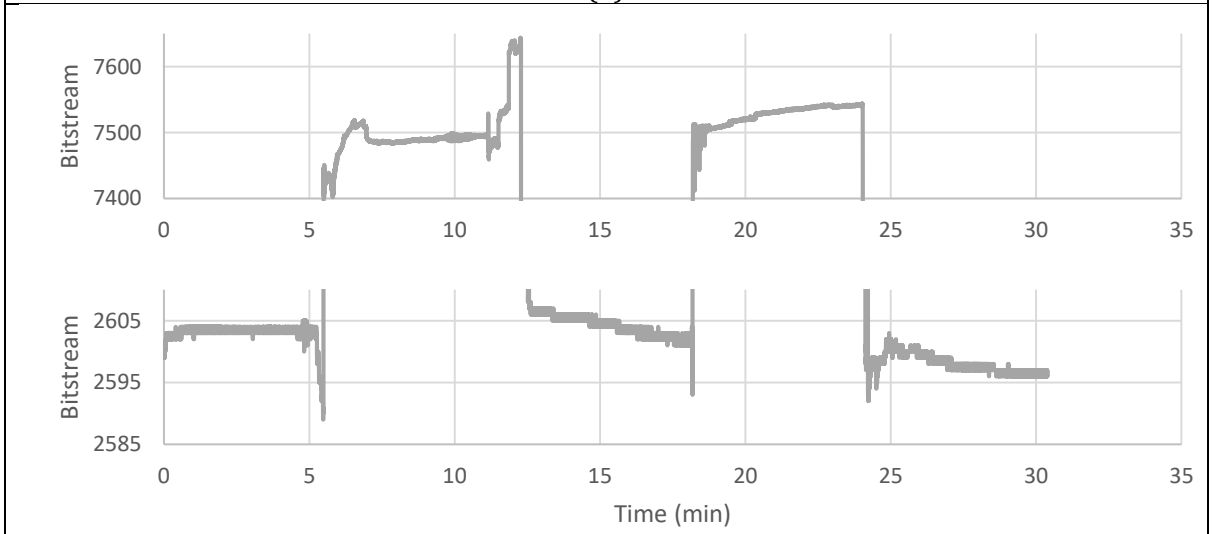
Bitstream
7600
7500
7400
0
5
10
15
20
25
30
35
Bitstream
2605
2595
2585
Time (min)

(c)

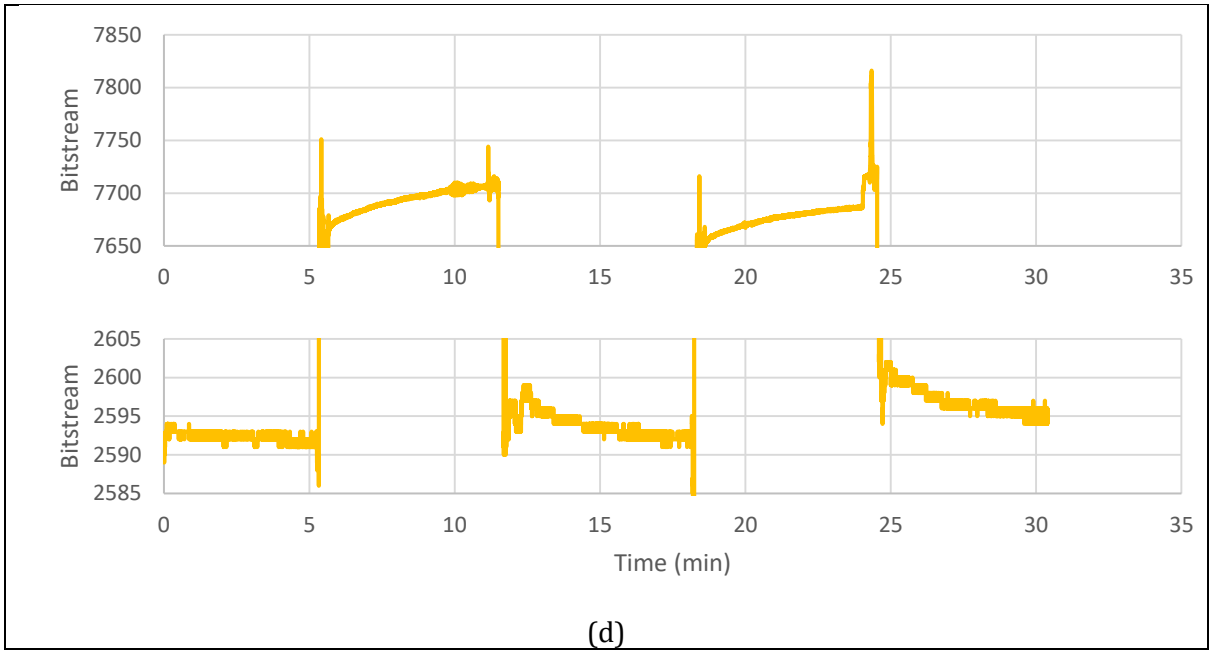

(d)

Figure 22: Sensor output over time over successive submerge-dry cycles zoomed on top and bottom values for sensors A, B, C and D in (a), (b), (c) and (d) respectively

The PHYTOS sensors were thus found to be consistent within individual tests. Figure 21 shows that the sensors are self-consistent in their maximum and minimum signals, with little to no variation or drift in signal after several submerging-drying cycles. Whilst long-term signal testing has not been conducted directly, the lack of noticeable variation over the 18 months that the 16-bit Arduino datalogger has been in use suggests that these PHYTOS sensors are stable over time when stored in lab conditions. Transient effects are visible in Figure 21, with the sensor signal gradually growing towards some steady-state equilibrium over the 5 minutes of submerge time, but this effect does not change between trials. A similar transient response can be seen after drying, though this is on a smaller scale. Of equal note is that the variation in maximum signal is larger than that of minimum signal, though it is unclear whether this is due to the sensor or due to the difference in dielectric material (water when covered, air when dry) in each circumstance. It may be simply proportional to signal level. This variation is characterised by approximately 30 bits (0.6% maximum signal range) for the submerged sensor and approximately 10 bits (0.2% maximum signal range) for the dry sensor. These transient responses are likely due to the dissolving of micro-scale air bubbles adhering to the surface of the sensor when submerged, or due to the evaporation of micro-scale droplets of water whilst drying respectively. They are not expected to affect measurements from these sensors significantly enough to introduce meaningful error.

Of more note than the transient response are the sudden changes in signal when the sensor is moved. It is unknown whether this is due solely to the movement of the sensor signal cable or whether it is due to crosstalk between adjacent cables. It is unlikely that it is due to magnetic field effects, but care should be taken to ensure that the sensor cables are as still as possible, especially relative to one another, when in use.

4.4.2 Testing the relative sensitivity of the front and back sides of the sensor

Another test was performed to determine the relative sensitivity of the front and back sides of the sensors. A sensor was placed face down on the surface of the water such that no water flows onto the back of the sensor. The sensor was then removed, dried, turned over and placed back onto the water. This was repeated for two more sensors. This test produced Figure 23.

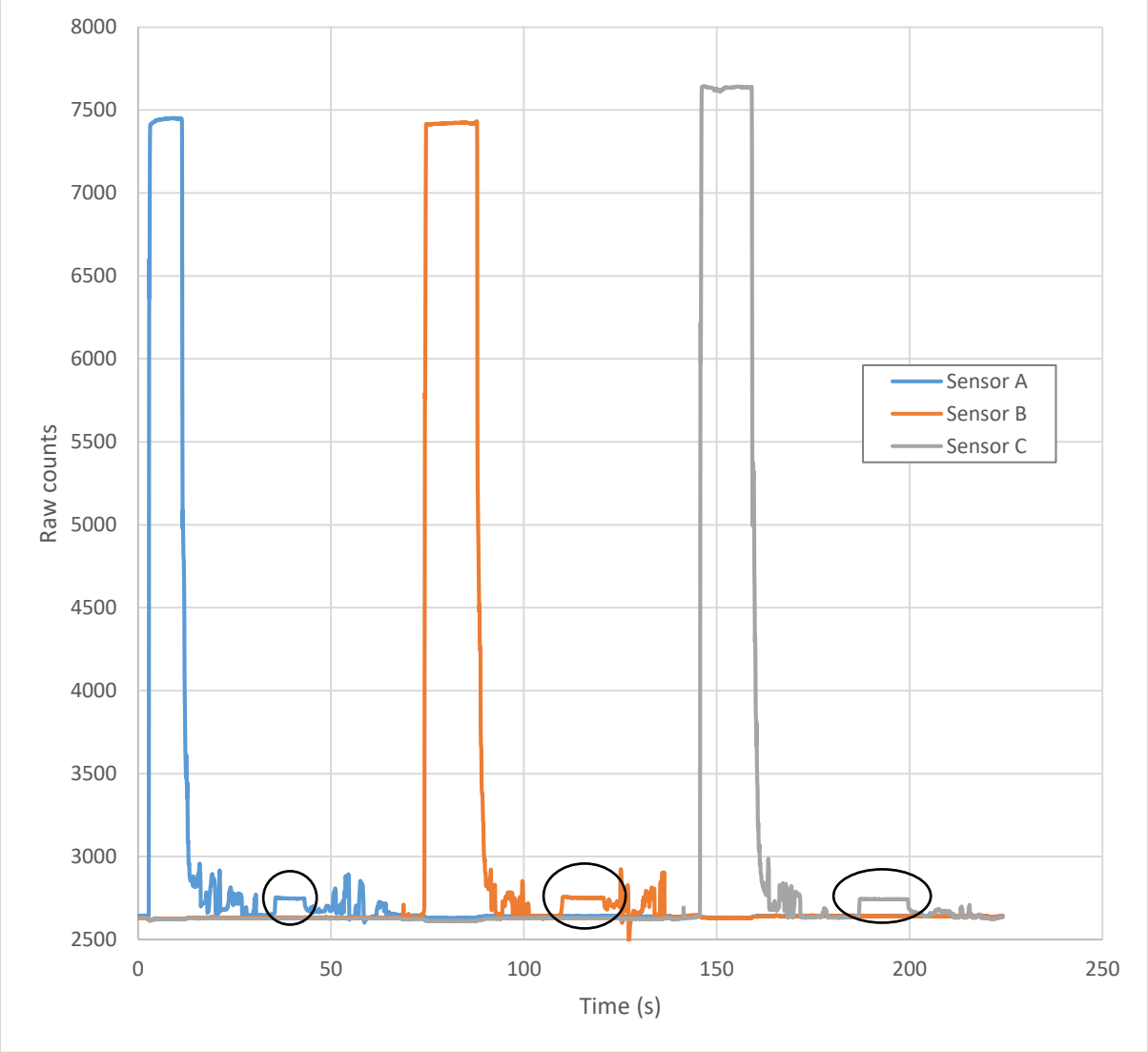

Figure 23: Sensor output over time for test in which first sensor front and then back is covered and dried. Circled sections indicate when the back was covered with water.

The periods of time in which the back side of the sensor was covered are highlighted with circles, and it can be clearly seen that the back side is much less sensitive. Specifically, the back side produces a maximum signal that is 2.3% to 2.6% as high as the signal produced by the front side. In most practical cases, this will produce a non-intrusive error, though in cases where the front of the sensor is kept dry and the back is covered (like in this experiment), care should be taken to ensure that results are not distorted. This level of sensitivity is unlikely to affect decisions based on the sensor signals.

4.4.3 Comparing the sensor signal for various methods of fully covering the sensor

There is also a difference in signal between a fully submerged sensor and a sensor with just one side fully covered. To show this, a test was carried out in which the sensor was brought to "full coverage" via different methods.

1. A barrier of tape was applied to the edge of the sensor to create a bowl-like structure and was subsequently filled with liquid.
2. Underwater facing upwards to the surface
3. Underwater facing downwards towards the metallic base of the bucket

4. Underwater facing sideways towards the wall of the bucket. In this configuration, the onboard signal processing circuitry was kept out of the water
5. Placed face-down in the water such that the entire sensitive side is covered, but the back is kept dry (as in the earlier test seen in Figure 23).

The sensor was removed and dried between each submerge, and the whole test was performed once with the Arduino data logger and once the LabView data logger. This produced Figure 24 and Table 3. The 5th configuration (fully wetted sensitive side, dry back side) was chosen as the reference state for 100% coverage, and all measurements were normalised against this.

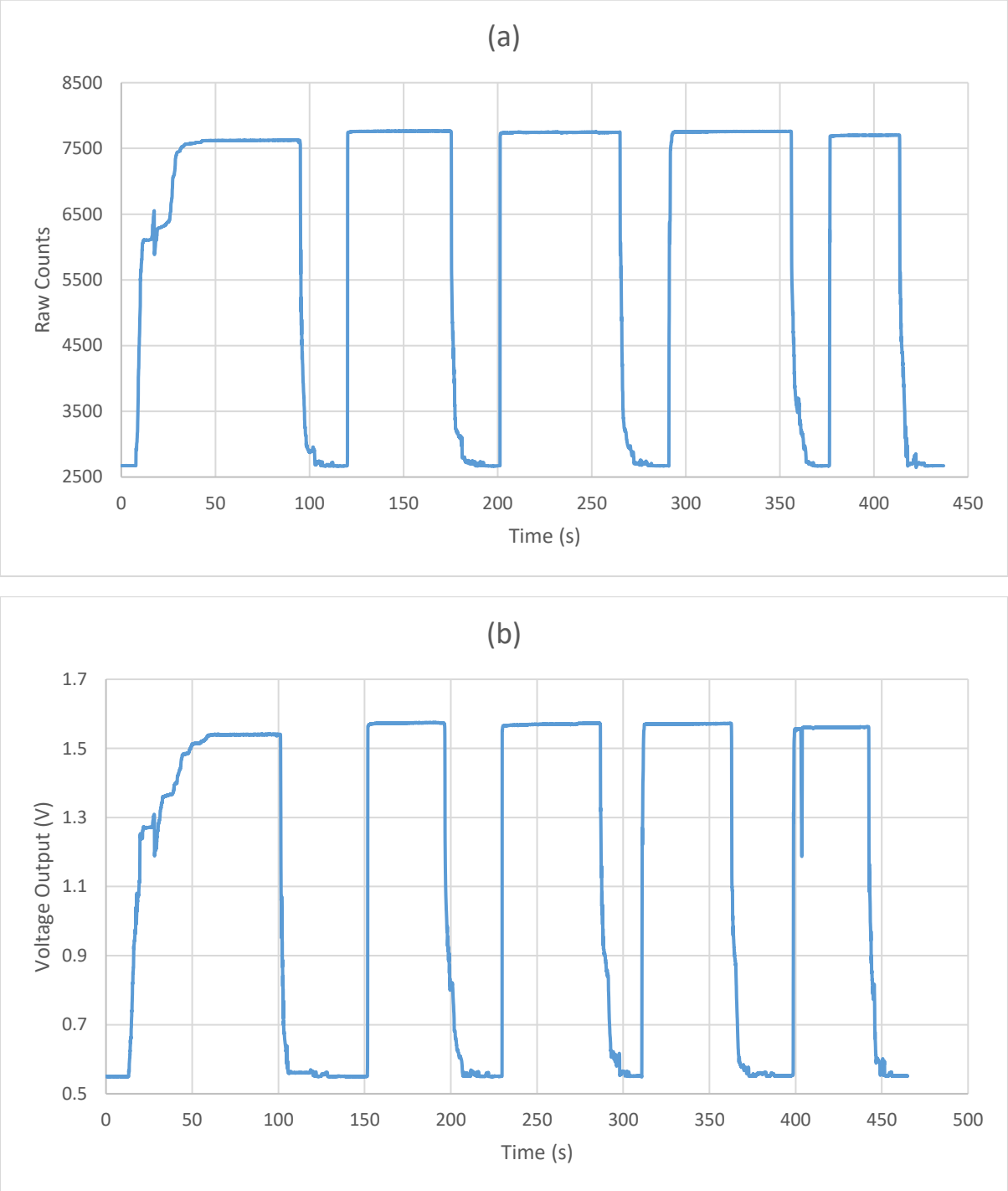

Figure 24: Sensor output over time as presented by (a) Arduino datalogger and (b) LabView datalogger for the sensitivity to full coverage test

Table 3: PHYTOS sensor output for a variety of different definitions of "fully covered". Also shown is the output normalised against case 5.

Peak	Description	Arduino		LabView	
		Mean	Normalised	Mean	Normalised
1	Covered with thin layer	7622	0.985	1.540	0.980
2	Submerged facing upwards	7761	1.012	1.574	1.013
3	Submerged facing downwards	7744	1.009	1.570	1.009
4	Submerged facing horizontally	7756	1.011	1.571	1.010
5	On surface facing downwards	7699	1.000	1.561	1.000

The effect of the thickness of the layer of water on the surface can be inferred to be relatively small by the differences shown in Table 3. The signal varies over a range of approximately 3% (from peak 1 to peak 2), with the smallest value occurring when the back of the sensor is not covered. This discrepancy may be explained in part by the back-side sensitivity of approximately 2.5%.

The effect of reducing the thickness further was investigated by gradually removing some of the liquid with a pipette until surface tension dictated that the lowest energy state of the liquid would be as beads of water and/or a small ring that lines the perimeter wall. This was done first with just water, and then again with a small amount of hand soap to act as a surfactant and allow the layer to become thinner again. Both the Arduino and the LabView dataloggers were used, once each. The results can be seen in Figure 25.

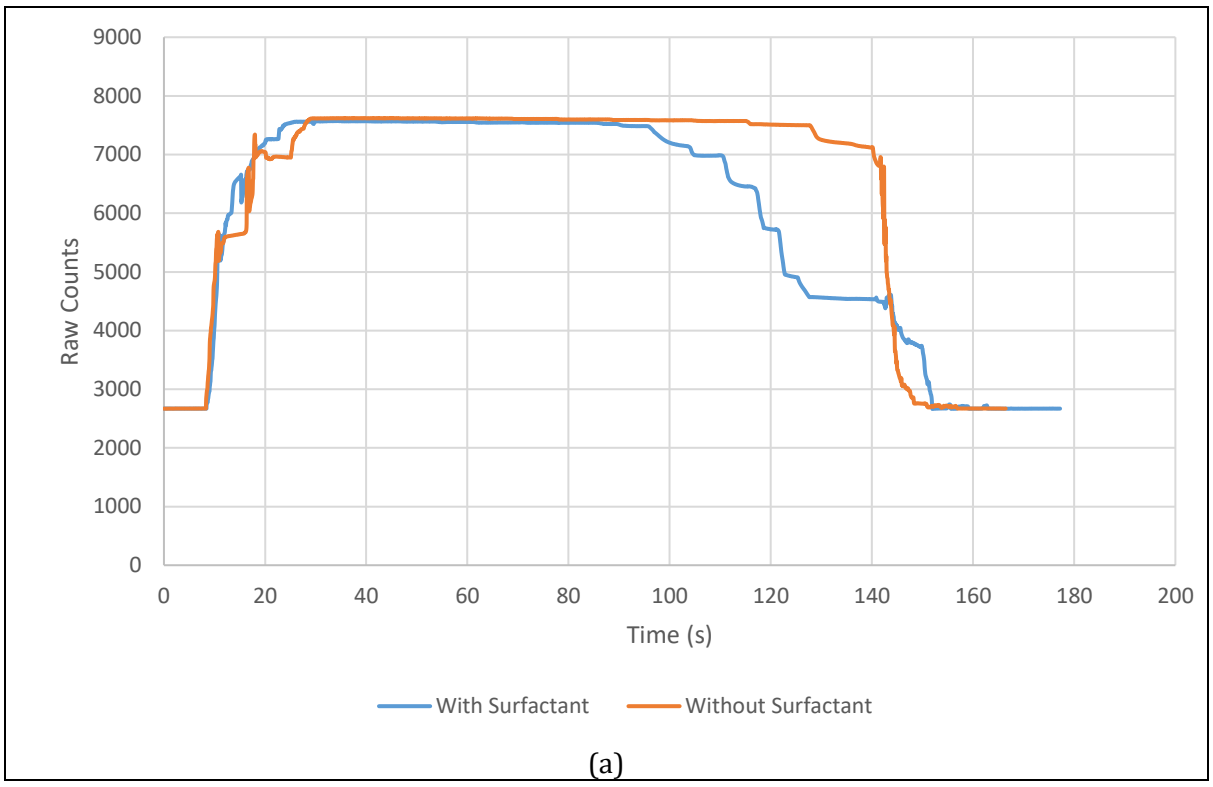

(a)

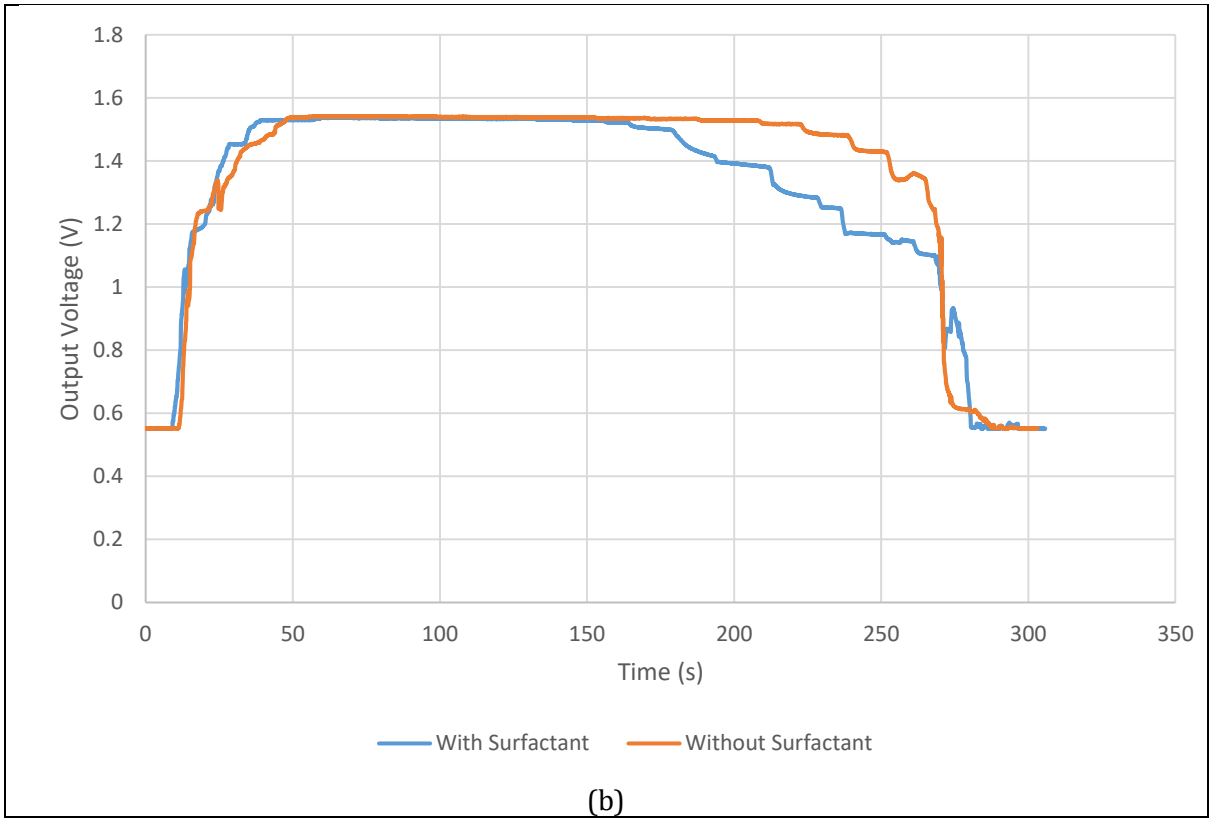

(b)

Figure 25: Sensor output for (a) Arduino datalogger and (b) LabView datalogger for test in which water was added and then removed from sensor surface with and without surfactant

It seems that adding surfactant does very little to the maximum value, though in both cases, the test without surfactant did have a slightly higher maximum (specifically, the Arduino test saw an average signal difference of 60 bits, or 0.47% of maximum signal range, and the LabView test saw an average signal difference of 0.012V, or 0.48% of maximum signal range).

An important discovery from this test is that the variation in readings in states which qualify as full coverage may be higher than the variation stated in Table 3. By covering the sensor in a layer of water (~1mm) and then gradually removing liquid from this layer, the sensor was able to be covered by a continuous layer of water of decreasing thickness. In the cases without surfactant, only a small amount of water could be removed before surface tension caused the remaining layer to bead up into smaller pools or droplets on the sensor, no longer covering the whole surface. This can be seen in Figure 25 as a series of small downwards steps before a large drop in signal indicates that the layer of water is no longer a continuous covering. However, when the surfactant is present, significantly more liquid can be removed before beading occurs, with the layer continually reducing its thickness until the layer looks more like a glossy coating than a layer of liquid. In this case, there is no sharp drop in signal (instead seeing a series of small steps downwards), implying that the sensor can be "fully covered" by a layer of soapy water of very small thickness (much smaller than the distance between conductive tracks under the surface) and produce a signal much smaller than the previous estimates (about 40%).

Most this investigation was carried out with the assumption that the maximum voltage output of roughly 1.54V or 7600 bits corresponded to a completely covered sensor, as the majority of the tests performed used water without surfactants which prevents the existence of these very thin layers. However, many agricultural sprays do use surfactants, and so further investigations may provide further insight into how the calibrations outlined below correspond to different chemical

mixtures. Further discussion about the possible impact of very thin layers can be found in section 4.5.1.

4.4.4 Effects of contaminants in water on sensor output range

Finally, the effect of adding certain contaminants into the water on the output signal was considered directly. The sensors were fully submerged in a series of solutions consisting of water and differing amount of red food colouring (Pillar Box Red, Queen Fine Foods, Brisbane, Australia). The results can be seen in Figure 26.

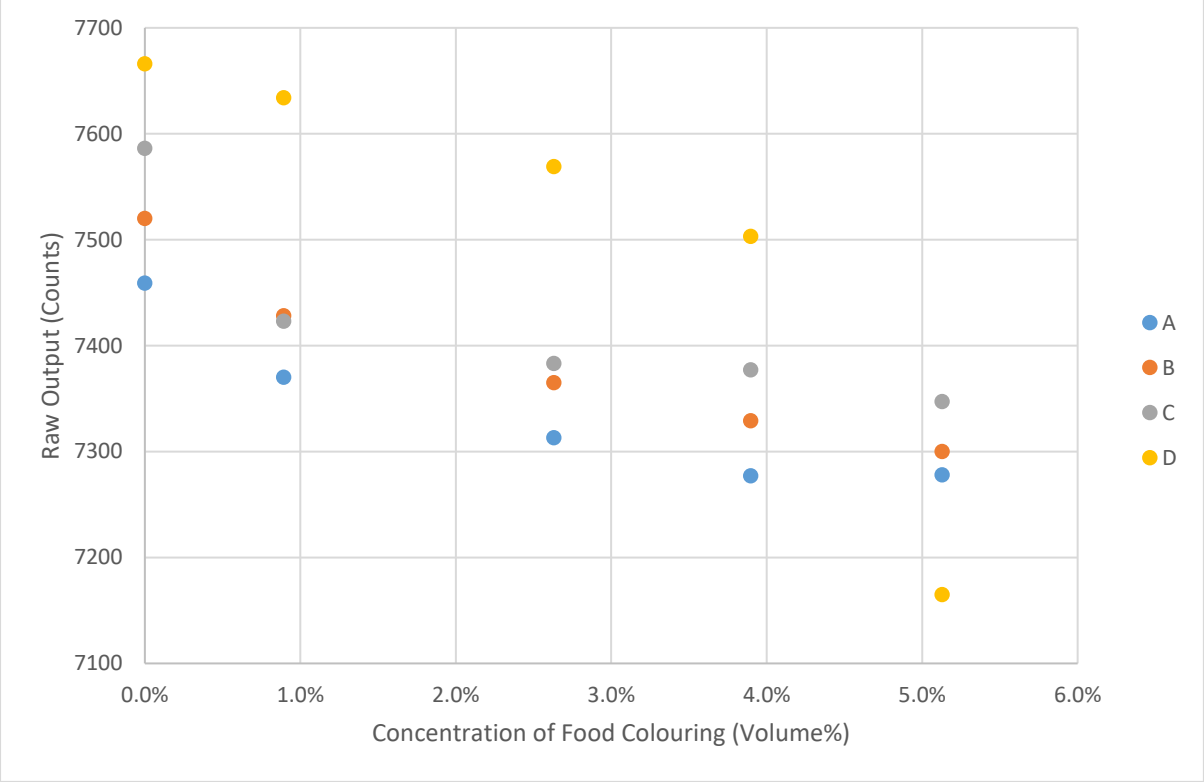

Figure 26: Maximum sensor output (A through D) with Arduino datalogger for increasing concentration of food colouring

All four sensors show a distinct downwards trend, with linear regression producing fits with R^2 of 0.8619, 0.9276, 0.7173, and 0.7811 for sensors A, B, C and D respectively. However, the actual maximum value only deviated by roughly 200 counts (except for D which had an outlier producing a deviation of 500 counts) out of a total range of roughly 5000 counts, meaning that contaminants are unlikely to produce error that is significant.

A similar experiment was performed with copper sulphate solution and the LabView datalogger, though only one sensor was tested. The resulting graph can be seen in Figure 27. Vertical error bars indicate the range of values over the measurement interval and horizontal error bars are determined by the smallest scale degree.

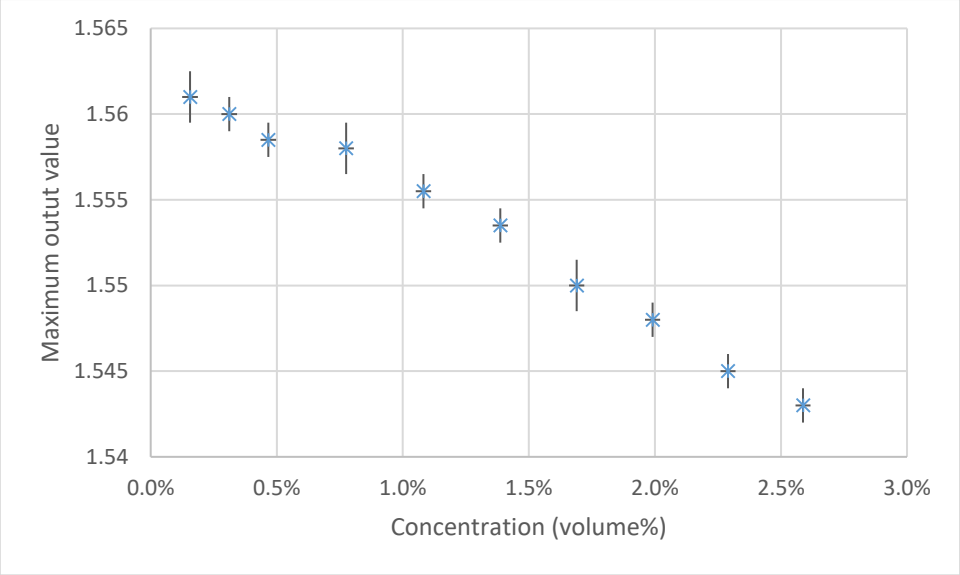

Figure 27: Maximum sensor output with LabView datalogger for increasing concentration of copper sulphate

These results are expected when the effect of altering the dielectric constant is considered. Contaminants tend to reduce the dielectric constant of an aqueous solution (Lyashchenko, Loginova, Lileev, Ivanova, & Efimenko, 2009) (Mohsen-Nia & Amiri, 2013), likely due to the contaminants affecting the orientation of the water molecules to arrange their dipoles to reduce electric field strength. This is true for both the copper sulphate solution (used as a fungicide), and the surfactant (used not as a pesticide directly, but rather to aid in spray coverage), but the difference was on such a small scale over reasonable concentrations that this effect is unlikely to affect the usefulness of the sensors over a range of different applications.

4.5 Calibration for Areal Coverage

The similarities between the signals of a sensor covered with a thin layer of water on one side and a sensor fully submerged in water suggests that the total mass of liquid on the sensor is not the primary variable being measured. Early experiments in which a fixed volume of water was deposited on the sensor first as a series of small droplets and then as a single, large drop showed that sensor output (which was significantly larger in the first case than in the second case) was not directly proportional to the amount of mass on the surface, strengthening this hypothesis. It was thus judged that a more worthwhile metric to measure would be the areal coverage. A series of experiments were carried out to generate calibration curves that would convert sensor output to areal coverage.

As previously mentioned, a few different dataloggers were used throughout this experiment, and as such there were several calibration curves generated over the course of these experiments. Throughout this next section the following calibration curves will be presented (with each test specification being referred to by these numbers):

1. Arduino datalogger with onboard ADC unit; liquid applied with pipette (equations 25 and 26; Figure 32)
2. Arduino datalogger with dedicated ADC unit; liquid applied with pipette (equation 29; Figure 35)
3. LabView datalogger; liquid applied with pipette (equation 30; Figure 37)
4. LabView datalogger; liquid applied with hand-pumped spray bottle (equation 31; Figure 38)

These experiments were all based on the same principle: a certain amount of stationary liquid on the sensor surface will cover a fixed proportion of the sensor area, and will produce a stable, constant signal. To this effect, the sensor was attached to the datalogger with a camera (Logitech, Lausanne, Switzerland) positioned directly above it. In most tests, a thin strip of waterproof tape was placed around the edge of the sensor to prevent run-off. A series of water droplets coloured with red food colouring were deposited onto the sensor surface by a pipette with small pauses in between. After each drop was deposited, a picture was taken at a resolution of 1280×720 pixels. The sensors went from completely dry to completely covered (with the water prevented from run-off by a wall of tape placed around the perimeter of the sensor) in the test. After some post-processing (outlined below), the two sets of data – one a datastream of sensor output and the other an album of photographs – were compared to each other in order to establish a link between the sensor output and the true areal coverage. A few example images of the sensors in these calibration tests is seen below in Figure 28, and an example of sensor output data can be seen in Figure 29.

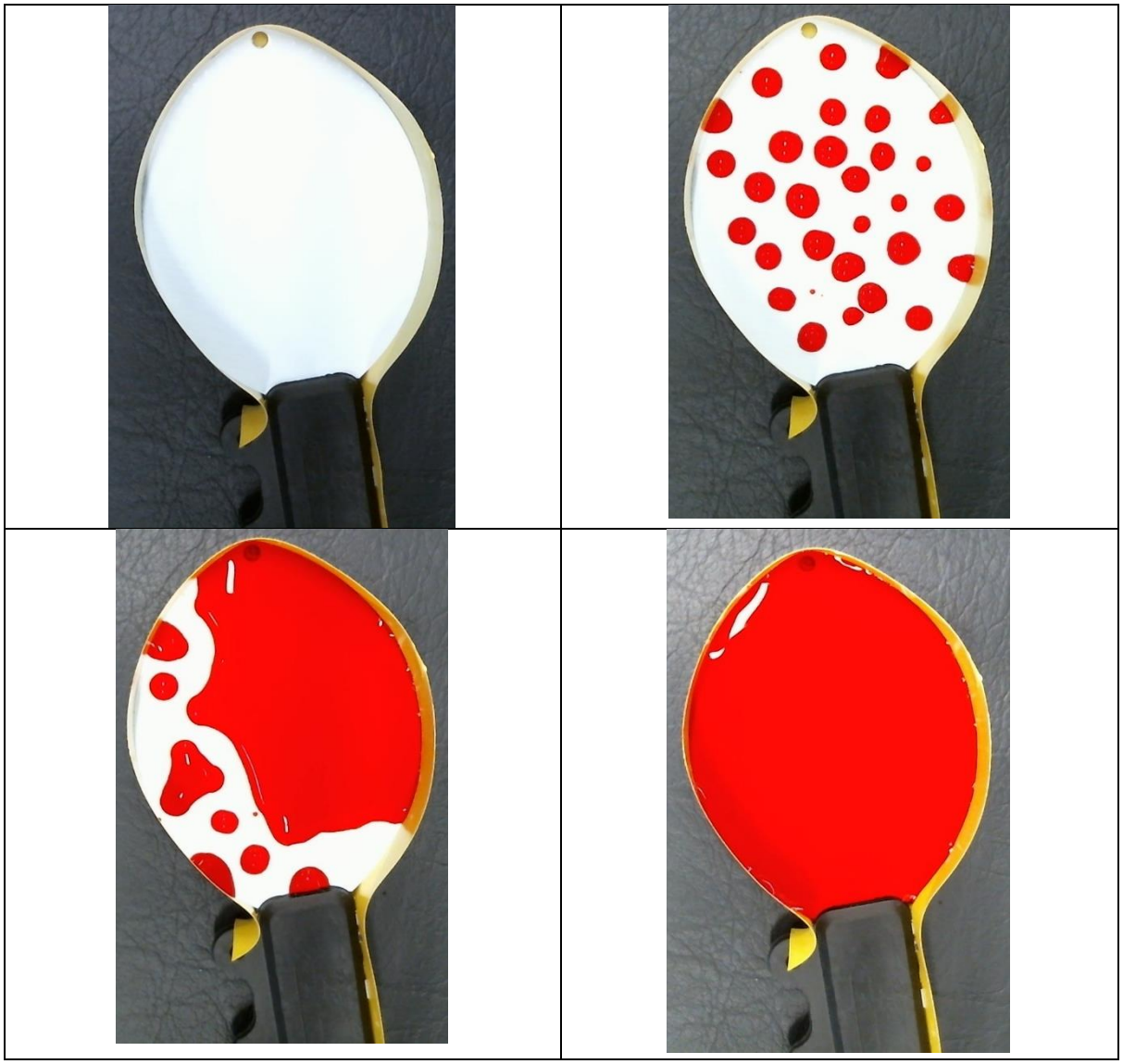

Figure 28: Example photographs taken of sensor during calibration. Notice the yellow tape barrier preventing runoff in latter cases, as well as reflection from lights

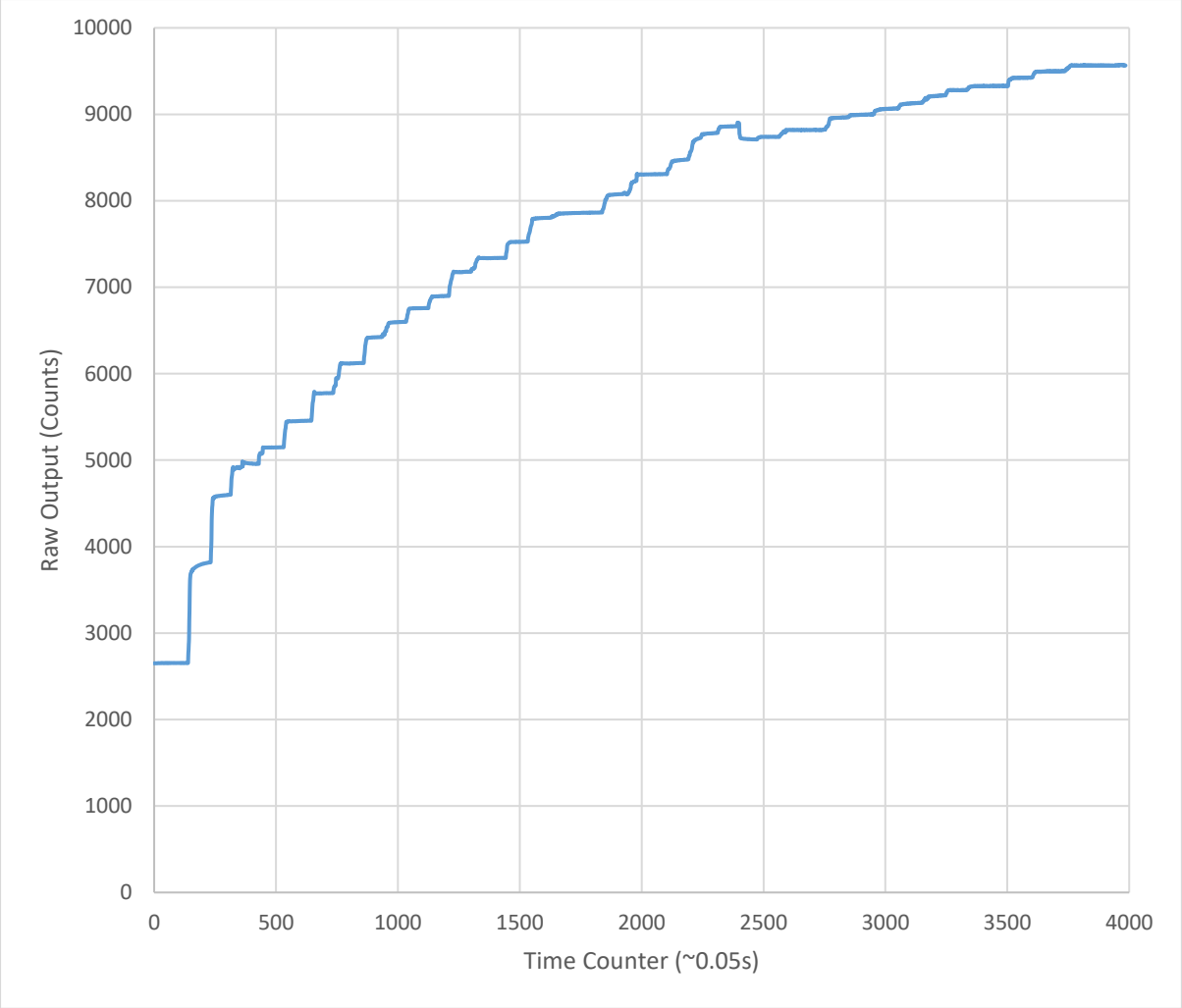

Figure 29: Example of raw sensor output during calibration as recorded by the Arduino datalogger

The sensor output was non-dimensionalised based on the minimum and maximum outputs of the sensor. Each data point then became a percentage of the total range of outputs. This had the advantage of making the results of each datalogger comparable to one another. The following equation (21) (a form of linear interpolation) was used:

$$Proportion\ of\ Sensor\ Output = \frac{Raw\ Output - Dry\ Output}{Maximum\ Possible\ Output - Dry\ Output} \quad 21$$

After this conversion took place, the graph in Figure 29 was converted to a series of points approximately in line with each of the "steps" in the staircase structure. The results of this can be seen in Figure 30, with the grey points corresponding to the coverage values generated from the photographs (outlined below).

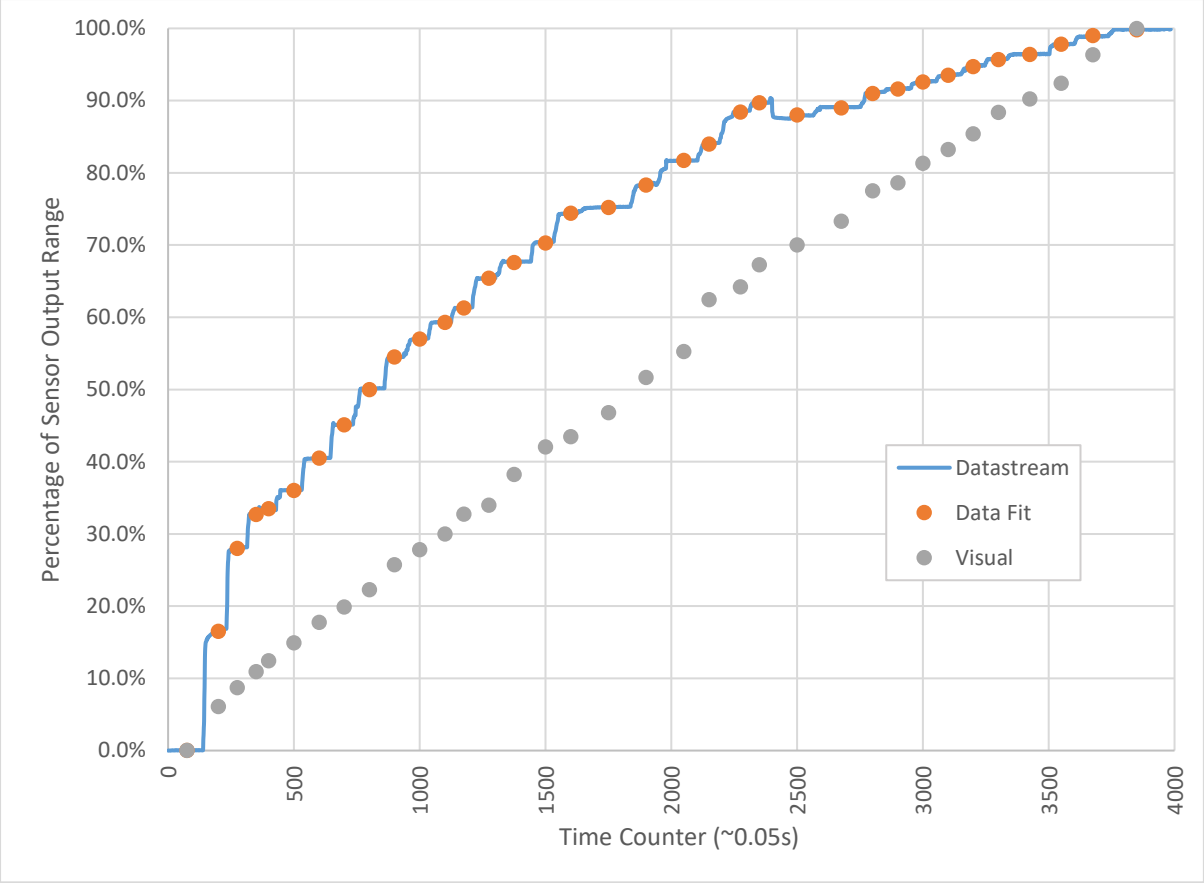

Figure 30: Example of datapoints (orange) fitted to raw sensor output (blue) compared to equivalent datapoints from the photographs (grey)

The photographs were processed using MATLAB (Mathworks, Natick, Massachusetts, USA) and its image processing toolbox. The specific MATLAB script used can be found in appendix 9.1. The script performed the following operations:

- Load the relevant image
- Separate the red, green and blue components
- Create an altered greyscale image by subtracting the magnitude of the green and blue components from the magnitude of the red components. The RGB components are 8-bit unsigned integers, so if the green and blue components combined are greater than or equal to the red component the subtraction will cause that pixel to overflow into the negatives and be set to 0. This means that any pixel which is does not have more red than blue and green combined will be completely black, with the rest of the pixels being varying shades of white-grey. This has the effect of "turning off" any white, black or grey pixels whilst leaving the red pixels "on".
- Binarise the image based on a threshold chosen such that red drops were now white, and the rest of the image was black. This threshold was usually arbitrarily low because the previous step caused all non-red pixels to be set at 0 already.
- Fill in any holes that were caused by white reflections in the drops using MATLAB's *imfill* command.
- Take the sum of the entire matrix describing the image. Because the image is binarised, every white pixel has the value 1 and every black pixel has the value 0, which means that this operation is equivalent to counting all the white pixels, which should closely correspond to the red pixels.

- The final image in each set is usually a completely covered sensor, so this summing operation will give the number of pixels in the whole sensor.
- The results were all saved to a CSV file.

The results were then compared to the largest value and converted to a percentage of that using the same equation as before but without the linear offset.

$$Percentage\ Areal\ Coverage = \frac{Number\ of\ Red\ Pixels}{Number\ of\ Pixels\ in\ Whole\ Sensor} \quad 22$$

These methods produced a dataset featuring pairs of percentage values; one that shows the proportion of the sensor output range and one that shows the percentage of the sensor area that is covered. These were graphed in a scatterplot such that the relationship between them could be visualised. If they were to line up in a straight line from (0,0) to (1,1), then there would be no calibration required, but unfortunately this was not the relationship.

The first round of tests (calibration 1) was performed on a single sensor with a variety of different test schemes involving different drop distributions. Three of the tests featured an even distribution of drops over the sensor, one test featured drops only around the edge of the sensor, and the final test featured a single, large drop growing gradually in the middle of the sensor. The results from this can be seen in Figure 31.

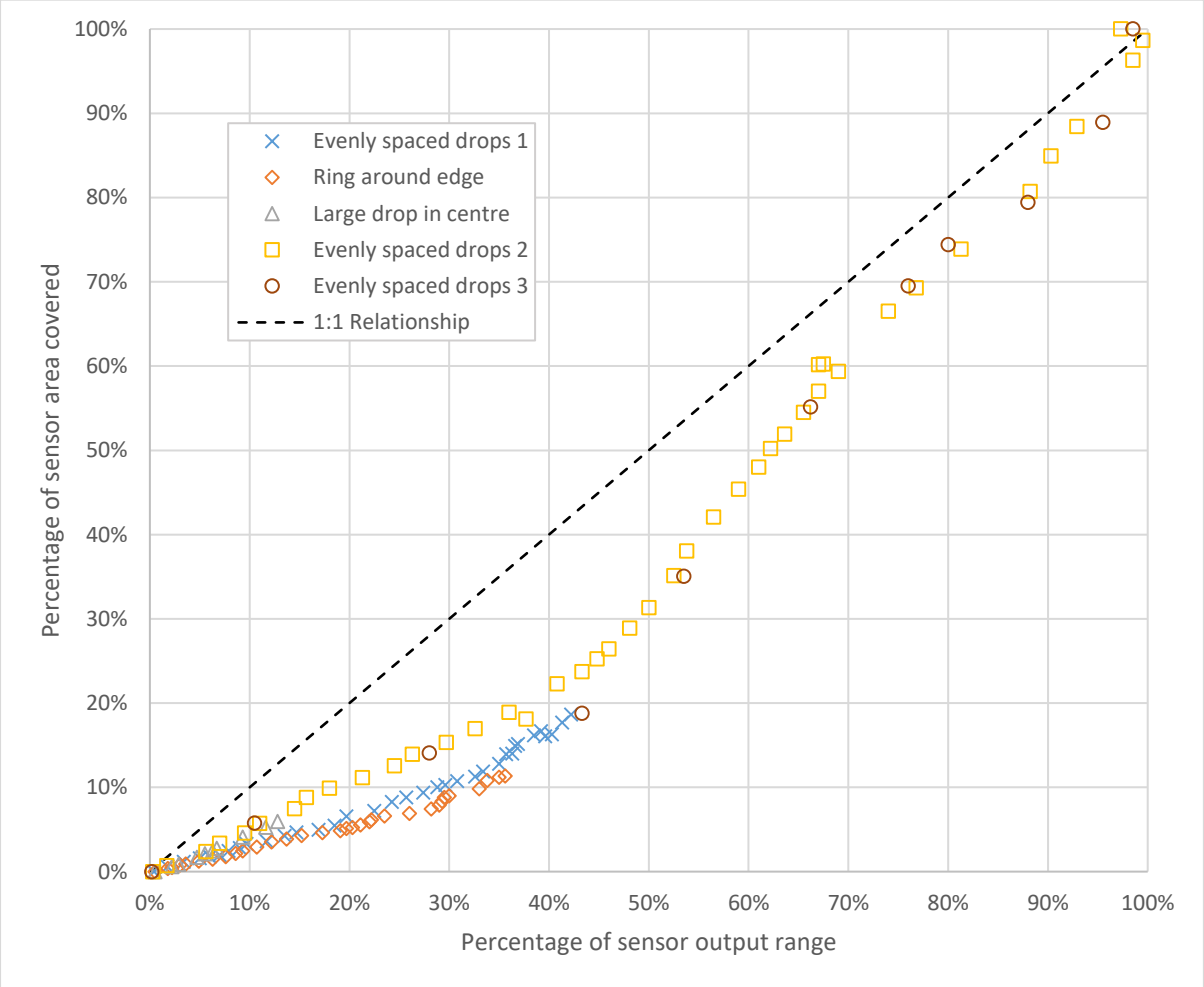

Figure 31: Compilation of all data points gathered in calibration 1(Arduino 10-bit datalogger) compared to a 1:1 relationship

The different droplet placement patterns produce very similar data, but they are not identical. Is The two tests featuring 100% coverage values produced sensor output values significantly lower for a given areal coverage than the other tests, even the other test with evenly spaced droplets. This discrepancy may be a result of the non-dimensionalisation (equations 21 and 22), as the "maximum sensor output" and "number of pixels in whole sensor" were not directly measured. This is discussed further below. The other two placement patterns produced slightly different results, with the large drop in the centre producing lower signals for a given areal coverage and the ring of droplets around the edge produced higher signals. This variation is likely to due to droplet thickness, which is discussed in section 4.5.1

Two fits were proposed: a bi-linear fit that had a shallow gradient for low inputs and a sharp knee leading to a steep gradient, and a quadratic fit. When accounting for the fact that the calibration must, by definition, go through the origin and (1,1), two forms of equation were produced:

$$y = \begin{cases} \dfrac{y_0}{x_0}x & 0 < x < x_0 \\ \dfrac{1-y_0}{1-x_0}x + \dfrac{y_0 - x_0}{1-x_0} & x_0 < x < 1 \end{cases} \quad \text{for some } x_0, y_0 \in (0,1)^2 \qquad 23$$

$$y = ax^2 + (1-a)x \quad \text{for some } -1 < a < 1 \qquad 24$$

Both of those equation formats satisfy the requirements and produce appropriate calibration curves. MATLAB was used to find the optimal value for the variable(s) that minimised the R^2 value for the fit. In the former case, (x_0, y_0) was optimised to (0.352, 0.124) with an R^2 of 0.9926, and in the latter case, a was optimised to 0.799 with an R^2 of 0.9848. The bi-linear option was chosen as the preferred fit because most coverage values when using these sensors for other tests were found in the early 35 - 50% (because liquid would coalesce into droplets and run off the sensor, limiting the total amount of liquid present), which just requires a linear scaling to be applied, and so error bounds were applied to the linear case only. These were of the same form but with different y_0 values, specifically 0.08 and 0.20. The bi-linear calibration fit (hereinafter referred to as calibration 1; equation 25) are shown below in Figure 32, with the error bounds (such that 98.5% of points are below the upper bound and 87% of points are above the lower bound) given in equation 26 and Figure 33.

$$y = \begin{cases} 0.35x & 0 < x < 0.352 \\ 1.35x - 0.35 & 0.352 < x < 1 \end{cases} \qquad 25$$

$$y = \begin{cases} \dfrac{0.28 \pm a}{0.704}x & 0 \le x \le 0.325 \\ \dfrac{1.72 \mp a}{1.296}x - \dfrac{0.424 \mp a}{1.296} & 0.325 < x \le 1 \end{cases} \quad \text{for some } a \in [0, 0.12] \qquad 26$$

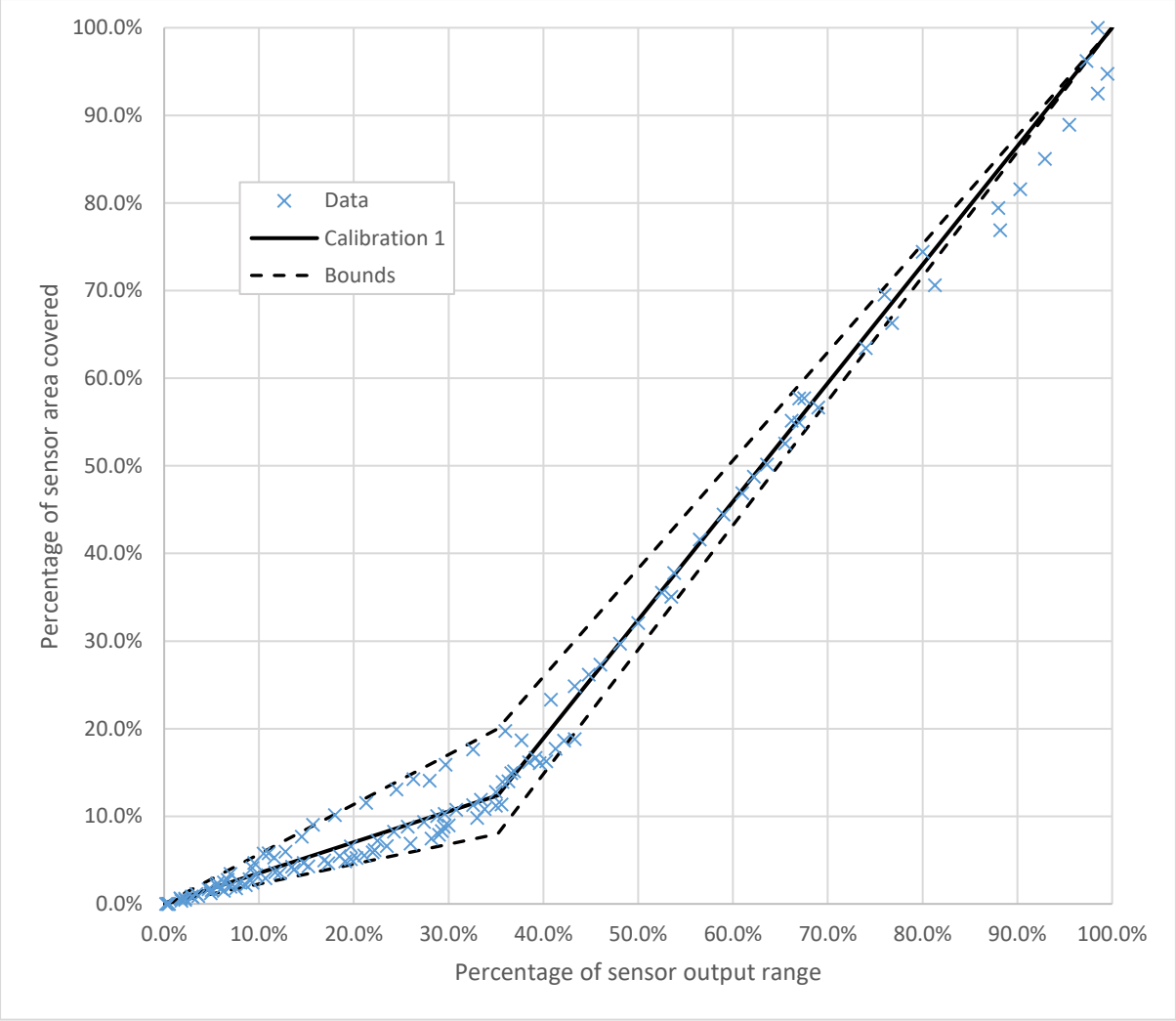

Figure 32: Compilation of all data points from calibration 1 (Arduino 10-bit datalogger) with a bi-linear fit and error functions

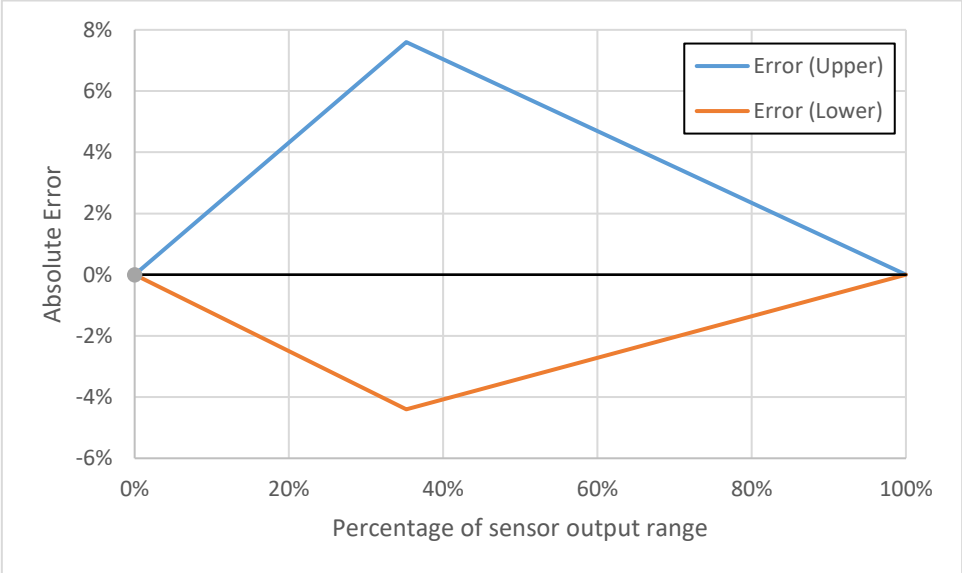

Figure 33: Error functions for calibration 1

The second set of calibration tests (calibration 2) were initially intended as a verification of calibration 1, but unexpectedly diverged significantly from the initial results. Calibration 2 featured the same droplet deposition method (though the tests were performed several months apart, so it is possible there is an unknown difference) and Arduino datalogger, but also the addition of a dedicated ADC unit, which is hypothesised to be the cause of a difference. Initially, a new pair of (x_0, y_0) points were selected to better fit the new data, specifically (0.713, 0.304), producing an R^2 of 0.9842. The compilation of data from calibration 1 and 2 can be seen in Figure 34.

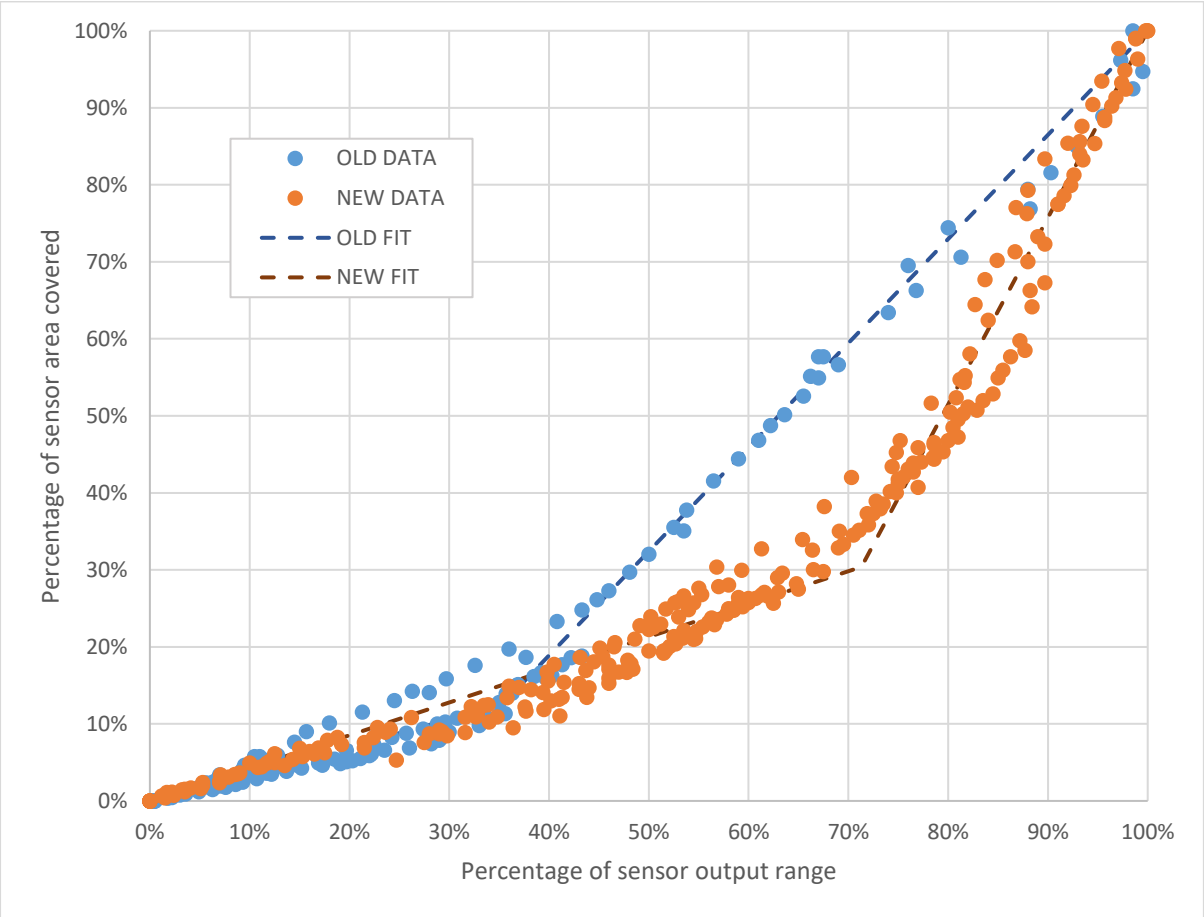

Figure 34: Comparison between calibration 1 (Arduino 10-bit) and calibration 2 (Arduino 16-bit) with associated bi-linear fits

It seems that the data from calibration 1 that did *not* feature a 100% coverage data point lines up reasonably well with the new data, whilst the other data does not.

It was noted that the new calibration curve does not fit the bi-linear shape as well as it previously did. Around the 30 – 40% mark, the calibration consistently overestimates the actual coverage value, and around the 70% mark it consistently underestimates. A quadratic fit was no longer suitable either, because the curvature changes significantly from start to end. A power fit was proposed, but these tended to either fit well at the start or at the end, never both. Eventually, it was suggested that a weighted sum of a linear function and a power function would suit. This would be of the following form:

$$y = a(bx + c) + d(x^f)$$

Multiplying the first bracket through by a and defining $a_1 = a \cdot b$ and $c_1 = a \cdot c$

$$y = a_1 x + c_1 + dx^f$$

Set y(0) = 0 and y(1) = 1

$$0 = a_1(0) + c_1 + d(0)^f = c_1$$

$$1 = a_1(1) + d(1)^f = a_1 + d \therefore d = 1 - a_1$$

Bringing the equation to the form

$$y = ax + (1 - a)x^b \qquad 27$$

Further restrictions were placed on these values such that the calibration function is one-to-one and restricted to (x,y) ϵ ((0,1),(0,1)). This was done by setting the derivative of the function to be strictly positive for all x on the relevant interval. It was observed that any negative value of b produced a discontinuity at x = 0, so these were discarded. It was then observed that for the function to be concave up (required to fit the data) and for the restriction on the domain and range to be satisfied, only values of a between 0 and 1, and values of b greater than 1 were suitable.

MATLAB was used to find the optimised combination of (a,b) which was (0.333,4.44), but it was deemed unsuitable at low values of x as the equation behaves like a linear function with gradient a at these values and 0.333 underestimates the data here. Thus, a modified equation was developed with (0.4, 5.2). This has an R^2 of 0.984 and is shown in equation 28.

Error functions were added to encompass the majority of the points, chosen by visually inspecting (a,b) pairs that best suited this. The function including error is equation 29, with the error given in terms of some variable m. When m is at the maximum value of 0.1, 86.5% of all points lie between the two error functions. The 13.5% outside these limits lies mostly in the 80% to 100% sensor output range, which are rarely reached in real tests. Thus, the equation should be read as "86% of data points are estimated to be predicted by this equation for some value of m on this interval". Or phrased alternatively: using the maximum value of m will provide you with two functions, the upper and lower bounds.

y refers to the percentage of the sensor surface that is covered, and x refers to the percentage of the total output range of the sensor.

$$y = 0.4x + 0.6x^{5.2} \qquad 28$$

$$y = (0.4 \pm m)x + (0.6 \mp m)x^{5.2 \mp 7m} \qquad \text{for some m } \epsilon\ [0, 0.1] \qquad 29$$

Figure 35 shows the compilation of all the new data along with the calibration function and error bounds. Figure 36 shows the error functions without the calibration curve or data points.

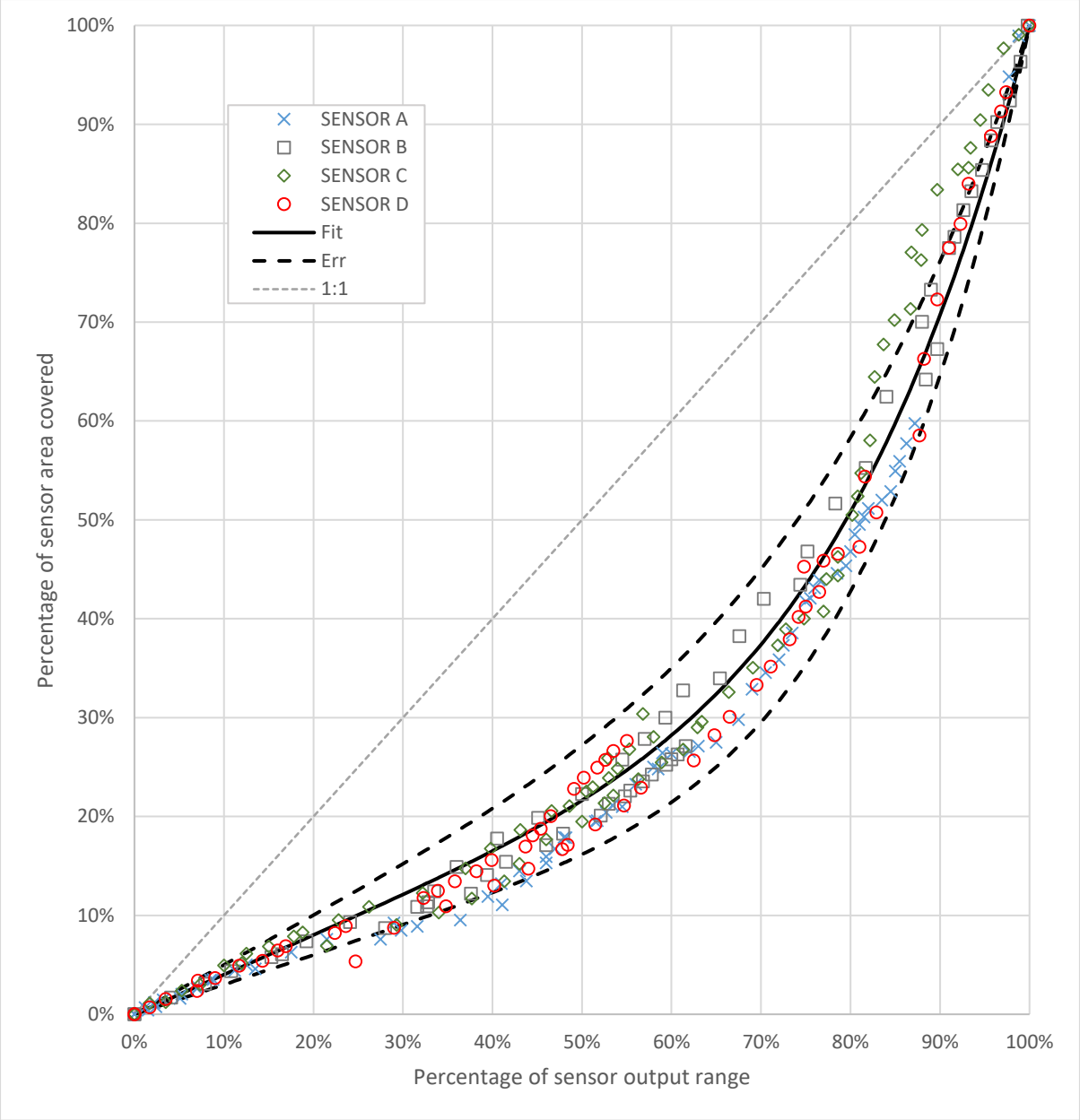

Figure 35: Data from calibration 2 alongside chosen calibration function, error functions, and a 1:1 linear relationship

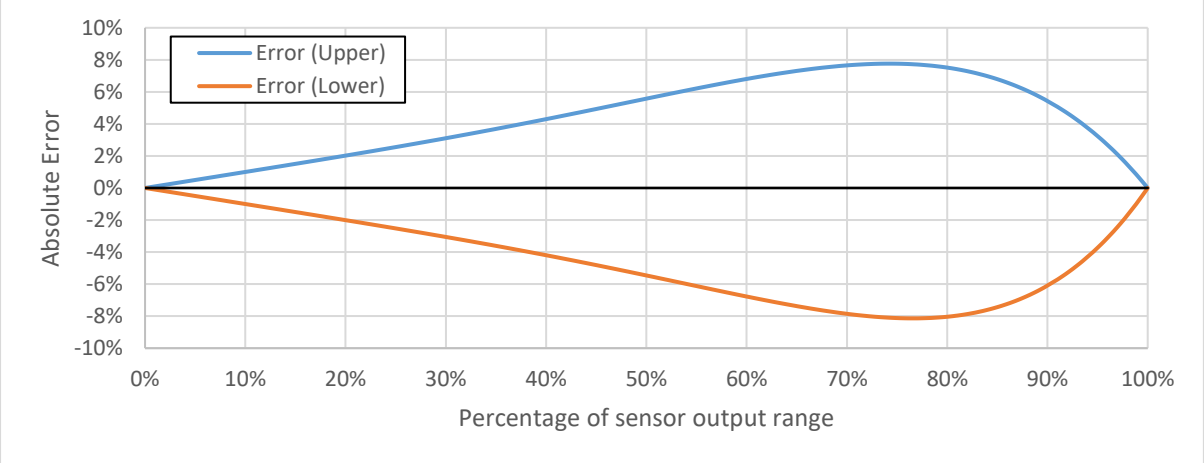

Figure 36: Error functions for calibration 2

The differences between the calibration 1 and 2 produced concerns that the LabView datalogger would produce a third, different calibration curve. Calibration 3 contains the data gathered from a series of tests almost identical to calibrations 1 and 2, but with the LabView datalogger. The results were largely similar to calibration 2, with minor differences for values between 50% and 100%. Figure 37 below shows the compilation of all data and calibration functions for calibrations 1, 2 and 3.

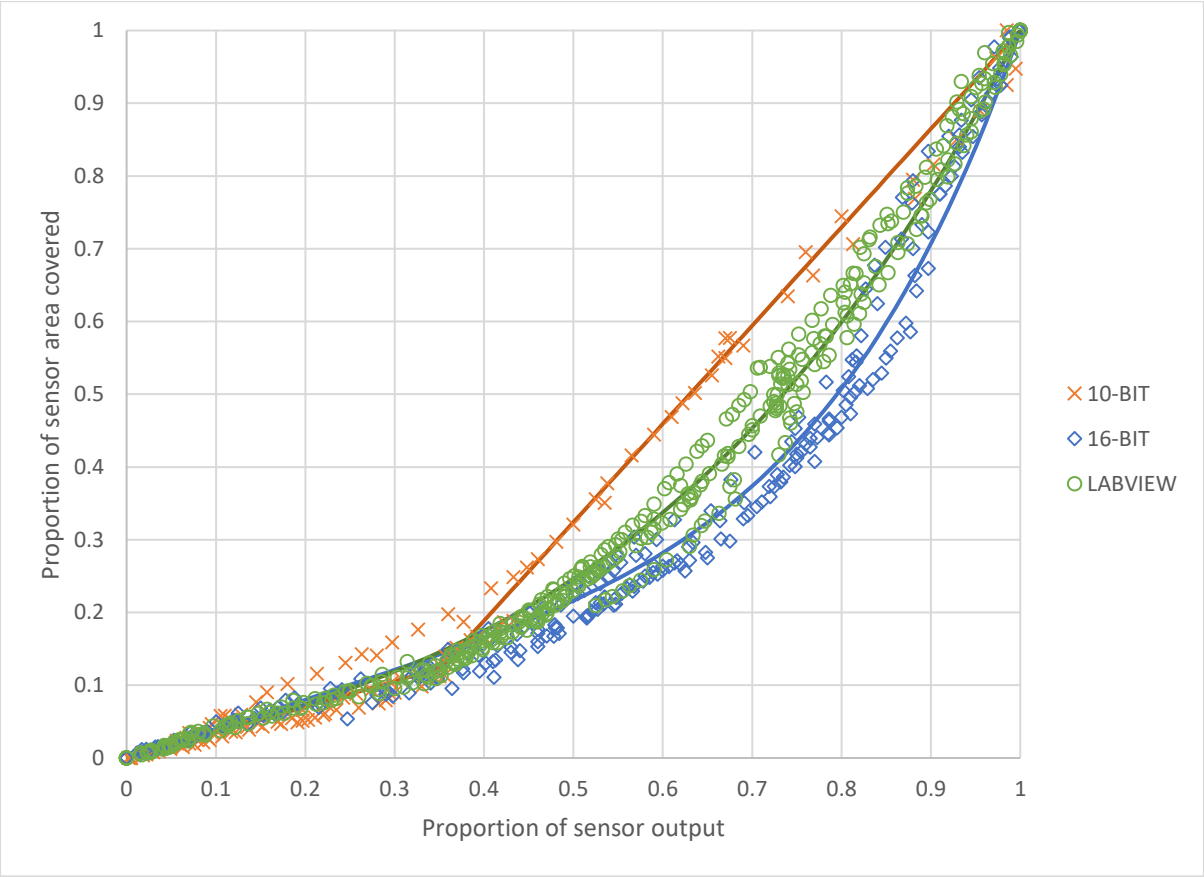

Figure 37: Data and associated calibration functions for calibration 1 (orange) calibration 2 (blue) and calibration 3 (green)

Calibration 3 produced the following calibration function:

$$y = 0.35x + 0.65x^{3.2} \qquad 30$$

Bounds of uncertainty were not calculated as no further experiments in this project featured coverage values exceeding 65% (with the majority of data being less than this) and so calibration 2 with associated error bounds was deemed suitable for all applications involving large droplets.

The final calibration (calibration 4) was carried out to better imitate a real spray. Previous tests performed using a pipette and large drops provided the highest possible resolution for the visual measurement, but in real spraying operations the drops will usually be significantly smaller. In calibration 4, the pipette was abandoned in favour of a hand-pumped spray bottle, though all other aspects of the calibration test remained the same. In some trials of calibration 4 a tape barrier was used to prevent run-off, but some trials did not use the barrier. In cases without the barrier the area of the total sensor was manually calculated each time because no trial successfully reached full coverage (the force of the droplets and pressurised air hitting the tape barrier caused leakages before 100% coverage was reached in all cases). The compilation of all

the new hand-pumped spray bottle data (calibration 4) with the existing calibration curve (calibration 2) can be seen below in Figure 38.

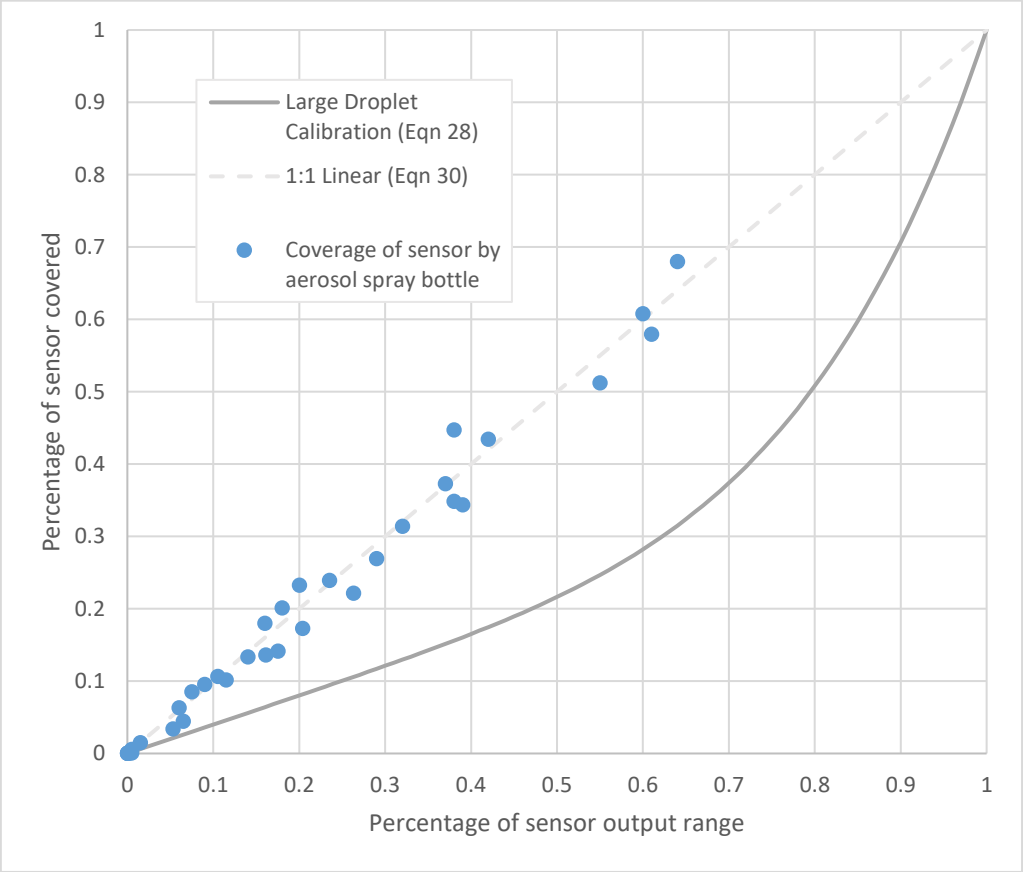

Figure 38: Data for calibration 4 (hand-pumped spray bottle/Arduino datalogger) compared to calibration 2 and a 1:1 relationship

It is clear that the new dataset is not in agreement with the calibration curve. In fact, the new dataset lines up with a direct 1:1 relationship with an R^2 of 0.9845. Error bounds were added, shown below in Figure 39 and equation 31.

$$y = 0.5x(1 + x^c) \; with \; c \; \in (-0.2, 0.4) \tag{31}$$

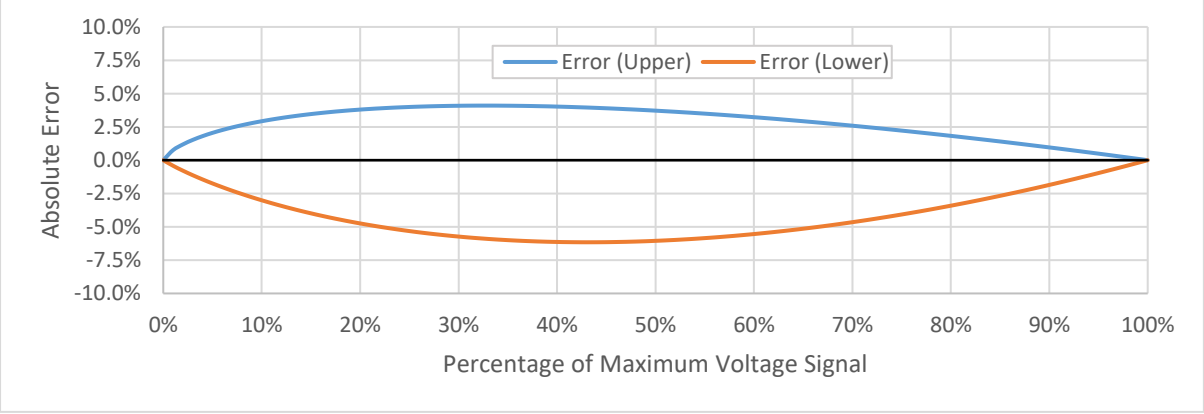

Figure 39: Error functions for calibration 4

Of these four calibration functions, the first three are similar in that they start with a slow linear increase before finishing with a steep incline, either curved or straight. The fourth is a 1:1

correlation (though there is a lack of data at the high end). The differences here may belie a fundamental difference in how the sensor interacts with liquid on the surface but may also be a by-product of the data processing. The following section discusses possible reasons for these differences and comments on the practicality of the calibration functions.

4.5.1 Difference between pipette application and hand-pumped spray bottle application

It is possible that the difference in droplet thickness between application methods is affecting the calibration curves here. Whilst it is clear from Table 3 that a small (~1-2mm) layer of pure water is fairly approximated by a layer of infinite thickness, none of the layers tested were of sizes comparable to the distance between interdigitated electrodes (<0.5mm) on the sensors. Figure 25 suggests that very thin layers that are on this distance scale produce a very different signal for a '100% covered' sensor. It is possible that the effect of the depth of the liquid on the sensor signal is non-linear, with changes to thickness when thickness is around the size scale of the interdigitation causing significant changes in signal, but changes when the thickness is anything greater than that producing very little change to signal. This would mean that the spray calibration, which produces many, very small droplets, is producing signals that are smaller than they otherwise would be because they have a very small depth, whilst the pipette calibration does the opposite. If we consider a fixed areal coverage on the sensor, but allow the distribution of this coverage to change from a single concentrated location (i.e. a pipette application) to a disperse collection of smaller droplets (i.e. a hand-pumped spray bottle application), then according to the calibration graphs, we would expect to see a decrease in total sensor output. This reinforces the idea that larger, thicker droplets are contributing more to sensor output than smaller droplets with thicknesses more comparable to the spacing of the interdigitation.

4.5.2 Differences between calibration curves with different dataloggers

It is still unclear why the calibration curves with pipettes are distinct from one another with different dataloggers. Each dataset was analysed with the same technique, and so it seems unlikely that the calibration tests were performed differently enough to produce this difference. If the datalogger truly does influence the sensor signal output, the most likely origin of this source would be the excitation or ground signal sent to the sensor. The LabView connection featured an entirely different set of jacks for the sensors to connect to, with different excitation and ground cables to match. Whilst theoretically the excitation and ground were still at 5V and 0V respectively, there may be a different behaviour due to the stability of being passed from the mains to the sensors via a computer.

The Arduino circuit is battery powered, and though the excitation voltage is being provided by the Arduino Nano and should theoretically be stable, this was not checked. In particular, the addition of the dedicated ADC unit would have required a larger power draw than before, which could explain the difference in calibration curve after this was added. As a final point, it is possible that the data exceeding input values of 40% in calibration 1 experienced a measurement error. It is noted that the datasets that did not exceed this value lined up very closely with calibrations 2 and 3, so it is possible that these large differences are not actually present. Regardless, calibration 1 is not recommended for use with these sensors, so this should not be an issue in use.

It should also be noted that, as predicted, the LabView datalogger and the Arduino datalogger are functionally equivalent with some small error . For any fixed areal coverage, calibrations 2 and 3 (equations 28 and 30) always have a sensor output value within 4.8% of each other. This is strictly less than the error functions imposed on calibration 2, so the two dataloggers can be considered equivalent.

4.5.3 Practical use of the calibration functions

Ultimately, the differences between calibration 1, 2 and 3 are primarily in the latter half of the calibration curve, and since most practical uses of these sensors allow run-off, the maximum signal obtained from these uses will be unlikely to exceed 60% of the maximum sensor output, and the differences will be negligible. Of more note is the aforementioned discrepancy between small and large droplet application, and care should be taken to use an appropriate calibration depending on the application. It is possible that the large droplet calibration is more suitable for measurements involving rain or watering via hose, whereas the small droplet calibration is more suitable for spray applications such as spray heads for hoses or pesticide application.

As a final point, these calibrations operate on a scale that can be misleading for those wishing to spray to "full coverage". The sensor output was non-dimensionalised in all cases in order to produce a calibration function that was independent of material conditions such as spray substance or atmospheric conditions, as well as to make the function easy to manipulate algebraically. To do this, the sensor output was converted from a bitstream to a percentage of maximum output. The maximum output was chosen for the ease with which it is found, as well as its association with the calibration tests itself, but the physical meaning of a maximum sensor output is not necessarily intuitive. As mentioned earlier, most real testing situations allow for run-off, preventing the sensor from ever being fully saturated in this way. This maximum output value thus does not represent a realistic full coverage (which has been found to be 50% to 65% of the maximum sensor output and can be seen in Figure 40), nor does it represent the point at which the sensor has just been coated in a thin layer (which can be as low as 40% of the maximum sensor output). Care should therefore be taken when applying the calibration functions that a suitable threshold be chosen for the application.

Figure 40: A sensor that is arguably fully covered but still at approximately 50% of "full coverage" as defined by the calibration tests

4.6 Comparison to Water Sensitive Papers and Real Leaves

4.6.1 Processing of and comparison to water sensitive papers

Two tests were done to compare the results generated by the PHYTOS sensors to those generated by water sensitive papers, one in the vineyard and one in the laboratory. In each test a water sensitive paper was placed next to a sensor (in the laboratory, this was on a table, whilst in the field they were pegged to the sensor) and sprayed with a backpack sprayer, (or in the laboratory, both the backpack sprayer and the modified ESS nozzle) for 0.5 – 4 seconds. Some spray applications were done close to the sensor/paper and others were from further away in order to produce different spray patterns. It is assumed that the distribution of spray is the same on both the paper and the sensor so that the two sensing methods can be compared directly. The field data was gathered immediately after gathering the data shown in section 6.2, and the sensor layout was the same.

To obtain quantitative data from the papers, the MATLAB script from the calibration tests was modified to work for these papers. The new script performs the following operations:

1. Load the image
2. Separate the image into its red, blue and green components
3. Create a weighted greyscale image by taking the average of each RGB channel brightness and setting the brightness of the new greyscale pixel equal to that value. This operated slightly differently to MATLAB's image processing script "rgb2gray" in that the yellow parts of the paper were set to a darker grey than they otherwise would be.
4. Create a new image that just shows the drops by taking 255 (maximum brightness) and subtracting both the red and green components. This is equivalent to the subtraction of the blue and green components in the calibration script in that it essentially "turns off" every pixel that doesn't have a blue component larger than the combined red and green components.
5. Create a new image by inverting the weighted average image. Because the yellow is a darker grey in the image, this has the effect of turning all blue *and* yellow pixels on whilst turning all white pixels off. This is used to determine which parts of the image are paper and which are background.
6. Binarise both new images
7. Count the number of "on" pixels in the image containing only the drops and comparing to the number of "on" pixels in the paper image. This allows the calculation of percentage area covered

An example of a paper being processed can be seen below in Table 4.

Table 4: Examples of water sensitive paper processing accompanied by descriptions of the process. Numbers in brackets indicate the step number from the above list.

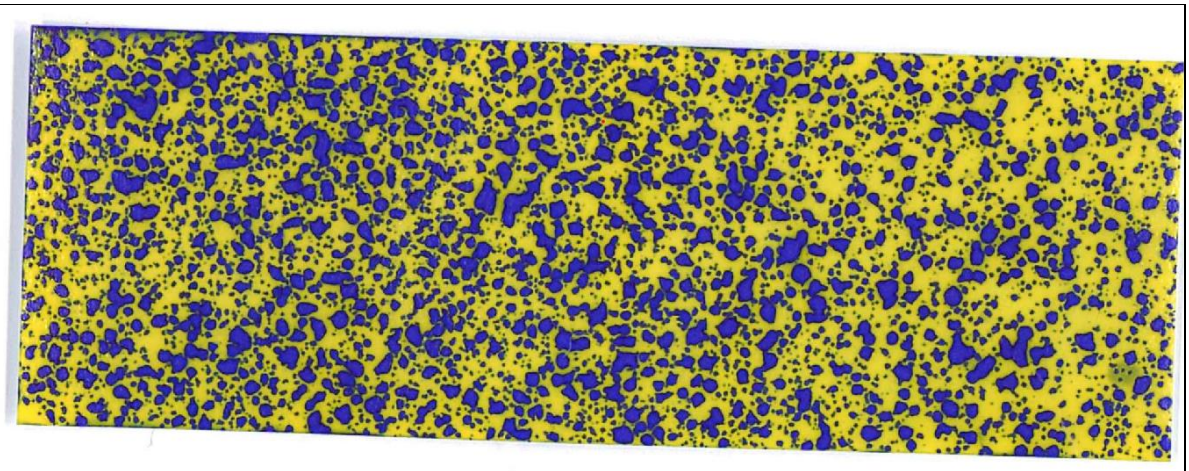

This is an example of the base image with no processing except for a crop. (1)

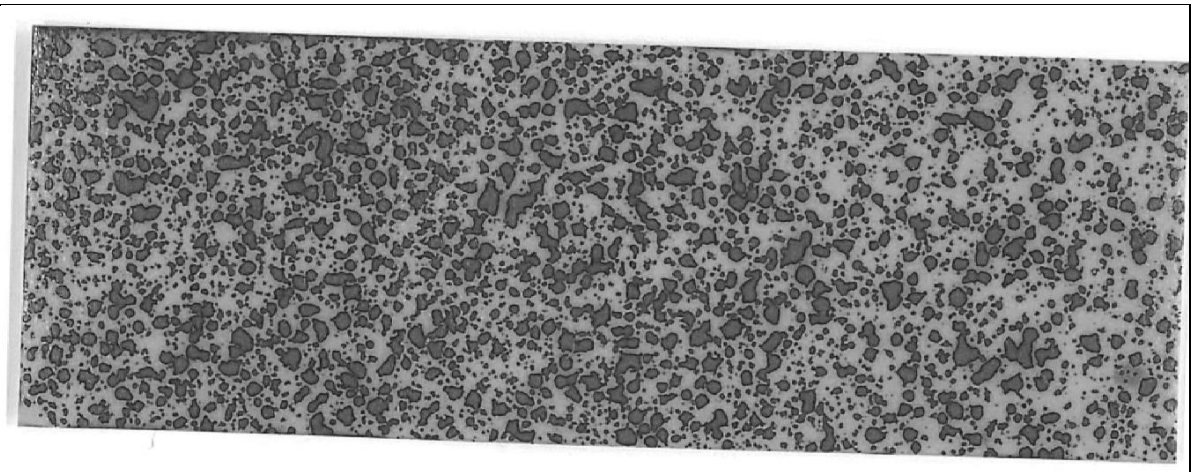

This image was produced by taking the RGB components of each channel and taking their arithmetic mean as the brightness in a greyscale image. (3)

Generated using the command:

```
>> ave = 3*(image(:,:,1)/3 + image(:,:,2)/3 + image(:,:,3)/3);
```

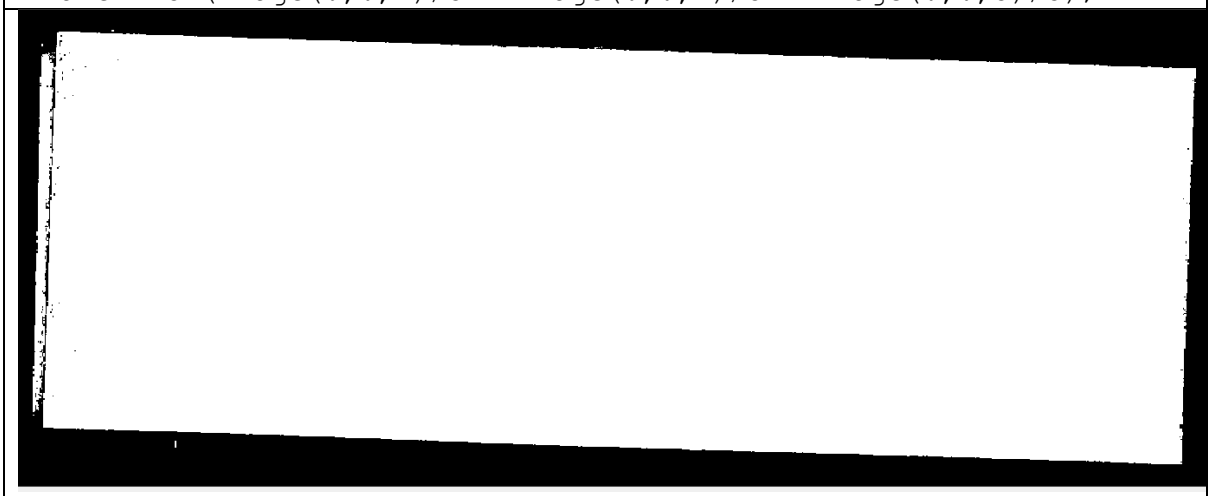

This image is the binarised form of the inverted previous image using a threshold of 15% brightness for white. (6)

```
>> imbinarize(255 - ave,0.15);
```

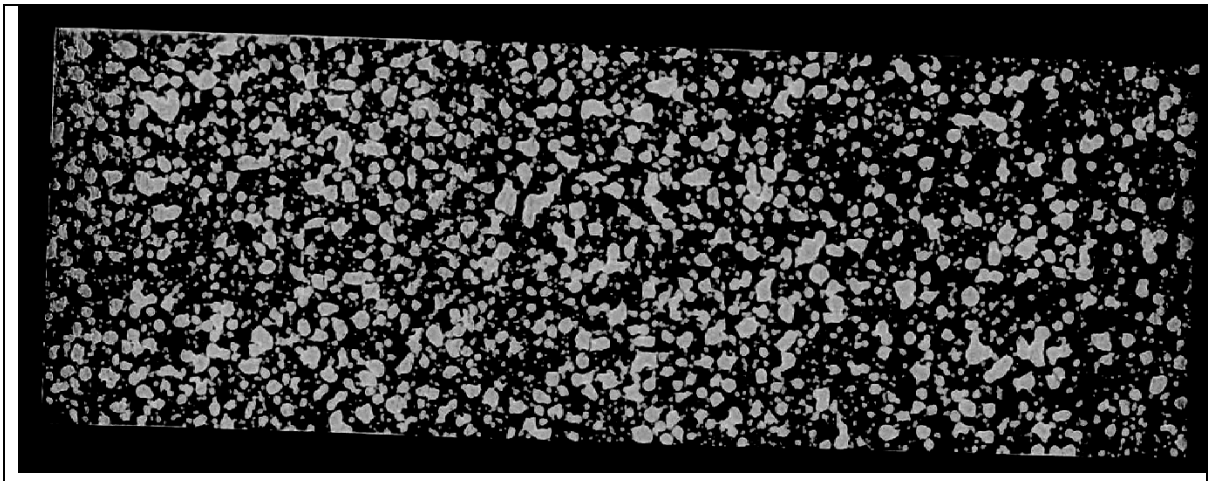

This image was produced by summing together the red and green components (which together make yellow) and inverting the image such that blue pixels are bright and any yellow or white pixels are dark. (5)

```
>> drops = (255 - red - green);
```

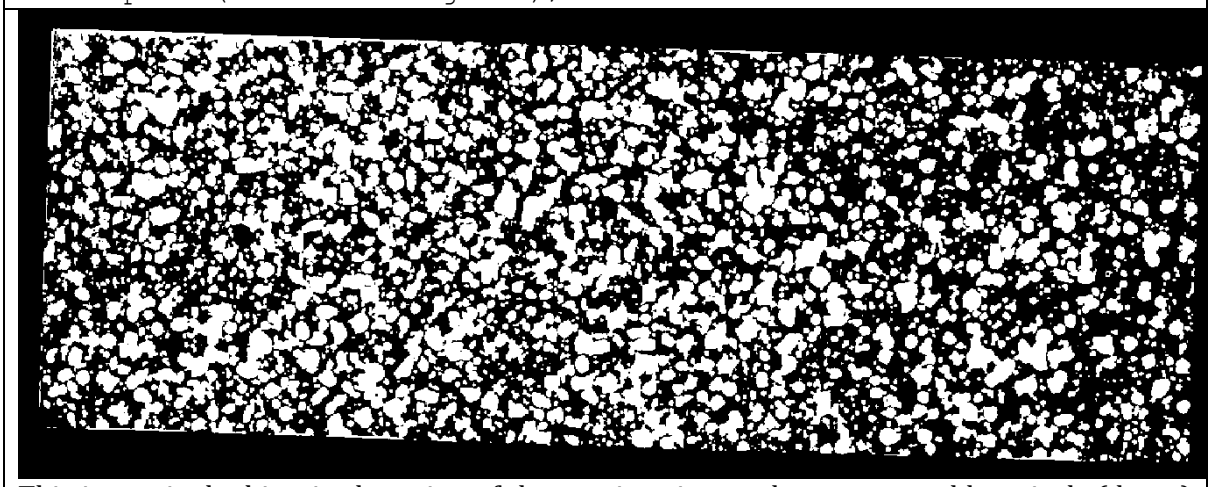

This image is the binarised version of the previous image that turns any blue pixels (drops) "on" whilst turning "off" any yellow or white pixels. (6)

```
>> imbinarize(drops, 0.001);
```

After the papers were all processed, the coverage values extracted were compared to those extracted from the sensors. The sensors were processed in the same way as previous tests and had the small spray droplets calibration applied (equation 31) to produce a coverage value. Figure 41 below shows this comparison, with the three different colours corresponding to whether the test took place in a controlled laboratory environment or in a vineyard, as well as comparing two different nozzles. The field tests were a combination of both the backpack sprayer (large droplets) and the ESS nozzle (small droplets).

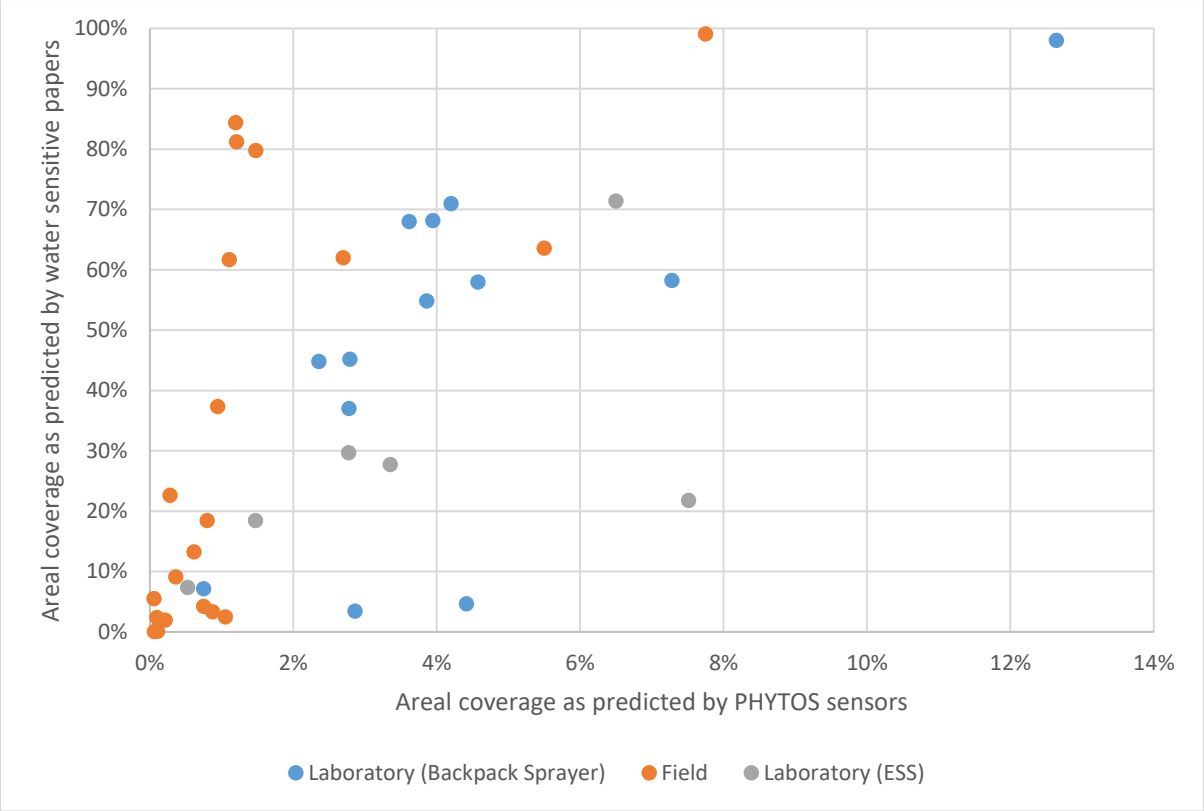

Figure 41: Scatterplot of areal coverage as predicted by the water sensitive papers (vertical axis) and PHYTOS wetness sensors (horizontal axis)

It is important to note the different scales on the axes of Figure 41. The two sensing methods are not particularly similar, though they do have a weak positive correlation, with the papers producing signals that are significantly higher than the PHYTOS sensors.

Due to the difference in the results generated by the papers and the sensors, a high speed camera was used to investigate the difference in the ways that water interacted with the two sensing mechanisms. The camera is a Photron SA5 (Photron, Tokyo, Japan), colour, 12 bit, 1024×1024 pixels. A series of different videos were recorded. The initial hypothesis was that the papers were producing an inaccurate signal due to water wicking through the paper fibres and covering an area with diameter significantly larger than that of the incoming droplet. This would not be possible with the sensors and would contribute to the understanding of the large overestimate of the paper results when compared to the sensor results. Because of this, the first video featured a single paper being sprayed by the backpack sprayer, with the intent of capturing the effect of droplet deposit size growing with time. The camera ran at 5000fps, with a shutter speed of 1/30000s and a resolution of 1024×1024. Some frames (chosen from a span of about 0.5 – 1 second to best illustrate the colouring process) from this video are included in Figure 42.

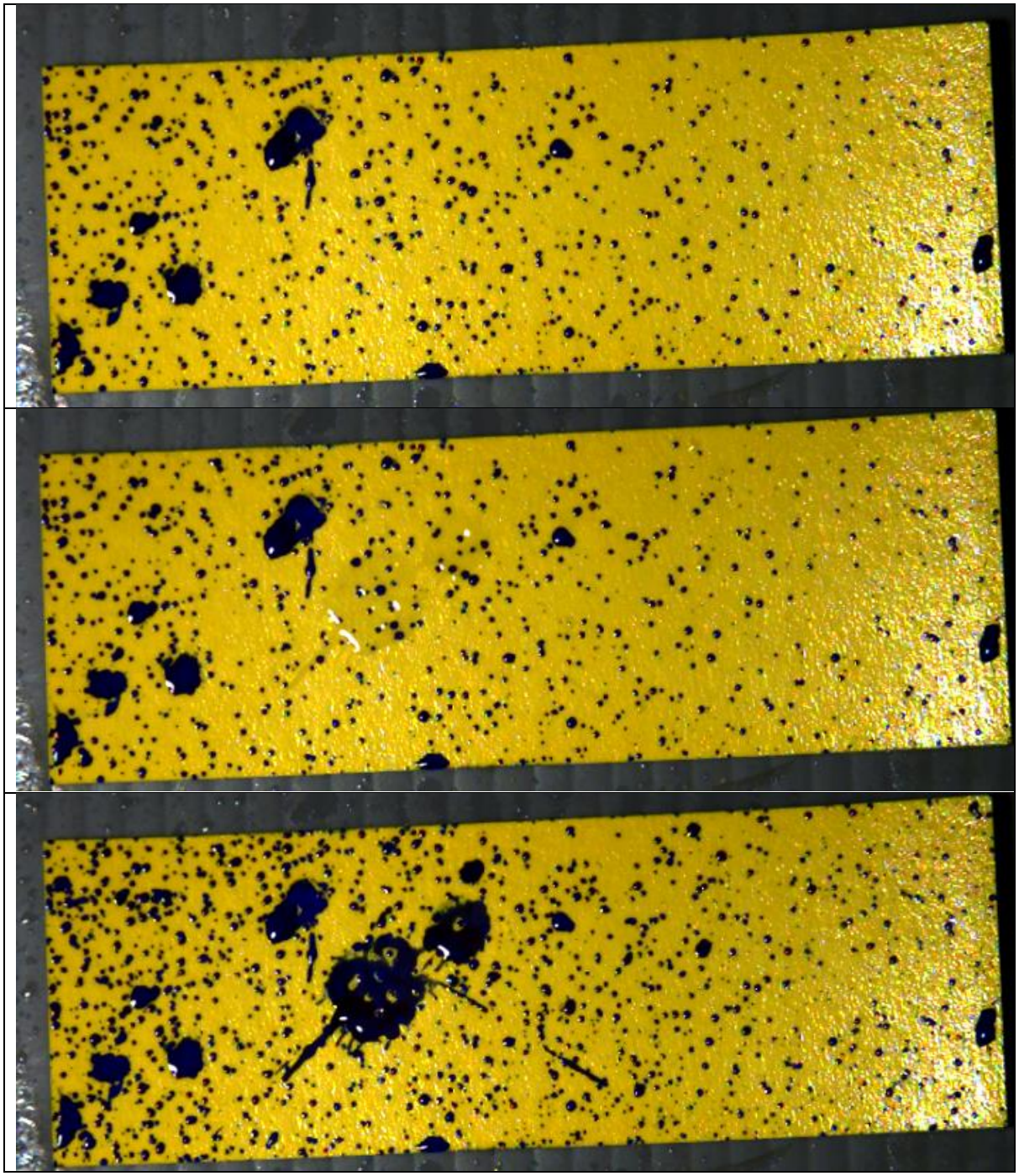

Figure 42: Three frames from the high-speed video showing the paper before a series of droplets hit, the paper as the droplets hit, and the paper shortly afterwards (after the chemical reaction has taken place)

The video captured a single spray, with some liquid being present prior to the start of the recording. The three frames shown are from the beginning, middle and end of the video, with the middle frame showing the paper immediately after the large drop in the centre-left hit the paper but before it had time to darken. The significance of this video is that, though there is more liquid on the paper after the spray, the individual droplets do not grow with time. The waxy coating of the paper that reacts with water to change colour prevents the water wicking through the fibres of the underlying paper, which invalidates the initial hypothesis.

The second video featured a paper and a sensor simultaneously being sprayed by the hand-pumped spray bottle filled with dyed water. This video proved more enlightening, and frames

from it can be seen in Figure 43 to Figure 47. This video was also shot at 5000fps, but with a 1/12000s shutter speed. It was also at a resolution of 1024×1024 (the maximum for the camera). The images of the droplet impact and subsequent retraction are only separated by a few frames.

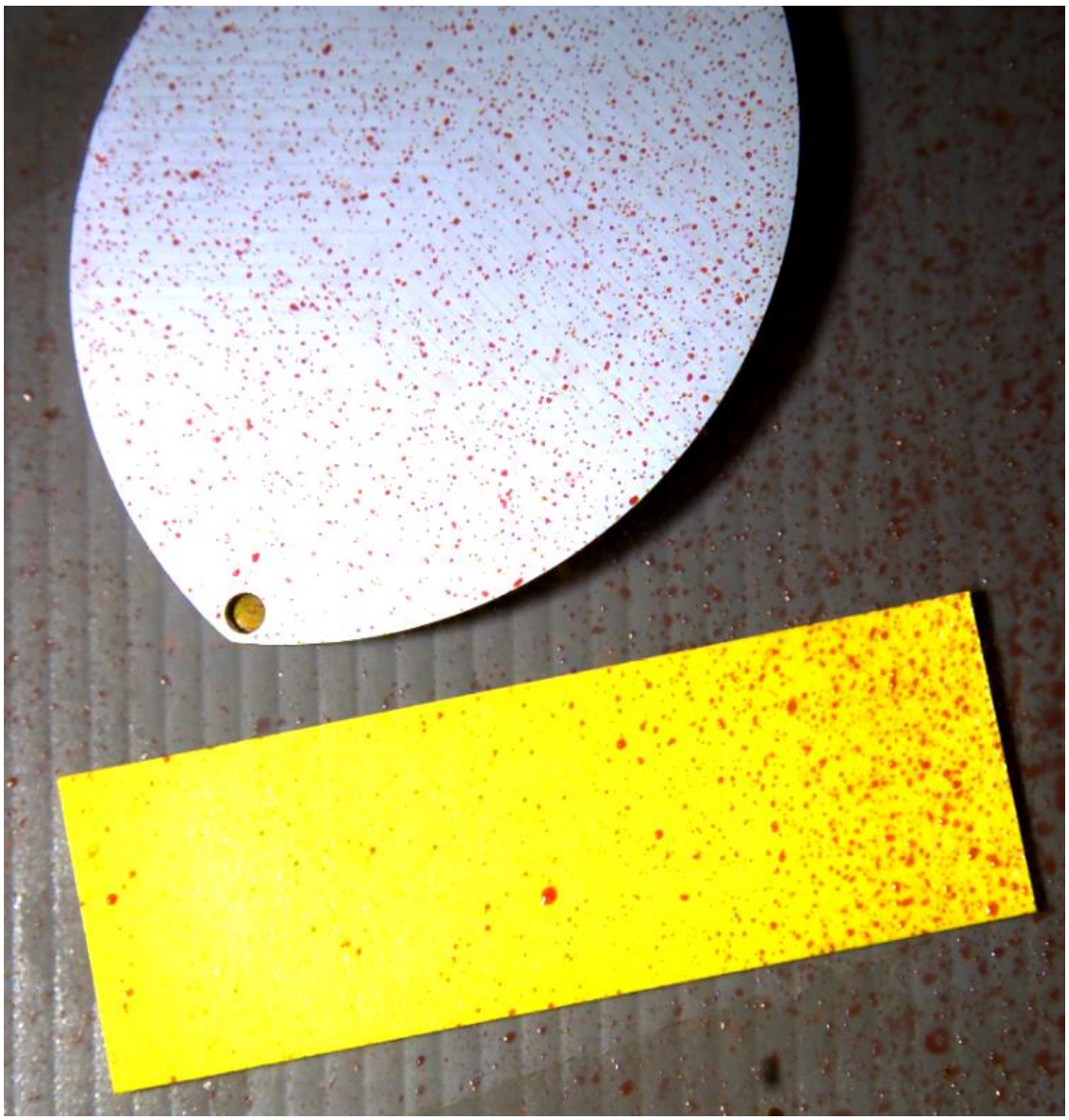

Figure 43: The PHYTOS sensor and paper immediately before the next series of droplets land

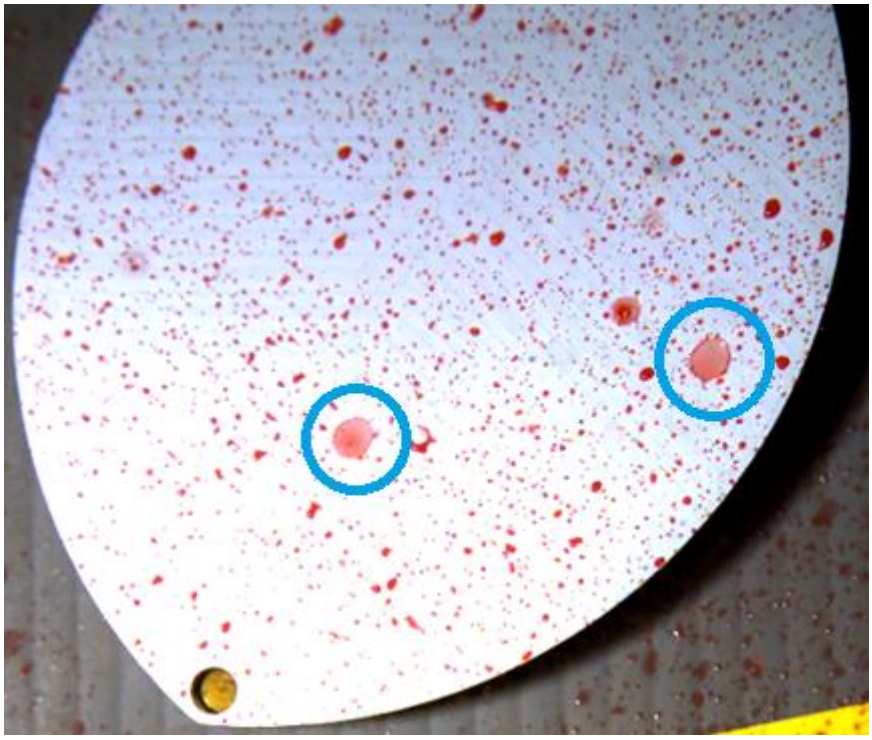

Figure 44: The PHYTOS sensor immediately as two droplets impact it

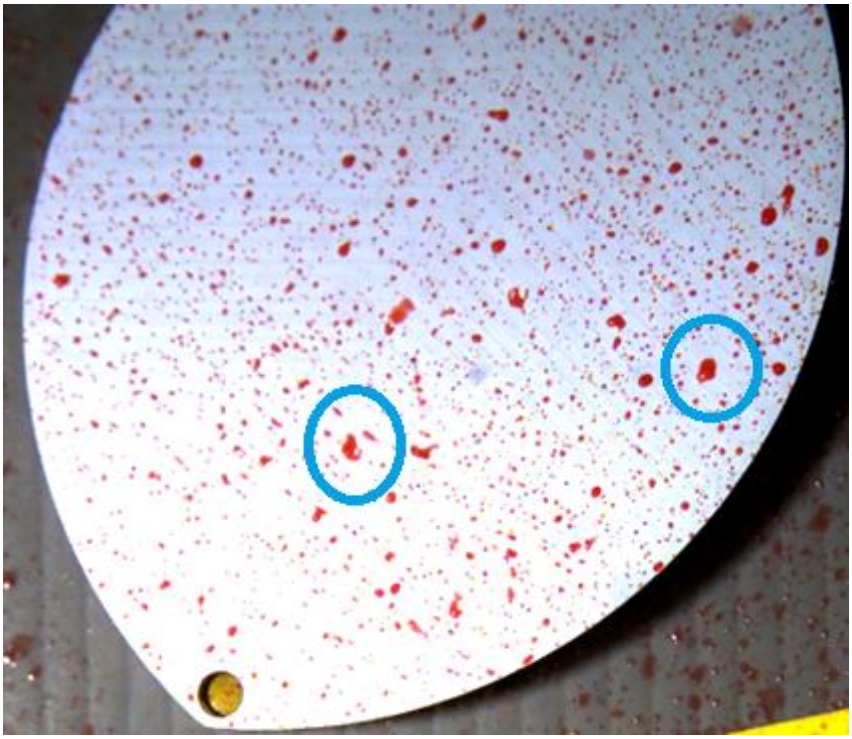

Figure 45: The PHYTOS sensor immediately after two droplets impact it

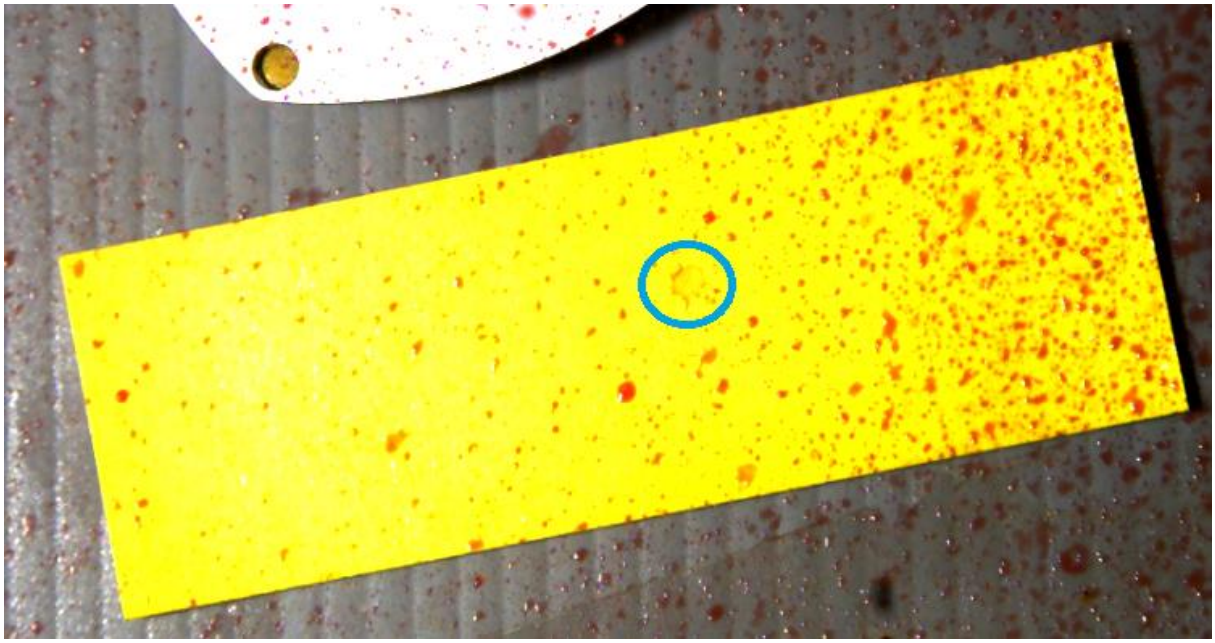

Figure 46: The water sensitive paper immediately as a droplet impacts it

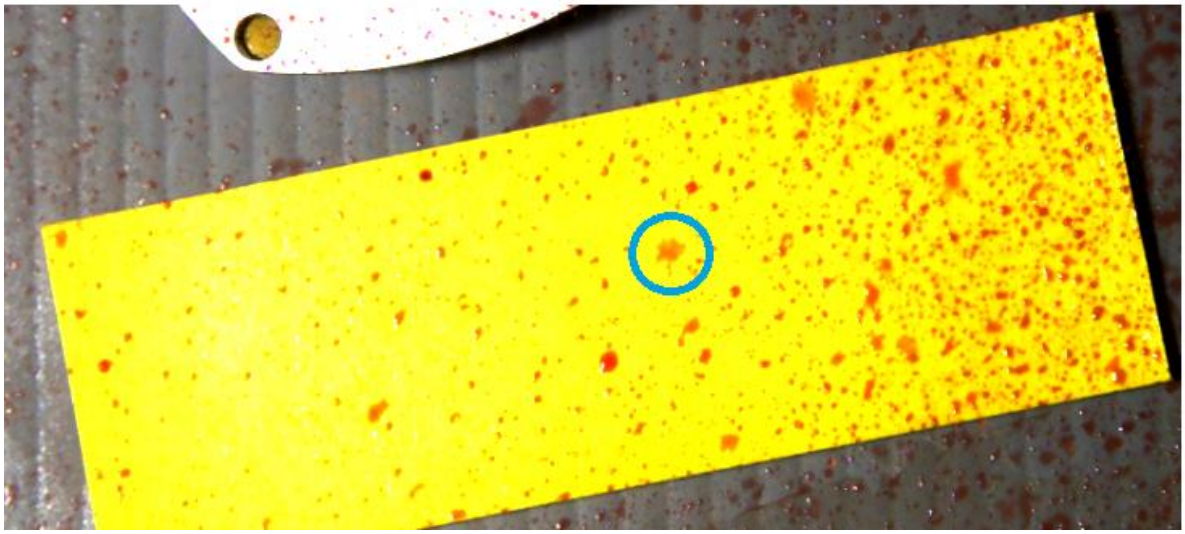

Figure 47: The water sensitive paper immediately after a droplet impacts it

The first image shows the layout of the paper and sensor, and shows that for small droplets, the overall distribution looks very similar between the two sensing methods. However, when larger droplets begin to impact the two different apparatuses, a difference in behaviour may be noted. On the sensor, the large droplets spread out before being pulled back into a small droplet by surface tension. On the paper, this happens to a much smaller degree, with the droplet remaining significantly more spread out.

The question is then raised: which of the two alternatives is closer to a real leaf? A selection of leaves picked from various plants from the grounds of the University of Canterbury were sprayed under the camera to test this. The camera settings were the same except for the shutter speed which was lowered to 1/6000s due to the darkness of the leaves compared to the previous test subjects. The final result of the spray is seen in Figure 48.

Figure 48: Spray pattern deposition of red-dyed water on various leaves. The upper right and central leaves are waxy, and the left and bottom leaves are softer.

It is less clear in this video what the behaviour of the spray droplets are because the colour and texture of the leaves is more complex than that of the sensor or paper. However, it seems that some leaves show a tendency towards the sensor behaviour and others show the opposite. Namely, the waxier leaves (top right and middle) show drops generally smaller, rounder, discrete droplets, whilst the softer leaves (left and bottom) show flatter, more spread out droplets.

To capture this spreading effect, several drops of water were dropped onto the sensor one at a time from roughly a metre up. The LabView datalogger was used in order to capture at a higher data save rate, specifically 100Hz rather than the usual 20Hz. Subsequently the test was repeated using a concentrated surfactant (50g/litre alkylaryl polyglycol ether, Sprayfix, Yates, Auckland, NZ) rather than water. The results are seen in Table 5. Take note of the scaling of the y-axis in each image.

Table 5: Excerpts from sensor output graphs comparing the effect of surfactant on the tendency of the droplet to retract after initial impact

No Surfactant	Surfactant
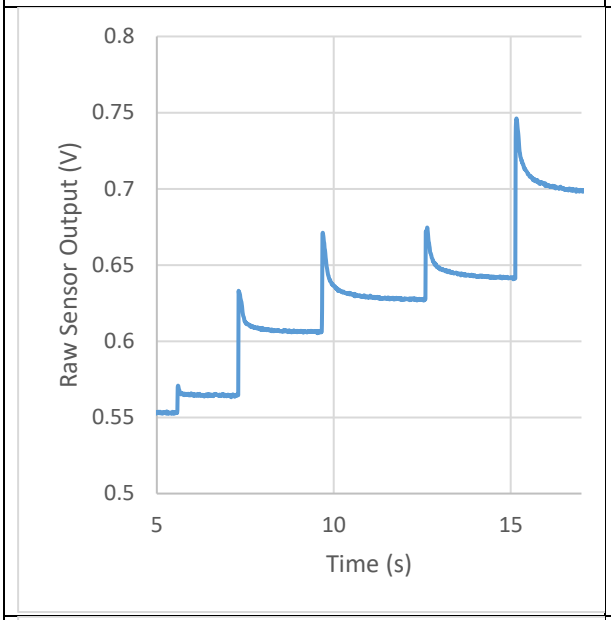	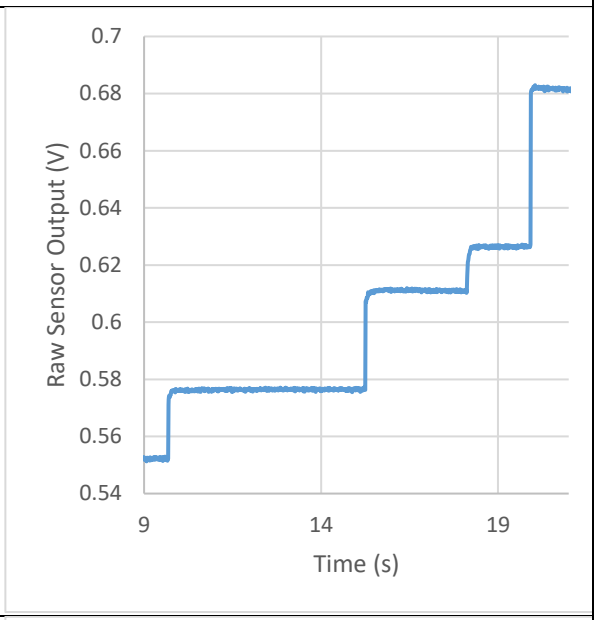
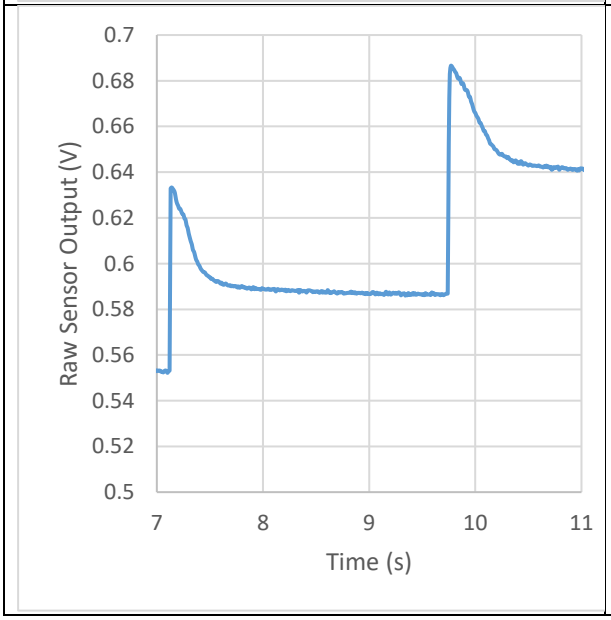	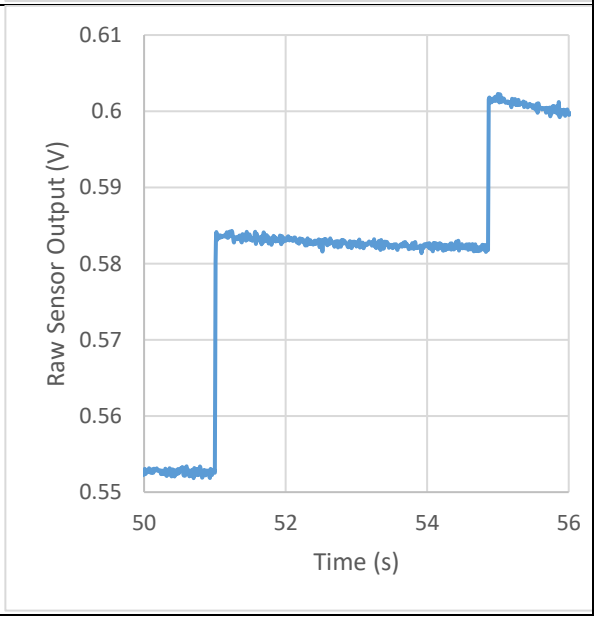

The spike in the signal when no surfactant was present was frequently twice the size of the equilibrium change, whereas with surfactant present there was no spike whatsoever. This reinforces the hypothesis that the PHYTOS sensors are underrepresenting the signal measured by the papers, as the change in signal on the paper may be twice as large as that on the PHYTOS sensor due to this retraction effect. Or, stated differently, the papers are measuring the size of the droplet as it expands on impact, whereas the PHYTOS sensors are only measuring the size of the droplet after the (much more significant) retraction. This is discussed further in section 4.6.3.

4.6.2 Contact angle investigation

An investigation was conducted to compare the PHYTOS sensors, the papers, and grapevine leaves in terms of the contact angle between a droplet of known volume and the surface. To do this, the same Photron SA5 camera was used, this time with a K2 DistaMax long working distance

microscope lens (Infinity Photo-Optical Company, Centennial, CO, USA) to see the micron-scale droplets with high resolution. Using an Eppendorf syringe, 1µL droplets were successively added to a site on the surface on which the camera was focused. Photos were taken in between each addition, giving a series of images of droplets sized 1 – 5µL to compare. This was done with and without surfactant of concentration 1.2g/L of active ingredient for the PHYTOS sensor, a paper, and the top and bottom surfaces of both an old and a young grape leaf.

To find the size of the contact angle, three pixels were selected on the image around the point of contact and the cosine rule was applied (equation 32).

$$\theta = 180° - cos^{-1}\left(\frac{a^2 + c^2 - b^2}{2ac}\right) \quad 32$$

The values a, b, and c correspond to side lengths of the triangle created by the three selected pixels and were calculated using Pythagoras' formula as below (equation 33). Pixels 1, 2 and 3 were defined by ordered pairs (x_1,y_1), (x_2,y_2), and (x_3,y_3) respectively.

$$\begin{aligned} a &= \sqrt{(x_2 - x_3)^2 + (y_2 - y_3)^2} \\ b &= \sqrt{(x_1 - x_3)^2 + (y_1 - y_3)^2} \\ c &= \sqrt{(x_1 - x_2)^2 + (y_1 - y_2)^2} \end{aligned} \quad 33$$

An example photograph and the corresponding geometry used to calculate contact angle can be seen in Figure 49 and Figure 50.

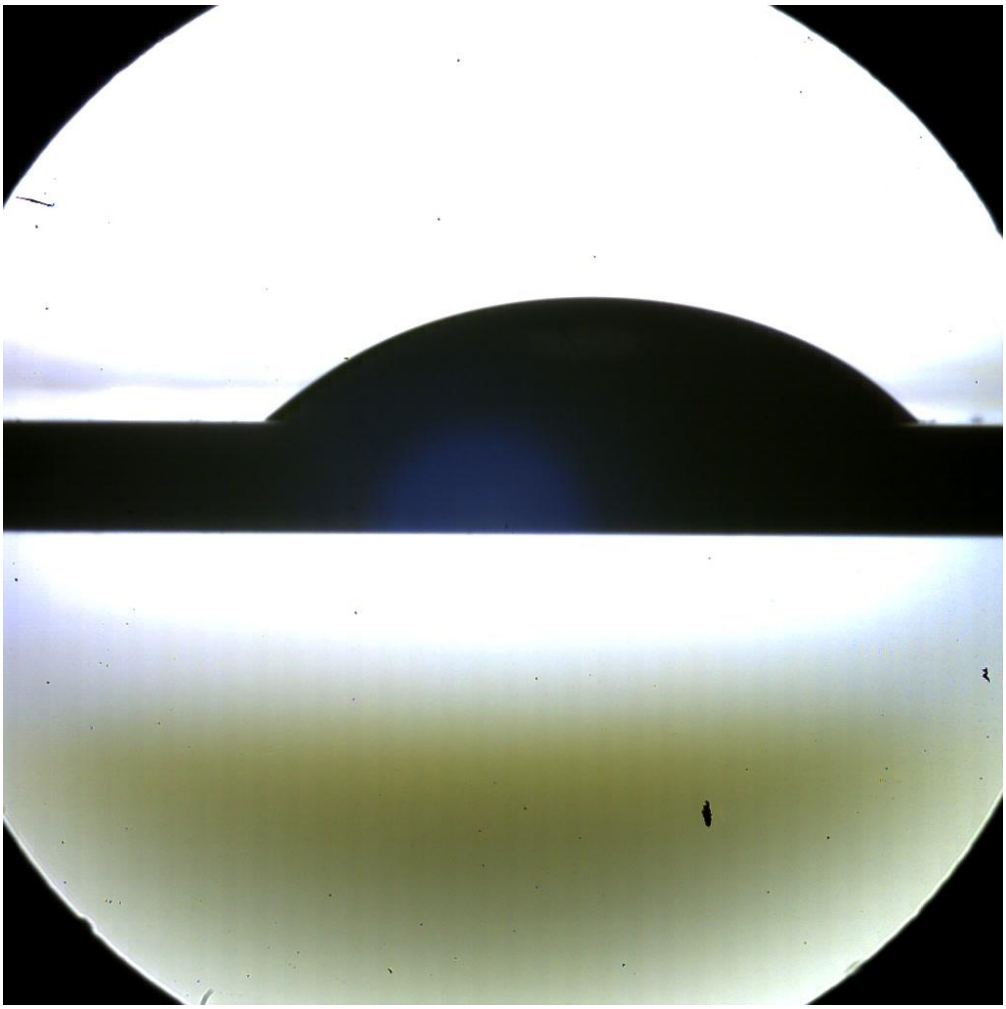

Figure 49: Photograph of droplet on PHYTOS sensor taken with magnifying lens

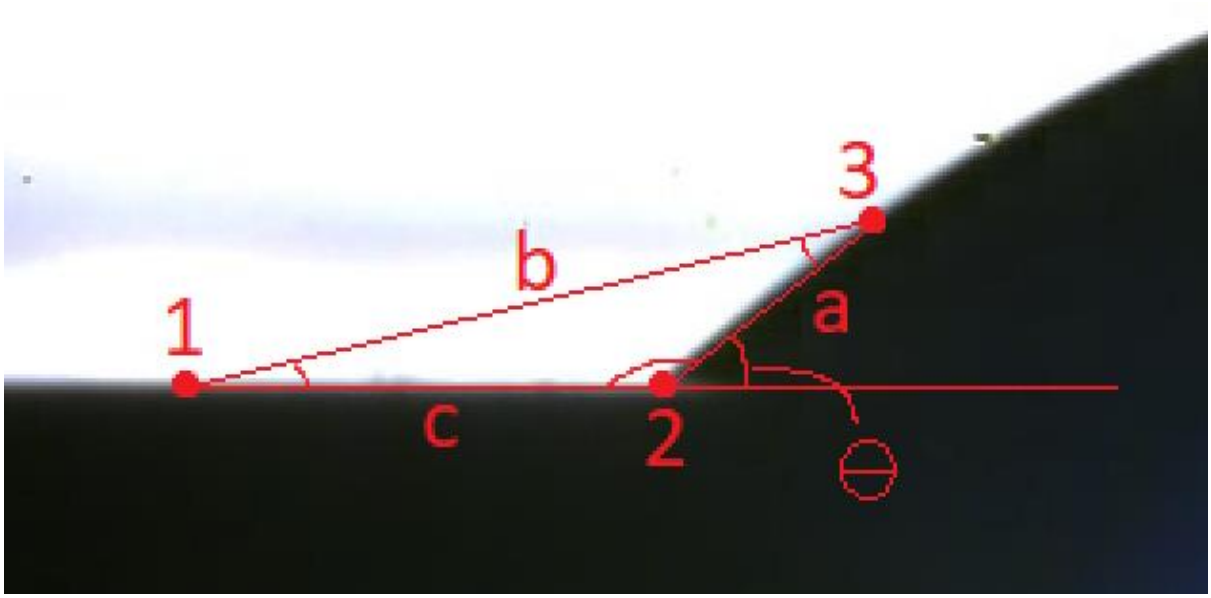

Figure 50: Example of lines and points used to calculate contact angle

Error can be introduced into this process in a few ways. Firstly, equation 32 assumes that the droplet surface is flat, which is untrue. Thus, points 2 and 3 must be sufficiently close to one another for the small-angle linear approximation to be true. Contrarily, if points 2 and 3 are too close to one another, a change in position can affect the calculated angle significantly. Finally, all lines are slightly blurred, filling a space approximately 3 pixels wide. Provided that point 1 is sufficiently far away from point 2, error is minimal. In addition to these potential measurement/calculation errors, any deviation from horizontal would introduce an extra force (gravitational) which will impact the measured contact angle.

It was assumed that errors introduced from slight deviations from horizontal would be small in comparison to measurement errors on this scale, so a brief investigation into the impact of point selection on contact angle calculation was performed. In the following list, when a point is fixed, it is fixed at the approximate location as seen in Figure 50.

- When fixing points 1 and 2 and moving 3 up the surface of the droplet, θ varies from 45° to 38°, with the shown location in Figure 50 producing an angle of 39°
- When fixing points 1 and 2 and keeping 3 near to 2, θ could change by up to 13° by only moving a few pixels
- When fixing points 1 and 2 and keeping 3 near to its shown location, small changes impact θ by up to 2°
- When fixing points 1 and 3, small variations in point 2 cause θ to vary by approximately 3°
- When fixing points 2 and 3, small variations in point 1 do not change θ.

This variation suggests that pixel selection can introduce errors of roughly 3°, with point 3 producing a tendency to underestimate due to the straight line approximation, increasing with distance from point 2. Thus, all measurements on flat surfaces (i.e. the papers and PHYTOS sensors) have been given an error of ±5° and measurements on curved surfaces (i.e. the leaves) have errors of ±8°.

A series of plots (Figures Figure 51 to Figure 55) were produced that compared the different surfaces to each other. In each of these plots, an x-shaped cross and solid line refers to a data point

with no surfactant, and a +-shaped cross and dashed line refers to a data point with surfactant (unless otherwise stated in the legend).

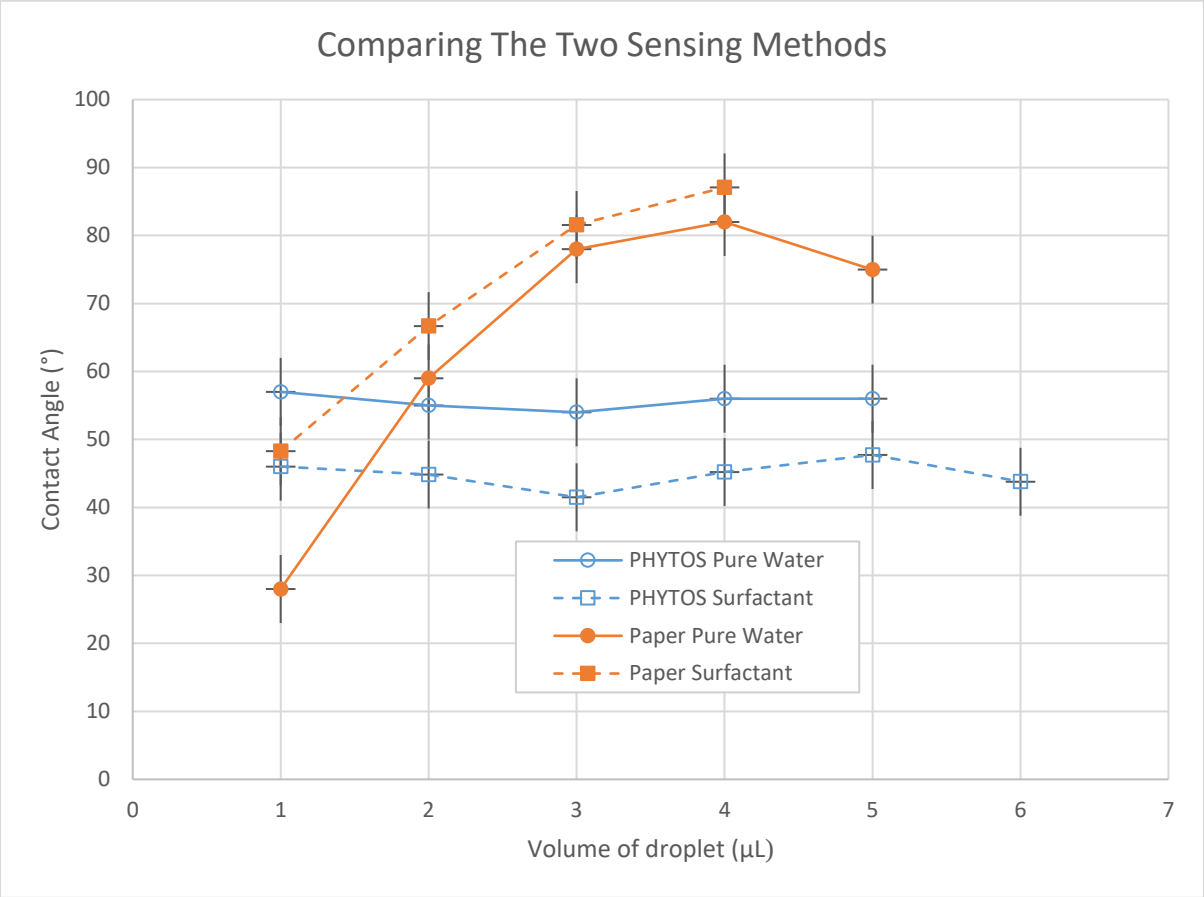

Figure 51: Contact angle with and without surfactant for PHYTOS sensor and water sensitive paper

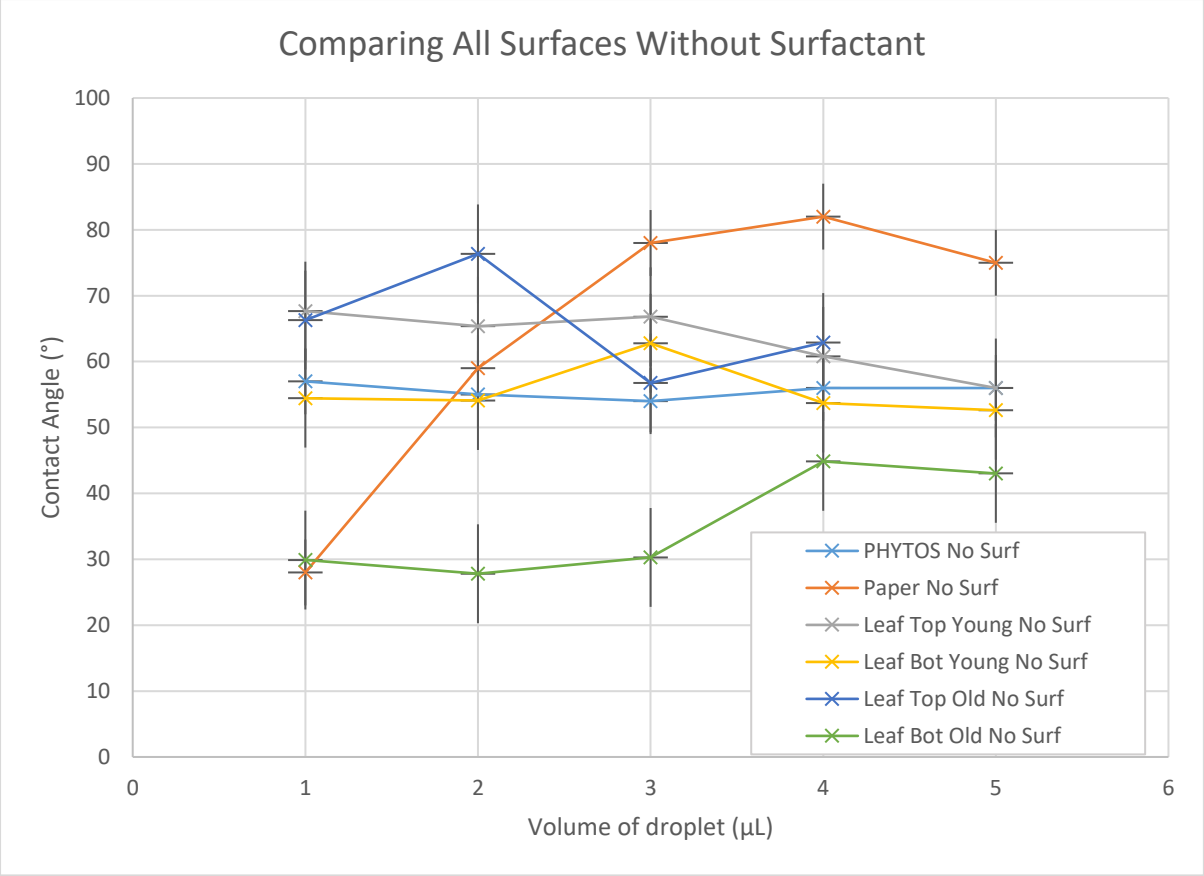

Figure 52: Contact angle without surfactant for all surfaces

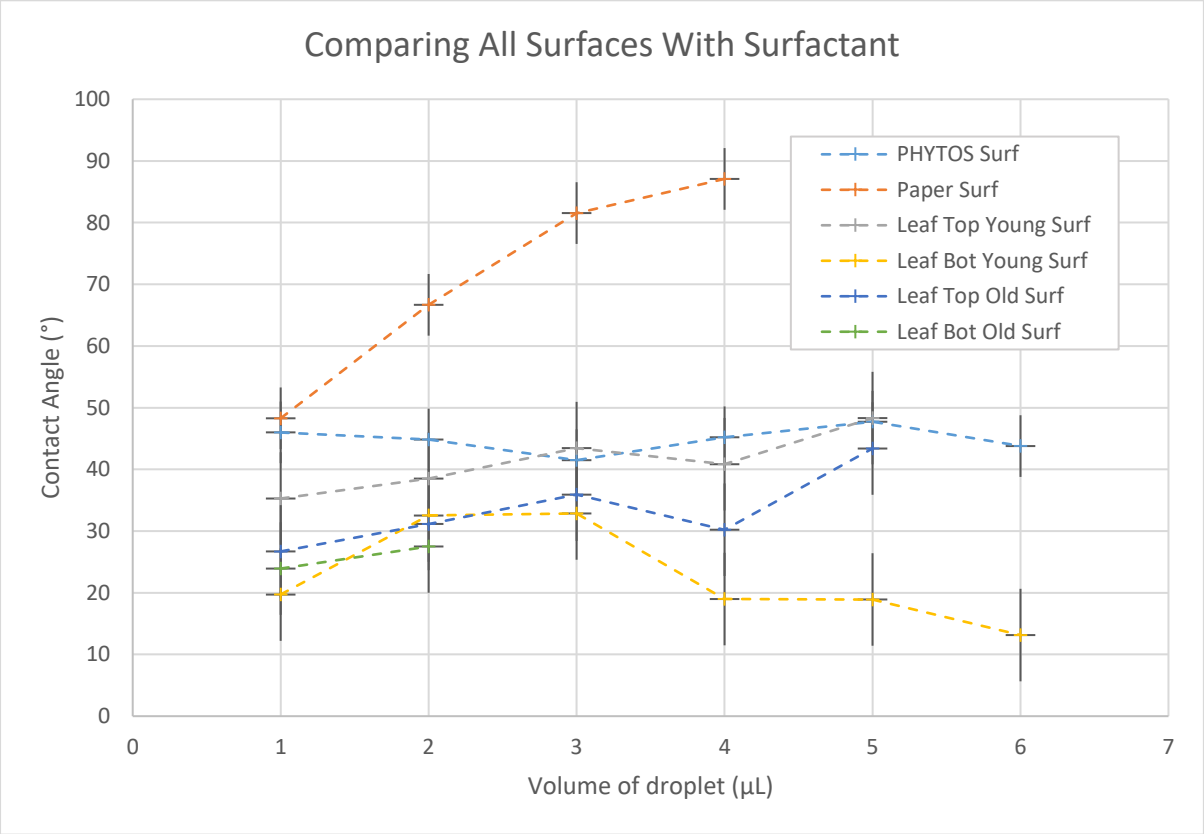

Figure 53: Contact angle with surfactant for all surfaces

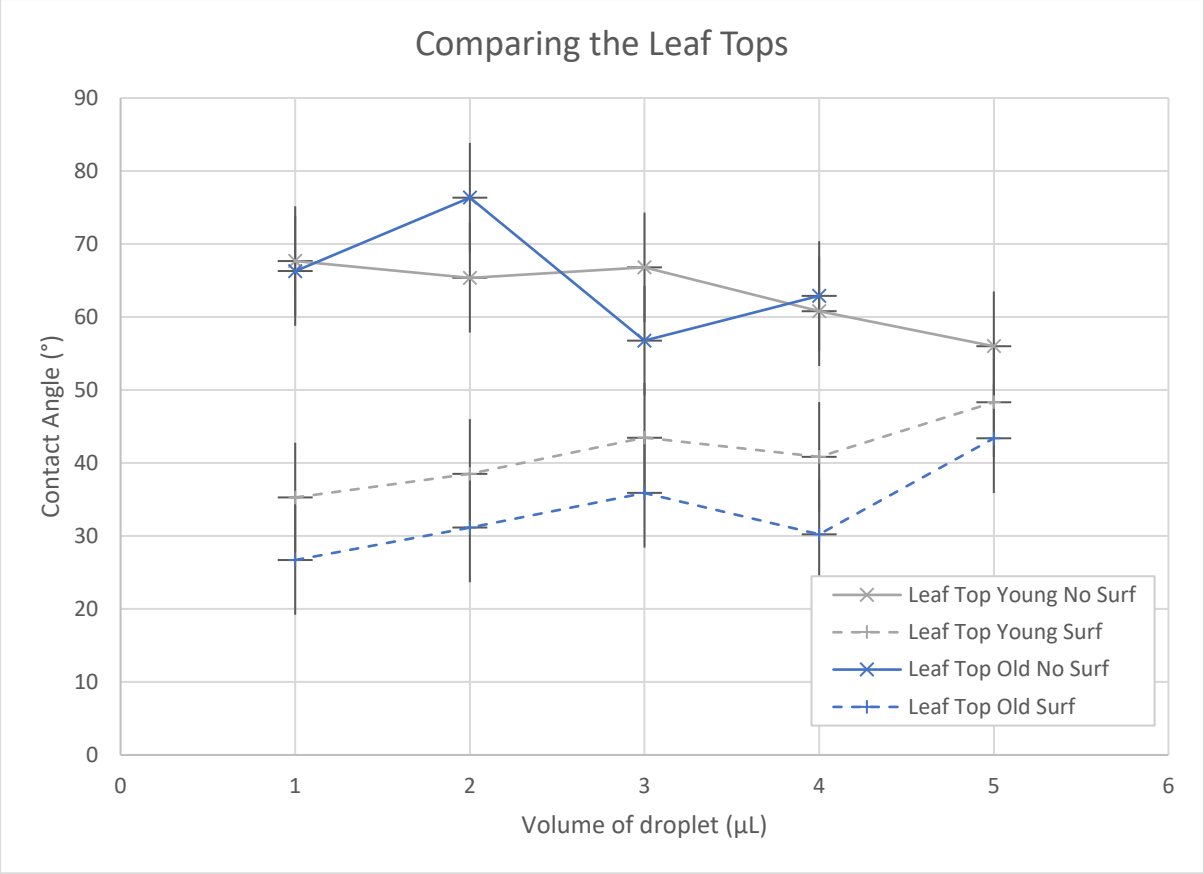

Figure 54: Contact angle with and without surfactant for top of grape leaf

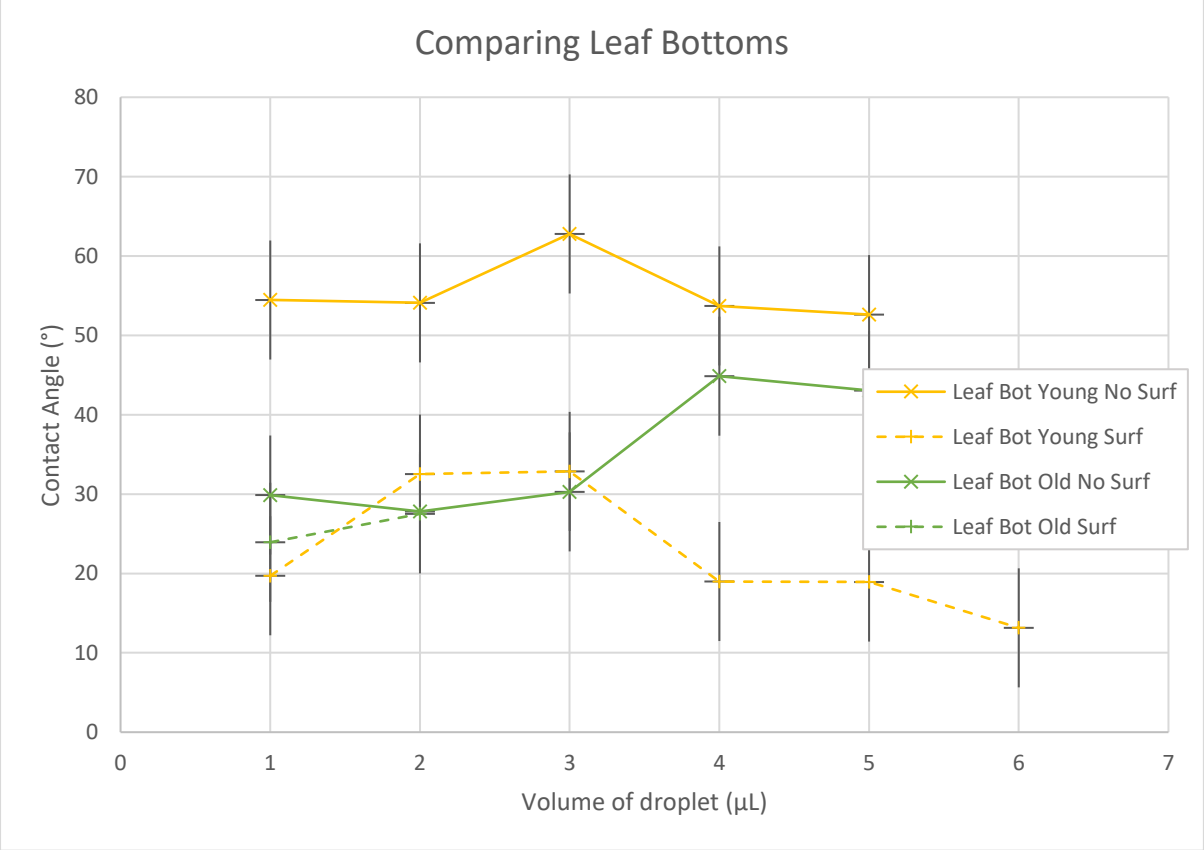

Figure 55: Contact angle with and without surfactant for bottom of grape leaf

The water sensitive papers are notable in that the contact angle seems strongly dependent on droplet size, with the contact angle varying from 30° to 80° in the no-surfactant trial and varying from 50° to 85° in the surfactant trial. By contrast, the PHYTOS sensor stayed within a band of 10° in both trials, and whilst the leaves tended to see relatively large margins of roughly 20°, their patterns were less monotonic and more random than the papers. In almost all cases, the addition of surfactant caused the contact angle to decrease, with the exception again being the papers. It is hypothesised that this increase in contact angle with surfactant is due more to statistical variation than due to underlying phenomena, as the contact angle measurements are within acceptable error of each other in most cases and those particular measurements (i.e. the PHYTOS and paper measurements without surfactant and with surfactant) were taken on different days.

The contact angle on the leaves is presented with larger error bars, as it was difficult to flatten the leaves appropriately for photographing and thus there is more potential for an inaccurate trio of pixels to be selected for the calculation. In general, there is no clear relationship between the contact angle and the size of the droplet on the leaf surfaces. The PHYTOS sensors seem to be behaving more similarly to the leaves than the papers do, though there is significantly less variation in the PHYTOS sensors than in the leaves.

One observation made was that as more liquid was added to the droplet on the papers, the area of the paper that is covered by the liquid did not change – instead, the thickness of the drop (and thus the contact angle) increased. After the measurements were made, the droplet was observed to relax, returning to a lower contact angle. This suggests that the boundary between the droplet surface and the paper is being pinned by the fibrous texture of the paper, whilst the smoother surfaces of the leaf and the PHYTOS sensor do not cause this effect. This is reinforced by the observation in the high speed footage that suggests that after a high-speed impact, the droplets do not tend to contract or “de-wet” as much on the papers as they do on the PHYTOS sensors, which may be due to pinning in the opposite direction. This also suggests that the water sensitive papers are sensitive to the speed of impact.

Another observation is that the PHYTOS sensor results seemed remarkably unchanged by the addition of a surfactant. In the tests with no surfactant, the leaves tended to produce contact angles that were similar, but generally slightly higher than those of the PHYTOS sensor (excepting the bottom side of the older leaf). In the tests with surfactant, the opposite is true. This suggests that pinning plays more of a role on leaves than it does on the sensor, as pinning might be reasonably expected to reduce its effect in the presence of a surfactant due to the weakened surface tension forces. A final observation is that the top surface of the leaf tends to have higher contact angles than the bottom surface of the leaf. This may be due to the less hydrophobic bottom surface encouraging spreading via capillary or wicking effects.

Generally, it seems that the PHYTOS sensors produce a better approximation of leaf properties than the papers.

4.6.3 Differences between papers and PHYTOS sensors

There is a clear difference between the PHYTOS sensors and papers, with the former producing much lower coverage estimates than the latter. A key assumption made was that both sensing methods are measuring the same phenomena. In a sense this is true, because both sensing methods respond in a sensible and similar way to the same stimuli. Specifically, both the sensors and the papers report a higher result when there is more liquid on the surface of either. It is apparent in Figure 41 that there is a weak positive correlation, but while the sensing methods qualitatively agree, they quantitatively do not.

To examine the differences between the two, consider a single, large droplet deposited near the top of both the paper and the sensor. As the drop rolls down the paper, the chemicals will react at each point and the paper will ultimately report a signal that is identical to that which would be produced by a continuous line of water. In other words, the paper does not distinguish between water which is currently on the surface (current coverage) and water that was previously on the surface (the time-integral of coverage). Conversely, the sensor would measure a signal of similar intensity through the entirety of its descent. Any trail of water left behind by the drop would be sensed, but it is apparent in the video footage that droplets tend to bead together rather than leave films when no surfactant is present. With this understanding it is clear that the paper would be expected to produce results that are higher than those of the sensor, especially in situations where there is a continuous stream of spray being directed at the sensor causing run-off.

Additionally, even a stationary droplet would likely produce a higher result on the paper than on the sensor due to a difference in contact angle. This was observed in the high-speed footage, in which droplets landing on the paper tended to stay spread out whilst droplets on the PHYTOS sensor tended to retract to a much smaller shape. Thus, the PHYTOS sensor would produce a short spike in signal before dropping to a steady-state value, whilst the paper would retain the value generated by the spike in signal. This was verified in Table 5, with the surfactant test appearing to behave more like the papers. Interestingly, the contact angle measurement suggested that for a given droplet volume, the paper should tend to see a smaller projected area onto the paper due to a high contact angle. This is not necessarily a contradiction, as the mechanism through which the contact angle increases with droplet volume – pinning – would likely also act to prevent the droplet from retracting in size after an initial collision flattened the droplet.

The combination of these effects suggests that the papers and the PHYTOS sensors are not measuring the exact same phenomenon. Specifically, the PHYTOS sensors are producing a signal proportional to the amount of water currently on the sensor, whilst the papers are producing a signal (visually) that is proportional to the amount of water that has ever been on the paper. Stated differently, the papers are integrating moisture coverage over time, whereas the PHYTOS sensors report the instantaneous coverage. Seeing as negative areal coverage is not a possibility, it should follow that the papers produce a higher overall signal than that of the PHYTOS sensors. A further research question would then be whether or not the papers, as the industry standard, produce a realistic result compared to how sprays land on real plant matter, or whether they overestimate in that case too.

4.7 Summary

This investigation has examined the properties of the PHYTOS 31 leaf wetness sensors and discovered the following characteristics:

- A rise time of less than 0.2 seconds with the last 1% of the total signal settling over a long time period (greater than 5 minutes)
- Crosstalk between sensor cables may be significant when one is moved whilst near to another
- Constant signals have noise on the scale of 0.2% for low signals and 0.6% for high signals
- The back has a sensitivity approximately 2.5% that of the front side
- A sensor that is fully covered by liquid produces a signal that is almost independent of layer thickness (variation of <3%) unless the thickness is on a similar length scale to the gaps between interdigitated tracks on the surface, in which case the signal can vary widely (down to as low as 40% of maximum signal)

- Sensor signal is affected by contaminants in the water due to dielectric constant differences, but these effects are small (<5%) for reasonable concentrations (<5%)

Four calibration functions were produced, with the first three being comparable to each other. In sprays involving large drops (diameters >1mm), calibration 2 is expected to be suitable, with finer sprays being better estimated by calibration 4.

The PHYTOS sensors were compared to water sensitive papers and were found to consistently produce significantly smaller coverage estimates than the papers. This was hypothesised to be due to papers essentially measuring the integral of coverage over time, whereas the PHYTOS sensors measure the instantaneous coverage. There is also a difference in droplet pinning behaviour, with the PHYTOS sensors imitating a leaf more closely than the papers.

The PHYTOS sensors seem suitable for use in research purposes, generating self-consistent results that agree with the expected outcomes. However, further investigation into the effects of very small droplets should be made to better explain the dependency of the sensors to liquid application methodology. The sensors are best employed in conjunction with rather than in place of water sensitive papers, which provide different but pertinent information that the PHYTOS sensors do not; primarily droplet travel paths, distribution patterns, and a clear indication of saturation. The primary advantage of the sensors is the immediacy of the data availability, with future projects possibly implementing onboard signal processing to convert the bitstream to areal coverage using an appropriate calibration. Regardless of the specific calibration function used, the calibration data is monotonic over the relevant interval (and over the entire domain in the calibration function), allowing the sensors to be used easily and reliably in tests which seek to compare spray deposition to each other rather than quantify the exact areal coverage.

5 PARAMETRIC STUDIES (LAB)

5.1 SUMMARY OF RELEVANT LITERATURE

- Al-Mamury (Al-Mamury, Balachandran, Al-Raweshidy, & Manivannan, 2014) used a similar nozzle to that used in this investigation to test the effectiveness of the spray for differently shaped targets and verified these results with numerical simulations. Targets with sharper points or edges (e.g. a cone or a flat plate) experienced higher depositions
- Similarly, Zhao (Zhao, Castle, & Adamiak, 2008) performed numerical simulations which predict an increase of coverage on the back side of a target sphere with higher charge-to-mass ratio, as well as an increase of overall coverage with larger droplets.
- Cho (Cho, Kim, Lim, Choi, & Kim, 2019) noticed that most electrostatic spraying is performed vertically and thus investigated the efficacy of horizontal sprays for this purpose. They state that volume flow rate has a strong impact on spraying pattern, whilst voltage and spray distance impact the spraying "mode", which they define in their paper.
- Sasaki (Sasaki, et al., 2013) compare charge-to-mass ratios and liquid deposition efficiency at various spraying distances. They find that charge-to-mass ratio is inversely proportionate to spray distance. Additionally, this effect is more prominent when the target was aligned longitudinally with the spray axis, as opposed to transversely.

A variety of tests were carried out, both in a controlled laboratory environment and in a vineyard, to investigate the efficacy of electrostatic spraying. The laboratory tests (described in this section) aimed to identify important factors in nozzle placement and orientation, specifically the angle between spray axis and the sensor face, and the vertical offset between the nozzle and the sensor.

5.2 ANGLE STUDIES

One advantage of electrostatically charging a spray is the wrap-around effect. This refers to the tendency of spray that misses the target plant to experience an electrostatic attraction as it passes near the plant and then alter its flight path to land on the sides or back of the target plant. This is desirable because it increases the proportion of the spray landing on the plant and increases coverage on surfaces hidden from the nozzle. The first test done in the laboratory investigated the effectiveness of the wrap-around effect as a function of angle between wetness sensor and spray direction.

The nozzle was fixed in place with a clamp and pointed towards one of the PHYTOS wetness sensors held in another clamp stand. The nozzle was approximately 900mm away from the sensor, with an air pressure input of 50psi and voltage input of 1.25V. The sensor was positioned above a large protractor with predetermined angles. The setup can be seen in Figure 57. The independent variable of this experiment was the angle θ, which is defined as the angle between the spray nozzle central axis and the normal vector for the sensor's sensitive surface. This relationship can be seen from the top down in Figure 56.

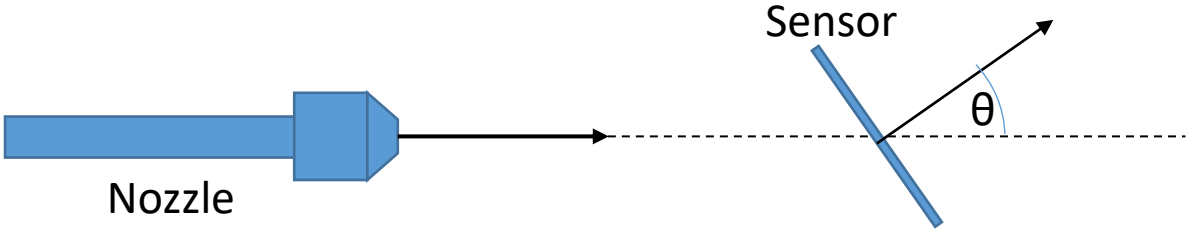

Figure 56: Schematic indicating the measure of θ

Figure 57: Photograph of contact angle measurement setup

Thus, a θ value of 0° is equivalent to the sensor facing directly away from the nozzle, and a θ value of 180° is equivalent to the sensor facing directly towards the nozzle. This angle was swept from 0° to 180° with step sizes varying from 10° to 20°, producing three trials each for charged and uncharged sprays at these angles. Each trial consisted of turning the nozzle on for 10 seconds whilst the sensor was continuously recording data. It was assumed that an angle of 20° would produce the same theoretical result as an angle of -20° due to the axis of rotation being vertical and gravitational settling was not expected to be significant for this drop size over distance.

The change in areal coverage was calculated by subtracting the average value of the sensor output over the first few seconds (before the spray started) from the average value of the sensor output for a few seconds after the spray finished. Over these intervals, the bitstream was very stable, with signal noise having an amplitude of approximately 0.001V (out of the total excitation range of 5V). Each of these values was converted to an areal coverage using calibration 4 (equation 31), and then the average change was considered for each value of θ. Figure 58 is a scatterplot with all results (the reflection is not applied in this case), and Figure 59 is a line graph showing the ratio between the areal coverage whilst charged (A_c) to the areal coverage whilst uncharged (A_u). The error bars are generated with a brute force method, in which the maximum and minimum possible ratios are calculated with the given data.

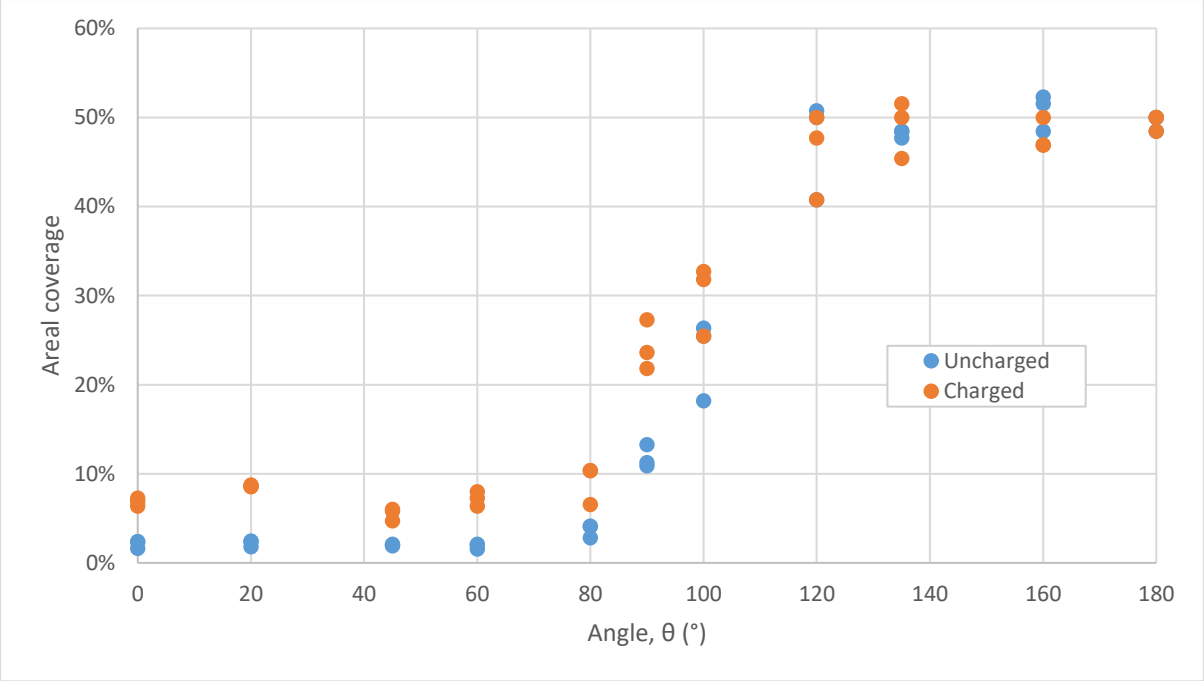

Figure 58: Compilation of all contact angle measurements, with uncharged spray in blue and charged spray in orange

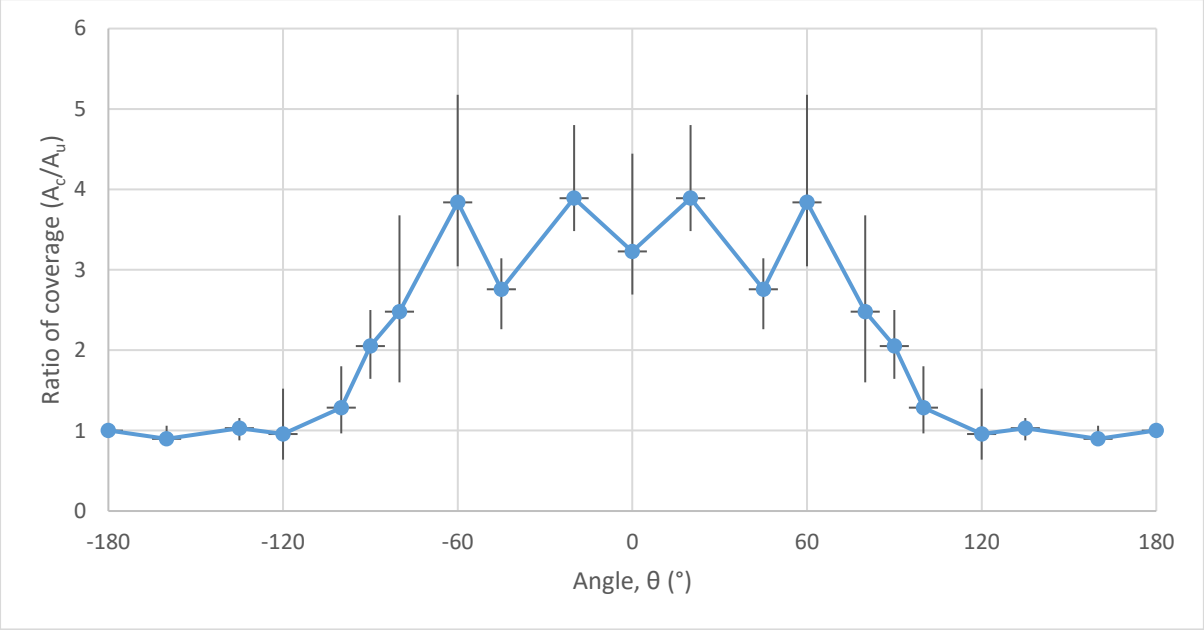

Figure 59: Ratio between average coverage for charged spray and average coverage for uncharged spray

Between 0° and 90° there is a clear increase in coverage when the spray is charged. The size of the increase varies from about twofold at 90° (when the sensor is facing directly perpendicular to spray axis), to around threefold to fourfold at 0°. From about 100° to 180° there is very little benefit to charging the spray, with the sensor reaching saturation within the 10 second period (an example can be seen in Figure 40). Even though the percentage increase is significantly larger from 0° to 90°, the absolute coverage is still much lower than when the sensor is facing the nozzle, so this only refers to the benefits of wrap-around specifically. There is an unusual alternating pattern in the 0° to 90° range, in which angles of 0°, 45° and 90° are low, whilst angles of 20° and 60° are quite high. In most cases, the error bars cover the variation, allowing for a relatively constant ratio over the middle section, but the 20° and 45° points are quite high and low

respectively, indicating that there may be some underlying effect. However, it is expected that this is a sampling error that would be smoothed with more data. As a final point, there may be some aerodynamic effects impacting the results at 0°, with droplets stagnating on the sensor. Again, this is not visible in this data.

5.3 OFFSET STUDY

A similar test was performed to investigate the efficacy of wrap-around, but this time the angle was fixed at 0° and the height of the sensor relative to the nozzle was changed instead. This experiment featured a nozzle height of 285mm, a horizontal displacement between nozzle and sensor of 820mm, and air supply pressure of 3 bar when in operation. The height of the sensor varied from 20mm to 370mm, which corresponds to a range of vertical offset distances, *x* values, of -186mm to +164mm. This was a deliberately asymmetrical range, as it became clear at the height of 164mm that gravity was affecting the spray such that none was reaching the sensor and it was deemed unnecessary to do the final test at +186mm. The test configuration can be seen in Figure 60.

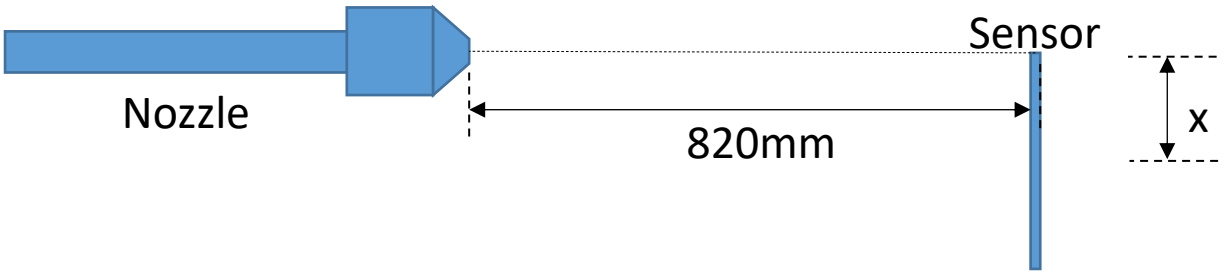

Figure 60: Schematic outlining the offset metric x

The data was processed in the same way as the previous angle study (section 5.2), with the average value before and after the spray took place converted to areal coverage using the spray-pattern calibration function, and then compared against each other. The vertical displacement, *x* (mm), was also converted to an angle, θ, using basic trigonometry so as to explain any effects in terms of angle from spray axis:

$$\theta = \tan^{-1}\left(\frac{x}{820}\right) \qquad 34$$

In this case, the ratio of deposition for charged and uncharged spray is not shown. This is because the deposition for uncharged sprays was very close to zero, and so the random error in the experiment causes large fluctuations in the ratio, producing very little in the ways of useful insight. The results for this study can be seen in Figure 61 and Figure 62.

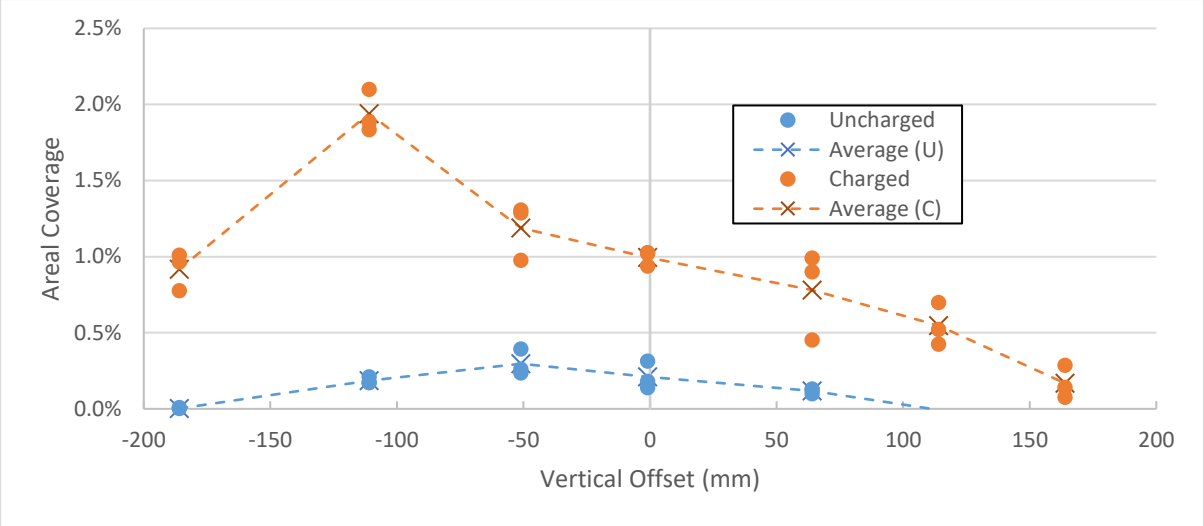

Figure 61: Coverage of sensor for different linear orthogonal offsets

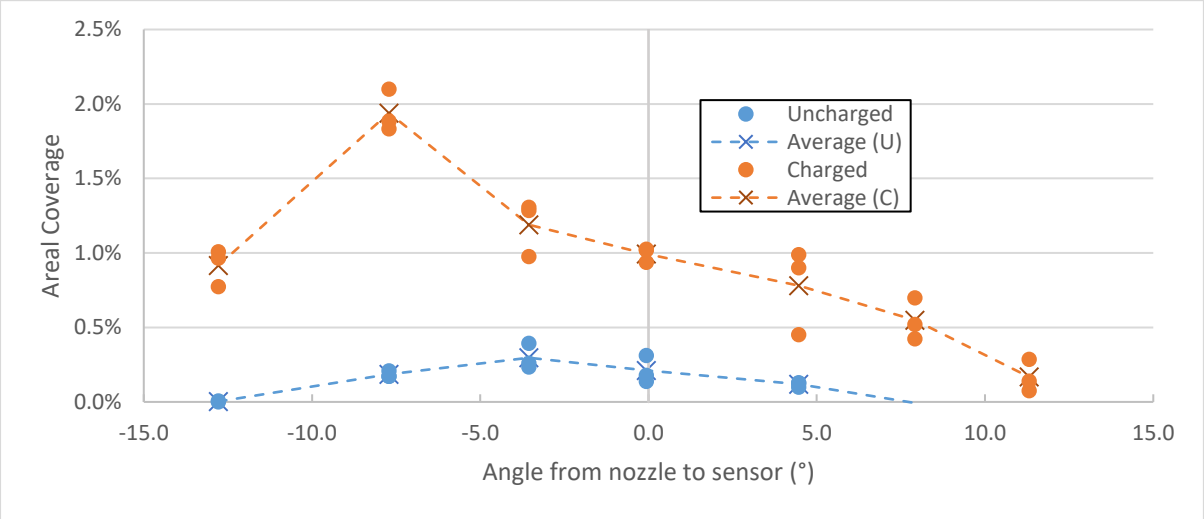

Figure 62: Coverage of sensor for different angles from spray axis

In all cases, the deposition was noticeably higher when the spray is charged, as expected due to the wrap-around effect. This increase was not symmetrical, with the deposition always being slightly higher when the sensor is below the nozzle. In all cases bar one, the areal coverage was lower than 2%, which seems low but may be a result of the non-linear behaviour of sensor output when considering very thin layers of droplets like this test. Converting to θ on the x-axis produced very similar results due to the small-angle assumption being valid for this range, though the data is more compressed towards the extremes.

The peak of the uncharged spray deposition curve was about 50mm below the nozzle (an angle of ~-4° downwards), whereas the peak of the charged spray deposition was at roughly 110mm below the nozzle (an angle of ~-8°). Charged spray will have a smaller average droplet size as well as a larger cone angle due to mutual repulsion of droplets. This suggests that at the sensor (which is at a fixed distance from the nozzle), droplets will have experienced more drag and slowed down, falling more in this time. This means that a charged spray may have a higher density of droplets at lower heights than an uncharged spray, causing this peak in coverage at a subsequently lower height. Additionally, droplets with a more vertical trajectory are likely to spend a longer period of time within 1 mm of the sensor, enhancing the effectiveness of the electrostatic attraction.

6 PARAMETRIC STUDIES (VINEYARD)

- Gan-Mor (Gan-Mor, Ronen, & Ohaliav, 2014) showed that an air-assisted induction charging electrostatic spraying nozzle can increase deposition on the underside of leaves by 200% and on the backs of grape bunches by 500%
- Law (Law & Scherm, Electrostatic application of a plant-disease biocontrol agent for prevention of fungal infection through the stigmatic surfaces of blueberry flowers, 2005) found that the use of electrostatic spraying can increase the density of a biological pest control agent per target 4.5-fold.
- Appah (Appah, Wang, Ou, Gong, & Jia, 2019) investigated the effect of electrode voltage on efficacy of sprays and found a critical voltage beyond which the charge-to-mass ratio starts to decrease and efficacy of spray decreases.
- Martin (Martin & Latheef, 2017) used fluorescent dyes to examine the effect of electrostatically charged sprays on canopy penetration in cotton plants, finding that lower layers of the canopy were unaffected by spray method even when top and bottom surfaces of leaves at the top of the plant saw two- to three-fold increases respectively.

Several tests were also performed in the vineyard on real grapevines to evaluate the efficacy of electrostatic spraying in a realistic context. These tests traded specificity for applicability, and as such they generally carry more error. All tests were conducted at Lincoln University (Lincoln, South Island, New Zealand) on the grapevine managed by Lincoln Agritech.

6.1 TRUNK WRAP-AROUND

Some spraying operations are performed on the stumps of the grapevine trunk during winter to prevent infection. Because most of the tests in this project were concerned with leaves or leaf-shaped objects, this type of spraying operation may not have been fairly approximated, so a dedicated test was created. The wrap-around effect is clearly effective on small, roughly planar targets, but it was not clear how effective it would be on a larger, rounder object such as a trunk.

Throughout this section it is assumed that the sensors will behave sufficiently similarly to a vine surface. The extrapolation of these results onto a spraying operation that excludes sensors may vary generally due to physical differences, and also through time as water content in the vines and surrounding earth changes.

The wetness sensors were attached the base of a vine trunk, one in the front, one on the side, and one on the back. An image of this arrangement can be seen in Figure 63. The BP1 electrostatic nozzle was used to spray the sensors for 10 seconds at a time from roughly 50 – 100cm away, with half of the trials having charged spray (with the electrode at roughly 1kV) and the other half having uncharged spray. The sensors were dried between trials. Following this, a set of tests were performed that were identical to the previous tests except that the sensors were not switched on and instead had a water sensitive paper pegged to them. After each trial, the water sensitive papers were placed in individual, labelled, dry, plastic zip lock bags. The papers were not used on the front sensor after the first test because they saturated completely in the 10 second test and were thus not a useful comparison.

(a) *(b)*

Figure 63: Sensor layout for (a) only sensor readings and (b) addition of water sensitive papers

The wetness sensor data was processed using the spray calibration 4 (equation 31) to produce an estimated areal coverage. The water sensitive papers were processed using the same method as in section 4.6. The results are shown in Table 6 and Table 7.

Table 6: Compilation of all trunk wraparound data

		Wetness Sensor			Water Sensitive Paper	
		Front	**Side**	**Back**	**Side**	**Back**
Uncharged	**1**	3.8%	0.4%	0.0%	N/A	0.8%
	2	6.6%	0.7%	0.1%	1.8%	0.0%
	3	7.4%	0.3%	0.1%	1.2%	0.0%
Charged	**1**	8.2%	1.4%	0.3%	N/A	2.7%
	2	6.6%	1.1%	0.9%	13.9%	2.1%
	3	5.8%	1.0%	0.5%	21.4%	0.6%

Table 7 is an amalgamation of these results; it shows the proportional increase in coverage when the spray is charged. The "average" row shows the mean of all charged trials divided by the mean of all uncharged trials. The "min" and "max" rows respectively show the smallest and largest value that could be calculated with the data. Because each average value is greater than 1, this gives the indication that charging the spray always increases the amount of liquid on the sensor or paper, though the amount of increase varies. Additionally, the range of min to max varies widely between tests.

Table 7: Ratio of charged spray deposition to uncharged spray deposition. Minimums and maximums found using brute force uncertainty methods.

	Wetness Sensor			Water Sensitive Paper	
	Front	**Side**	**Back**	**Side**	**Back**
Min	0.79	1.46	3.08	7.67	0.76
Average	1.16	2.47	8.54	11.72	6.37
Max	2.17	4.31	19.01	17.83	1254.87

6.2 CANOPY PENETRATION

The tendency of electrostatic spraying to draw spray to the target plant cast doubts on the ability of electrostatic spraying to increase the canopy penetration of sprays (with the fear being that spray would be attracted to the outer layers and thus would not travel further into the canopy). A test was created in the Lincoln University vineyard to investigate this.

The four PHYTOS sensors were placed in the grapevine canopy at different locations throughout the canopy, all intended to be close together (within the cone angle of the nozzle), but not obscuring each other. The sensors were facing the nozzle, as this test was intended to measure the total amount of liquid entering the canopy, not the effectiveness of wraparound at different canopy depths (the sensor resolution would likely be too small to detect any changes in deposition deep in the canopy with a backwards-facing sensor). Water sensitive papers were also used. This allows a comparison between them and the PHYTOS sensors, and their reputation as an industry standard helps to validate the findings. When used, the papers were secured to the top of the sensors such that the long side of the paper is parallel to the long side of the sensor (an example can be seen in Figure 63). The results from the PHYTOS sensors can be seen in Figure 64.

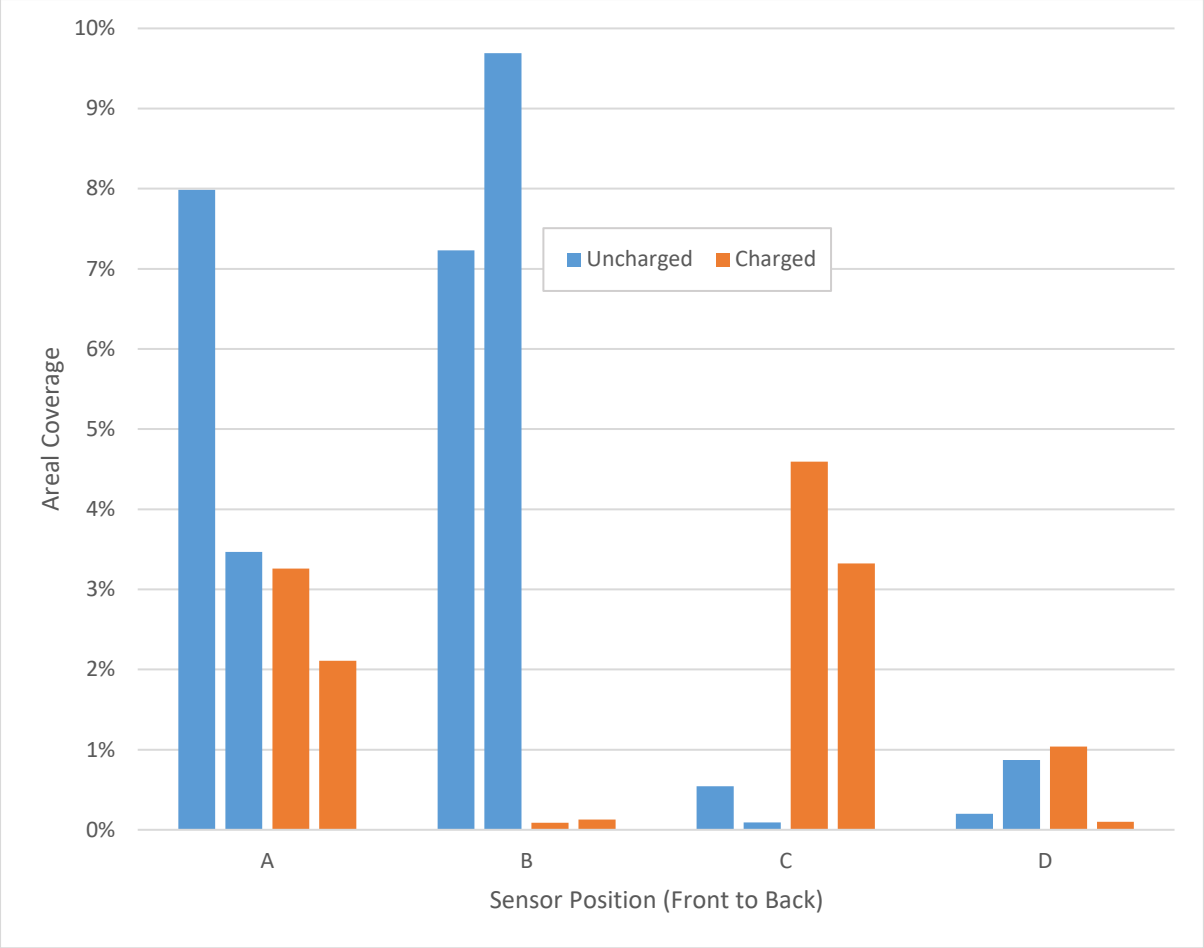

Figure 64: Areal coverage for various sensors ranging from A (closest to nozzle) to D (furthest from nozzle) inside the canopy. Dashed bars show results from PHYTOS sensors covered in part by paper

The sensors that were closer to the nozzle tended to have a decrease in deposition when the electrostatic charging was turned on. This was not expected; these sensors were predicted to have deposition that was independent of the charge, as they were expected to saturate quickly due to their proximity to the nozzle and lack of cover from the canopy. One reason for this may be an increased cone angle of the spray due to electrostatic repulsion. This could cause the spray to spread out further, with less total spray volume landing on the sensors at the front. Decreases in average droplet size due to this could also impact the results.

Conversely, sensor C (near the back) consistently experienced a much larger deposition when the spray was charged. This is unexpected, with a previous study (Martin & Latheef, 2017) finding this to not be the case, though the previous study sprayed downwards rather than horizontally. It may be due to decreased droplet size, with finer sprays being more able to penetrate through small gaps in the canopy due to lower mass and thus less resistance to changes in trajectory. This effect is not seen behind the canopy at sensor D, suggesting that this effect is lessened after passing nearby many surfaces.

When the papers are considered (though they were only used for one set of tests), the following results are generated (Figure 65).

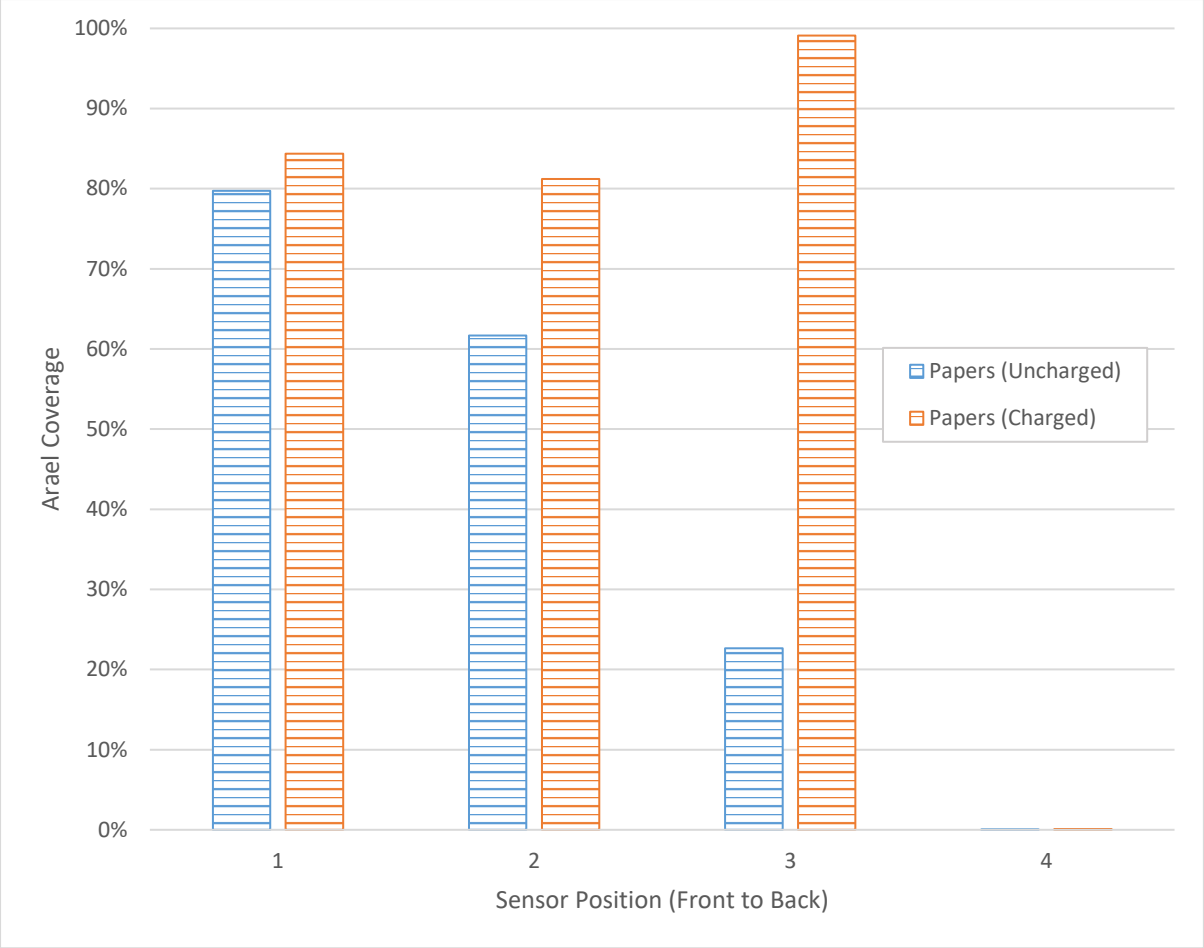

Figure 65: Areal coverage as measured by water sensitive papers (1 corresponds to A, etc)

The papers tell a somewhat different story, in which the charging of the spray invariably causes an increase in deposition at all locations. This reinforces the finding that deposition on the inside of the canopy increases when the spray is charged, with a drastic increase in coverage on sensor C. It is not clear why the papers show an overall increase in sensors A and B, but it is possible that this is simple statistical variation requiring further trials to smooth. Additionally, the uncertainty of the papers is unknown.

6.3 Voltage Parametric

As a final field study, the effect of electrode voltage on the spray efficacy was tested. This test had a very similar method to the previous test in section 6.2, but rather than testing a fixed voltage and comparing it to a zero-voltage, the voltage input was swept from 1.25V to 5.96V. Two sensors were placed near the front of the canopy, with one further away and facing the nozzle (sensor B) and the other angled more upwards and sideways (sensor A). One was in the centre of the canopy (sensor C) and one was behind the canopy attached to a net (sensor D), also both facing towards the nozzle. The results can be seen in Figure 66.

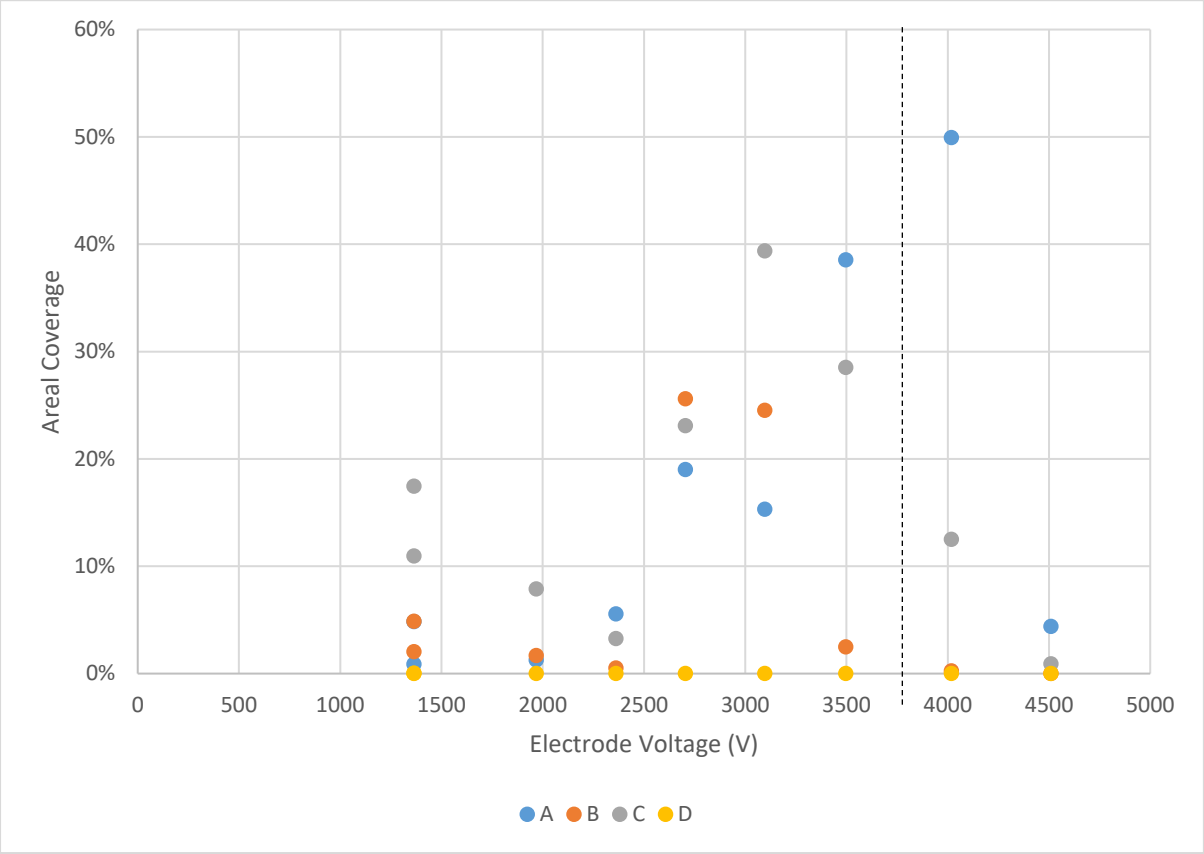

Figure 66: Areal coverage for sensors A to D (A closest to nozzle, D furthest away) for various electrode voltages.

Anything to the right of the vertical line was a test recorded after the sensors were mistakenly moved and then replaced as accurately as possible.

Sensor D never received any spray deposition regardless of charging level, which suggests that a single electrostatic sprayer is not a replacement for a pair of conventional sprayers spraying from both sides of the vine. However, all three other sensors saw a general increase in coverage as the voltage was increased. The overall rise was preceded by an initial drop, with sensors B and C lowering between electrode voltages of 1300V to 2400V. Sensor B also saw a drop in coverage just before the dashed line.

It was noted in section 3.4 that the charge-to-mass ratio was largely determined by air flow rate rather than voltage. Despite this, voltage seemed to be a more useful parameter to vary for these tests, as an increased flow rate would not just increase the charge-to-mass ratio but also the total spray volume deposited, which would impact the results. There is much existing knowledge about streamlines around objects, so the impact that charged spray has on the trajectory of droplets in that airstream is potentially the more important metric. This suggestion that higher voltages can result in a greater deposition in most locations also suggests that increased flow rates would improve results in two different metrics – total spray output per unit time, and amount of spray actually landing on the plant. This may indicate the possibility of faster spray rig movement for similar results with this technology.

7 SUMMARY OF RESULTS, CONCLUSIONS AND FUTURE WORK

This thesis discussed experiments that produced the following knowledge:

1. An electrostatic nozzle was modified for testing purposes
    a. The relationship between input parameters and important performance metrics were discovered
    b. The liquid and air flow rates can be related to supply air pressure via equations 4, 5 and 6
    c. The electrode voltage can be inferred from the supply voltage via equation 3
2. The relationship between these metrics and spray characteristics were determined for this particular sprayer
    a. The charge-to-mass ratio of the spray can be predicted using equation 17
    b. The Sauter Mean Diameter of the spray can be predicted using equation 18
    c. The charge-to-mass ratio and SMD can be related to each other through equations 19 and 20
3. These findings suggest that charge-to-mass ratio is impacted much more significantly by liquid flow rate than it is by electrode voltage within reasonable values for each. They also suggest that flows with higher charge-to-mass ratio are associated with a lower SMD, indicating that sprays that aim to maximise electrostatic effects should expect more spray drift to occur. Perhaps these systems should aim to keep the nozzle as close to the canopy as possible
4. The PHYTOS 31 leaf wetness sensors were fully characterised and compared to the existing industry standard for spray measurement of water sensitive papers.
    a. Their specifications as measured by this investigation can be read in section 4.7
    b. Two dataloggers were constructed: One operated by an Arduino Uno, the other operated by a computer running LabView with associated NI DAQ equipment.
    c. Four calibration functions were produced, of which calibration 2 (equation 29) is suggested for use with large (>1mm diameter) droplets and calibration 4 (equation 31) is suggested for use with fine sprays
    d. Whilst the papers and the PHYTOS sensors are both accurate, they generally do not produce equivalent results. The papers measure the integral of coverage over time whilst the PHYTOS sensors measure instantaneous coverage. This means that the papers consistently measure higher results than the sensors, exacerbated by a tendency of papers to experience contact line pinning more than the sensors and prevent droplet retraction after a high velocity impact.
    e. The contact angle of droplets on surfaces was measured for the PHYTOS sensors, papers and leaves, both with and without surfactant. Surfactant was found to reduce contact angle in most cases (excepting the papers), and the PHYTOS sensors were found to give a better estimate of a leaf surface for the small sample of leaves tested.
    f. Both measurement tools are useful, though the PHYTOS sensors have the advantage of an instantaneous reading and little post-processing required
5. The modified nozzle and PHYTOS sensors were used to perform two parametric laboratory studies
    a. It was found that electrostatically enhanced spraying produced no deposition increase on the front surface of the target object, but increased coverage on the back surfaces (wrap-around effect) up to four-fold.

    b. This effect may be reduced when a leaf-shaped target object is facing directly away from the nozzle, with the maximum increase occurring when the target object is facing on an angle away from the nozzle (20° - 60°)
    c. This effect is at a maximum when the target object is offset to a location slightly below the nozzle (approximately 8° cone angle), with gravity aiding the flow trajectory to land on the back surface. This effect diminishes with large offsets and does not occur above the nozzle, only below.
6. The modified nozzle, PHYTOS sensors, and water sensitive papers were also used in parametric studies in a vineyard
    a. The wrap-around effect was shown to exist for large, blunt bodies such as the base of a grapevine trunk, with deposition increasing two- to eleven-fold on the sides of the trunk and six- to eight-fold on the back of the trunk.
    b. PHYTOS sensors placed near the front of the canopy tended to experience reduced deposition when the spray was charged, though the papers saw a slight increase. This may be due to increased cone angle and drift. PHYTOS sensors placed in the centre of the canopy did see an increase in deposition, as did the papers. Sensors behind the canopy experienced little to no deposition in either case.
    c. As electrode voltage was increased, deposition seemed to generally increase, though there was a threshold above which the deposition may have begun to decrease. This critical voltage coincided with a slight adjustment to sensor location, so it is not clear whether this is a result of the electrical properties of the spray, or experimental error

Overall, it is clear that electrostatic spraying has much to offer, with increased coverage on hidden surfaces via the wrap-around effect and a suggested increase in canopy penetration. This latter point contradicts previous findings (Martin & Latheef, 2017), though the previous tests were performed with a vertical spray direction and this thesis used a horizontal direction. This supports existing literature that near-unanimously states that electrostatic spraying produces an increase in spray efficacy. The novel aspects of this thesis provide insight into the specific mechanisms of electrostatic spraying best suited to increase this efficacy; namely the geometry of the spraying system (relative locations and orientations of nozzle and target) and the differing levels of effectiveness at different locations in the canopy of a grapevine.

This thesis also provides new insight into spray sensing, providing calibration functions for capacitive wetness sensors that span the entirety of the sensor output range, as well as providing output in terms of areal coverage rather than mass coverage. It provides comparisons to water sensitive papers which allows for a good point of reference when using these sensors and discovered shortcomings of the commonly used papers in terms of the differences in surface properties to that of leaves, as well as an overestimate of coverage due to impact velocity.

7.1 Future Work

Future research in this area may include more investigations into the geometry of the spray system; relationships between target offset and relative angle have been inferred, but these can be extended into other axes of rotation or offset. Further data showing the effectiveness (or lack thereof) of canopy penetration would be valuable, as natural variation in leaf growth and water content could play a significant role in determining results, which look promising when using a horizontal spray axis. As liquid flow rate and charge-to-mass ratio have been shown to be linked together, as well as to the average droplet size, future work investigating the maximum wind speed before loss in efficaciousness due to wind speed may be useful.

The capacitive wetness sensors could benefit from further research too, primarily in the form of an investigation into the effect of droplet thickness on sensor output. Ideally, calibration 2 and calibration 4 could be unified into a single equation that has two inputs: raw sensor output and average droplet size. This would allow easy use of the sensors in a wide range of applications. Additionally, the resistivity properties of tank mixes varies between different spray operations, so further testing may be beneficial to reinforce the results found using water here. Finally, a more robust connection between water sensitive paper results and capacitive sensor results would prove beneficial in understanding how to best use the two sensing methods in complementary ways.

8 BIBLIOGRAPHY

Acharya, B. S., Stebler, E., & Zou, C. B. (2017). Monitoring litter interception of rainfall using leaf wetness sensor under controlled and field conditions. *Hydrological Processes*, 240-249.

Al-Mamury, M., Balachandran, W., Al-Raweshidy, H., & Manivannan, N. (2014). Computation Model of Electrostatic Spraying in Agriculture Industry. *COMSOL Conference.* Cambridge.

Appah, S., Wang, P., Ou, M., Gong, C., & Jia, W. (2019). Review of electrostatic system parameters, charged droplets characteristics and substrate impact behavior from pesticides spraying. *Int J Agric & Biol Eng, 12*(2), 1-9.

Asano, K. (1999). Electrostatic Pesticide Spraying. *The Modern Problems of Electostatics with Application in Environment Protection*, 363-377.

Bailey, A. G. (1988). *Electrostatic Spraying of Liquids.* Taunton: Research Studies Press Ltd.

Balsari, P., Grella, M., Marucco, P., Matta, F., & Miranda-Fuentes, A. (2019). Assessing the influence of air speed and liquid flow rate on the droplet size and homogeneity in pneumatic spraying. *75*(2).

Camuffo, D., della Valle, A., & Becherini, F. (2018). A critical analysis of one standard and five methods to monitor surface wetness and time-of-wetness. *Theor Appl Climatol*, 1143-1151.

Cho, Y., Kim, S., Lim, H., Choi, S., & Kim, M. (2019). Experimental study of electrostatic spray modes of high-flowrate water with horizontal nozzle. *Journal of Mechanical Science and Technology*, 4563-4572.

Clark, S. (2018). *Remote Monitoring of Cherry Wetness Using a Leaf Wetness Sensor and a Wireless Sensor Network.* New Orleans: University of New Orleans.

Dorr, G. J., Hewitt, A. J., Adkins, S. W., Hanan, J., Zhang, H., & Noller, B. (2013). A comparison of initial spray characteristics produced by agricultural nozzles. *Crop Protection*, 109-117.

Ebert, T. A., Taylor, R. A., Downer, R. A., & Hall, F. R. (1999). Deposit structure and efficacy of pesticide application. 1: Interactions between deposit size, toxicant concentration and deposit number. *Pesticide Science, 55*, 783-792.

Ehlert, K., Himmelmann, L., Beinhorn, J., & Kollar, A. (2019). Comparison of wetness sensors and the development of a new sensor for apple scab prognosis. *J Plant Dis Prot*, 429-436.

Electrostatic Spraying Systems. (2011, March). *Backpack Sprayer Data Sheet.* Retrieved from Maxcharge: http://maxcharge.com/pdf/BP_PI(WEB).pdf

Ferguson, J. C., Chechetto, R. G., Hewitt, A. J., Chauhan, B. S., Adkins, S. W., Kruger, G. R., & O'Donnell, C. C. (2016). Assessing the deposition and canopy penetration of nozzles with different spray qualities in an oat (Avena sativa L.) canopy. *81*.

Foque, D., Dekeyser, D., Langenakens, J., & Nuyttens, D. (2018). Evaluating the usability of a leaf wetness sensor as a spray tech monitoring tool. *Aspects of Applied Biology 137*, 191-200.

Gan-Mor, S., Ronen, B., & Ohaliav, K. (2014). The effect of air velocity and proximity on the charging of sprays from conventional hydraulic nozzles. *Biosystems Engineering*, 200-208.

Gomez, A., & Tang, K. (1998). Charge and fission of droplets in electrostatic sprays. *Physics of Fluids*.

Hislop, E. C. (1988). Electrostatic Ground-Rig Spraying: An Overview. *Weed Technology*, 94-105.

Hornero, G., Gaitan-Pitre, J. E., Serrano-Finetti, E., Casas, O., & Pallas-Areny, R. (2017). A novel low-cost smart leaf wetness sensor. *Computers and Electronics in Agriculture*(143), 286-292.

Inculet, I. I., Castle, G., Menzies, D., & Frank, R. (1981). Deposition studies with a novel form of electrostatic crop sprayer. *10*.

Jahannama, M. R., Watkins, A. P., & Yule, A. J. (1999). Examination of Elecrostatically Charged Sprays for Agricultural Spraying Applications. *The Institute for Liquid Atomization and Spray Systems*, (pp. 1-6). Toulouse.

Kabashima, J. N., Giles, K., & Parrella, M. P. (1995). Electrostatic sprayers improve pesticide efficacy in greenhouses. *California Agriculture*.

Kawahara, Y., Lee, H., & Tentzeris, M. M. (2012). SenSprout: Inkjet-Printed Soil Moisture and Leaf Wetness Sensor. *ACM Conference on Ubiquitous Computing*, (p. 545). Pittsburgh.

Kesterson, M. A., Luck, J. D., & Sama, M. P. (2015). Development and Preliminary Evaluation of a Spray Deposition Sensing System for Improving Pesticide Application. *Sensors, 15*, 31965-31972.

Kishi, M., Hirschhorn, N., Djajadisastra, M., Satterlee, L. N., Strowman, S., & Dilts, R. (1995). Relationship of pesticide spraying to signs and symptoms in Indonesian farmers. *21*(2).

Law, E. S. (2001). Agricultural electrostatic spray application: a review of significant research and development during the 20th century. *Journal of Electrostatics*, 25 - 42.

Law, S. E. (1983). Electrostatic Pesticide Spraying: Concepts and Practice. *IEEE Transactions on Industry Applications*, 160-168.

Law, S. E., & Lane, M. D. (1981). Electrostatic deposition of spray onto foliar targets of varying morphology. *24*(6).

Law, S. E., & Scherm, H. (2005). Electrostatic application of a plant-disease biocontrol agent for prevention of fungal infection through the stigmatic surfaces of blueberry flowers. *Journal of Electrostatics*, 399-408.

Law, S. E., Marchant, J. A., & Bailey, A. G. (1985). Charged-spray deposition characteristics within cereal crops. *IA-21*(3).

Law, S. E., Marchant, J. A., & Bailey, A. G. (1985). Charged-spray deposition characteristics within cereal crops. *IEEE Transactions on Industry Applications, IA-21*(3).

Lobo, N. S. (2016). *Wireless Pesticide Spray Drift Sensor System.* Auckland: Department of Mechatronics Engineering University of Auckland.

Longworth, L., Hendrickson, H., Steel, J., Cannon, E., & Gleadow, J. (2018). *End of Year Report, M22: Electrostatic Spraying.* Christchurch: Unpublished.

Lyashchenko, A. K., Loginova, D. V., Lileev, A. S., Ivanova, N. A., & Efimenko, I. A. (2009). Dielectric Constant and Dielectric Relaxation in Aqueous Solutions of K2[PdCl4] and K2[PtCl4]. *Russian Journal of Coordination Chemistry, 35*(9), 633 - 639.

Lyttle, N. S. (2017). *Artificial Leaf for Spray Coverage Detection.* Auckland: Department of Mechanical Engineering University of Auckland.

MacGregor, A. (2016). *Management of grapevine diseases.* Retrieved May 1, 2019, from The Australian Wine Research Institute: https://www.awri.com.au/wp-content/uploads/2016/11/spray-application-workshop-grapevine-diseases.pdf

Malborough District Council. (2015, July). *Rules relating to the application of agrichemicals.* Retrieved from Marlborough District Council: https://www.marlborough.govt.nz/repository/libraries/id:1w1mps0ir17q9sgxanf9/hierarchy/Documents/Environment/Air%20Quality/Rules_for_Application_of_Agrichemicals.pdf

Martin, D. E., & Latheef, M. A. (2017). Aerial electrostatic spray deposition and canopy penetration in cotton. *Journal of Electrostatics, 90*, 38-44.

Mohsen-Nia, M., & Amiri, H. (2013). Measurement and modelling of static dielectric constants of aqueous solutions of methanol, ethanol and acetic acid at T = 293.15 K and 91.3 kPa. *J. Chem. Thermodynamics, 57*, 67- 70.

Nazarko, O., Schoofs, A., Van Acker, R. C., Entz, M. H., Derksen, D., Martens, G., & Andrews, T. (2002). Pesticide-Free Production (PFP). (3).

Patel, M. K., Sahoo, H. K., Nayak, M. K., Kumar, A., Ghanshyam, C., & Kumar, A. (2015). Electrostatic Nozzle: New Trends in Agricultural Pesticides Spraying. *SSRG International Journal of Electrical and Electronics Engineering*, 6-11.

Patel, M. K., Sharma, T., Nayak, M. K., & Ghanshyam, C. (2015). Computational Modeling and Experimental Evaluation of the Effects of Electrode Geometry and Deposition Target on Electrostatic Spraying Processes. *International Journal of Computer Applications*, 10-15.

Peyrous, R., & Lapeyre, R.-M. (1982). Gaseous products created by electrical discharges in the atmosphere and condensation nuclei resulting from gaseous phase reactions. *16*(5).

Post, S. L., & Roten, R. L. (2018, July). A Review of the Effects of Droplet Size and Flow Rate on the Chargeability of Spray Droplets in Electrostatic Agricultural Sprays. *American Society of Agricultural and Biological Engineers*, 1243-1248.

Salyani, M., & Serdynski, J. (1990). Development of a Sensor for Spray Deposition Assessment. *Transactions of the ASAE*, 1464-1468.

Sasaki, R. S., Teixeira, M. M., Fernandes, H. C., Monteiro, P. M., Rodrigues, D. E., & de Alvarenga, C. B. (2013). Parameters of electrostatic spraying and its influence on the application efficiency. *Revista Ceres, 60*(4), 474-479.

Shujie, W., Hujun, W., Chun, L., Xiangmei, Z., Hui, H., & Yajun, Z. (2016). Adsorption characteristics of droplets applied on non-smooth leaf surface of typical crops. *International Journal of Agricultural and Biological Engineering, 9*(1), 35-41.

Syngenta. (2019, April 26). *Miravis.* Retrieved from Syngenta New Zealand Web site: https://syngenta.my.salesforce.com/sfc/p/#24000000Yk1o/a/1o0000005A1J/UqeMSjCjr6d6efxcEFBda4tXKA_f6TzZPrhtBmO4G20

The Australian Wine Research Institute. (2010). *Equipment adjustment and evaluation to maximise spray coverage.* Retrieved May 01, 2019, from The Australian Wine Research Institute: https://www.awri.com.au/wp-content/uploads/spray_equipment.pdf

Wang, P., Yu, W., Ou, M., Gong, C., & Jia, W. (2019). Monitoring of the Pesticide Droplet Deposition with a Novel Capacitance Sensor. *19*(537).

Wei, Z., Yongrui, H., Xin, L., Qi, L., Xiaoming, F., Bo, Z., . . . Yingqian, W. (2017). Wind tunnel experimental study on droplet drift reduction by a conical electrostatic nozzle for pesticide spraying. *10*(3).

Wen, Y., Zhang, R., & Chen, L. (2019). A new spray deposition pattern measurement system based on spectral analysis of a fluorescent tracer. *Computers & Electronics in Agriculture*, 14-22.

World Health Organisation. (2018, February 19). *Pesticide residues in food*. Retrieved from World Health Organisation: https://www.who.int/en/news-room/fact-sheets/detail/pesticide-residues-in-food

Zhang, W. (2018). *Global pesticide use: Profile, trend, cost / benefit and more.*

Zhao, S., Castle, G. S., & Adamiak, K. (2008). Factors affecting deposition in electrostatic pesticide spraying. *Journal of Electrostatics, 66*(11-12), 594-601.

9 APPENDICES

9.1 CODE TO PROCESS PHYTOS WETNESS SENSOR CALIBRATION VISUAL SIGNAL

```
%% Image processing code (avoiding imageJ)
% This code is used to calculate the total number of red pixels in an image

% For ease of use, at least one image should feature the sensor entirely
% covered in red dye so that you can use the total number of pixels to
% calculate the areal coverage

close; clear; format compact; clc

%% Initialisation
n = 49; % Highest image number
threshold = 0.5;

mkdir("processed\")

results = zeros(n+1,1);

for ii = 0:n
    i = string(ii);
    filename = strcat(i,".jpg");
    % Load image
    image = imread(filename);
    red = image(:,:,1);
    green = image(:,:,2);
    blue = image(:,:,3);
    image_grey = red - green - blue;
    image_grey = imbinarize(image_grey,threshold);
    image_grey = imfill(image_grey,"holes");
    numPixels = numel(image_grey);
    results(ii+1,1) = sum(image_grey(:));
    % Filename manipulation
    newname_grey = strcat("processed\",i,".jpg");
    imwrite(image_grey,newname_grey);
end

results_table = table(results,'VariableNames',{'total_white_pixels'});
results_filepath = strcat("processed\","results.csv");
writetable(results_table, results_filepath);
```

9.2 CODE TO PROCESS WATER SENSITIVE PAPER COVERAGE

```
close; clear; format compact; clc

%% PreProcessing

% These are the thresholds - adjust these until the 2nd image looks like
% just the dots, and the 3rd image looks like just the paper. Generally
% tdrops should be very low, unless you have some sections that are
% blue-green instead of yellow but aren't really drops, in which case as
% high as 0.6 might be good. tpaper should be around 0.15 - 0.20.
```

```
% Make sure this file is saved to the same folder as your images, then all
% you need to do is change the file name. You could also name your images
% "0", "1", "2", etc. and use a for-loop to go through all of them if you
% want.
ii = 12;

image = imread(strcat(num2str(ii),".jpg"));

tdrops = 0.001;
tpaper = 0.15;

imshow(image)

pause

close
%% Processing

red = image(:,:,1);
green = image(:,:,2);
blue = image(:,:,3);

ave = (red/3 + green/3 + blue/3);
drops = imbinarize(255 - red - green,tdrops);

paper = imbinarize(255-ave,tpaper);

sizeDrops = sum(sum(drops));
sizePaper = sum(sum(paper));

areaCover = sizeDrops/sizePaper % Print percentage coverage to the command
window
```